Laser Doppler Vibrometer for Efficient Structural Health Monitoring

A Thesis
Presented to
The Academic Faculty

by

Vinod K. Sharma

In Partial Fulfillment
of the Requirements for the Degree
Doctor of Philosophy

School of Aerospace Engineering
Georgia Institute of Technology
December 2008

Laser Doppler Vibrometer for Efficient Structural Health Monitoring

Approved by:

Dr. S. Hanagud
School of Aerospace Engineering
Georgia Institute of Technology, Committee Chair

Dr. M. Ruzzene
School of Aerospace Engineering
Georgia Institute of Technology

Dr. G. Kardomateas
School of Aerospace Engineering
Georgia Institute of Technology

Dr. N. Apetre
School of Aerospace Engineering
Georgia Institute of Technology

Dr. S. Engelstad
Lockheed Martin Aeronautics Company

Dr. B. Glass
NASA Ames Research Center

Date Approved: _____

I dedicate this thesis to my wife Mary and my children, Arun, Aneil, Jonathan, and Tresa for their unwavering support throughout this endeavor. This thesis is also dedicated to my mother Anar Devi who taught me all about perseverance.

ACKNOWLEDGEMENTS

I wish to thank Dr. Sathya Hanagud for his guidance and sharing his vision of the futuristic Structural Health Monitoring concepts. I am thankful to Dr. Massimo Ruzzene who provided many ideas at all stages of this research effort. Exchange of ideas with Dr. Nicole Apetre throughout the research effort were crucial to the successes reported in this thesis. My lifelong dreams are coming true through the help of all my teachers and colleagues.

Contents

List of Tables

List of Figures

SUMMARY

The research effort in this thesis is devoted to develop techniques to accurately and rapidly identify the location, orientation, and magnitude of the defects by using structural health monitoring concepts that use Laser Doppler Vibrometer as a non-contact sensor with multi-point sensing capability. The first research area addresses the formulation and validation of an innovative Damage Measure that is based on the ratios of the strain energy distributions of the damaged and undamaged structure. The innovations include use of a single set of actuator/sensor pair to excite and detect the responses of a structure for low frequency vibrations as well as guided wave propagation studies. A second new capability is the estimation of the Damage Measure without requiring any knowledge of the undamaged baseline structure. This method is made possible because of the development of these new technologies: Spatial Decimation and Wavenumber/Frequency filtering. The third contribution is to develop analytical models for the structural dynamics of damaged structure and seek solutions that use perturbation methods to detect damage in a plate structure. The fourth contribution is the development of a comprehensive damage detection technique over a wide frequency dynamic range. The fifth topic of research involves automation in Structural Health Monitoring based on the comprehensive Damage Measure formulation. Under the control of software the Scanning Laser Doppler Vibrometer is used to acquire the low frequency vibration mode data for a coarse identification of all the suspect regions of damage using a threshold criterion on the Damage Measure. Each suspect region of damage is further investigated using the high frequency elastic wave propagation to clearly identify the location, orientation, and extent of the damage. The computer control of the Laser Doppler Vibrometer and a quantitative assessment of the damage provide the enabling technologies for the automation proof of concept. Finally the developed techniques of damage detection are successfully demonstrated on practical structures such as a turbine blade in the laboratory and an F-15 vertical tail in field maintenance conditions.

Chapter I

INTRODUCTION

1.1 Structural Health Monitoring

Goals of Structural Health Monitoring (SHM) are to develop techniques to detect flaws in a given structure by global monitoring of the structural dynamic response to avoid possible catastrophic failures. In depot, on-board, and field structural health monitoring, the dynamic response result from excitations such as the impinging of elastic waves or vibrations excited by special devices or normal operation of the vehicle. In general, structures are designed for specific design criteria with a margin of safety, to account for the unknowns during the use of the structure. In actual usage, it is entirely possible for a structure to encounter loads that are different from the loads considered during the design. For example, the buffet loads that are experienced on the vertical tails of a high performance twin tail aircraft are different from those considered during the design. Such loads result in the initiation and growth of fatigue cracks in the vertical tail structure [1]. To enhance safety, current practices are to perform inspections of the major structural components at regularly scheduled intervals.

However, the goals of SHM are to rapidly determine without structural disassembly 1) the existence and type of damage, 2) location of the damage, 3) size of the damage, and 4) prognosis. The information on damage and loading condition are useful in a complete evaluation of the state of the health of the structure to permit its continued use or proceed with the maintenance and repairs. In comparison to non-destructive examination (NDE) there is a clear distinction between SHM and the current practices of NDE. The NDE supports the notion of examination per scheduled maintenance or with prior knowledge that a damage has occurred. Through the use of established practices of NDE such as die-penetrant, ultrasonics, and magnaflux, the damage location is confirmed. The NDE concept is different from a global structural health monitoring.

1.2 Potential Benefits of SHM

A properly developed SHM has the potential benefit of reducing the cost of maintenance, enhancing the safety of operation of the vehicle, by avoiding catastrophic failures, enhancing the life of the structure and providing the prognosis concerning the residual life of the structure. For example, the potential benefit of SHM to aircraft such as US Navy's P-3 Orion aircraft [2] is as follows. In terms of flight hours, most P-3s are operating today beyond the designed fatigue life of the airframe. They are also operating in an environment where exposure to salt is unavoidable. In addition, their low altitude flight profiles where air is more turbulent, lead to the initiation and growth of fatigue damage in the airframe. Following the early observations of stress corrosion and fatigue cracks in the aircraft, most suspect regions are now identified and fatigue life enhancement programs [2] are being implemented to enhance the useful life of the aircraft for additional 10 years. The enhancement program consists of structural component redesigns by the use of newer materials that have better stress corrosion resistance. It is envisioned that life enhancement program includes structural health monitoring concept that would allow inspection of the airframe, including the structural enhancements, without "tear-down". Thus, SHM offers a significant benefit in operating the aging fleet of P-3 aircraft.

A second example that suggests benefits of SHM is to the fleet of F-15 aircraft. Figure 1 illustrates an F-15 aircraft that has suffered a structural failure of the left vertical tail. The vertical tails on F-15s are known to experience buffet induced vibrations during high angle of attack maneuvers and consequently structural failures due to fatigue [1] over hours of flight are observed. Thus it is possible to use SHM successfully to reduce the cost of maintenance.

A third example of potential benefit of SHM is to the fleet of commercial transport aircraft. A tragic incident of ALOHA Flight 243 in 1988 is due to fatigue failure of a Boeing 737 fuselage structure. The results of the investigation by National Transportation and Safety Board are presented in Reference [3]. The fatigue damage of this aircraft is due to excessive pressure cycling and is attributed to island hopping in the State of Hawaii. Goals of a properly designed SHM technology are to detect such damages before a catastrophic

Figure 1: F-15 Damaged Vertical Tail; Consequence of Fatigue Damage Accummulation

failure occurs.

1.3 A Comparison of SHM with Current Practices in Aircraft Maintenance

Current practices in the aircraft industry require a tear-down inspection of the major airframe components to allow access to critical locations. For example, the F-15 wing skins are removed from the airframe for inspection of the stringers underneath the skins as well as the ribs and the spars every 1000 flight hours. Not all inspections lead to repairs because of no damage. However, aircraft are removed from the active service for a considerable duration while the inspections are taking place. In airline industry, such inspections amount to a significant cost of operation.

The current inspection procedures include visual, ultrasonic, magnetic field, Eddy current, radiography, and thermal field investigation. The current paradigm of ensuring safety enforces an inspection schedule throughout the operating life of the structure. Under the

current practice of schedule-based maintenance, the structure is quite often found to free from damages, hence requiring no repairs. There is a great impetus to move away from schedule based maintenance towards the condition based maintenance where SHM plays a critical role in terms of improving safety and reducing the cost of operation. Hence, there is an acute need for developing procedures for a robust and rapid structural health monitoring concept.

1.4 Goals of this Research

In this thesis the goals are to advance the state of the art of SHM techniques through the use of non-contact Laser Doppler sensors to identify the structural dynamic responses to detect small anomalies from Laser sensor information. The next goal is to develop analytical models and seek solutions from perturbation methods for small defects and formulate innovative Damage Measures. Damage Measures require a synthesis of corresponding dynamic responses of the undamaged structure. Then, the third goal is to develop procedures to obtain the undamaged structure dynamic response from the detected dynamic responses on damaged structure by different techniques such as decimation and innovative filters. Research goals are to explore both vibration-based SHM and elastic wave-based (guided wave) SHM and develop "Damage Measures" through Laser Dppler sensor measurements. The final goals of the research are to conduct tests, validate the formulated techniques, automate and demonstrate the basic research results on practical aircraft structures and turbine blades. Advances in the application of LDV are also explored to increase the efficiency of the test techniques. In Figure 2, a road-map to achieve these goals is sketched.

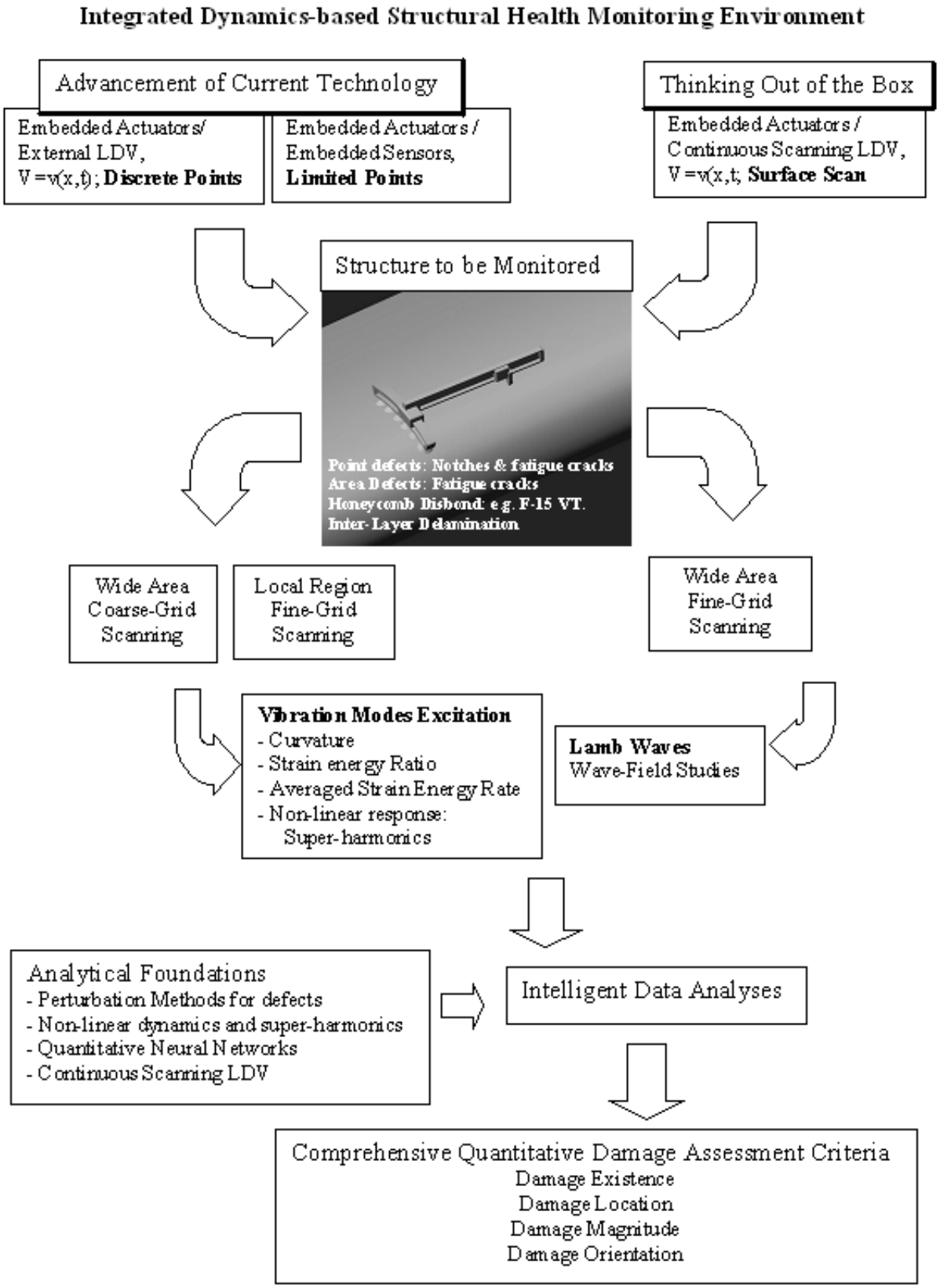

Figure 2: A Road Map for Comprehensive Structural Health Monitoring Approach

Chapter II

BACKGROUND AND LITERATURE SURVEY

2.1 Dynamics Response Based Structural Health Monitoring

A structural health monitoring (SHM) technique relies on the changes of dynamic responses due to damages in the structure. Damages result from fatigue, environmental corrosion, stress corrosion, and impact. Both metallic and polymer based composite structures experience fatigue damage. Sandwich structures are also susceptible to disbonds between the facesheet and the core of the structure. A direct consequence of such damages is the local loss of stiffness of the structure. Dynamic characteristics such as the interaction of elastic waves with defects, natural frequencies, the mode shapes, and the damping characteristics of the structure change due to a change of the stiffness due to damages. Thus, a measure of the change in the dynamic characteristics is used in SHM to identify the damage in a structure. In early efforts SHM techniques rely on exciting vibrations of a structure, measuring the dynamic response and identifying the dynamic characteristics such as the natural frequencies, modes, and damping ratios. The dynamic characteristics of the current state of the structure are then compared with the dynamic responses of the healthy structure. However, it is to be noted that the dynamic characteristics also change due to effects other than the defects, such as the operational conditions and usage of the structure. For example, an aircraft structure exhibits appreciable changes in its natural frequencies with the varying quantity of fuel and payload. Furthermore, variation in operating temperature leads to changes in the dynamic characteristics. Thus, a robust health monitoring system needs to discriminate between the operational, usage, and environmental conditions and changes in dynamic responses due to the real damage or degradation in the structure. In Reference [5] Sohn, et al. present a valuable review of the literature on structural health monitoring up to the year 2001. Their review is focused on damage detection based on

changes in vibration modes shapes and changes in the natural frequencies of the structure. In addition to the use of structural dynamic response to identify natural frequencies , mode shapes, and damping characteristics, interaction of the elastic waves with the damages in the structure [7] are also used in SHM. These damages are in the form of notch defects. In references [9, 10, 11] the Lamb waves are used to identify flaws.

With the advent of the Laser Doppler Vibrometer, now it is possible to include non-contact vibration measurements and to eliminate a need for a physical placement of an accelerometer at a particular location of interest. The beam placement is controlled such that a large region is scanned through a set of discrete points. The scanning LDV allows the use of a large array of non-contact sensor locations that can be dynamically varied during a test to discretize a large area of interest.

2.2 Literature Survey

There is a vast amount of literature on dynamics based damage detection concepts. In References [5] and [6], researchers at Los Alamos reviewed some of the recent work on the subject of structural health monitoring. In this review, all damage detection techniques are classified in one of the two broad categories. The first category is SHM based on modal data while the second category is based on study of elastic or guided wave interaction with defects.

2.2.1 SHM Techniques based on Modal Parameters

2.2.1.1 SHM Techniques based on Changes in Modal Parameters

In early attempts, changes in the modal parameters such as natural frequencies, mode shapes, damping ratios, and frequency response functions, due to structural defects, are associated [5]. In some cases, the acquired modal data are further processed through the use of spatial derivatives to obtain curvature modes [22] and modal strain energy distributions [5], which exhibit a significant amount of sensitivity to damages and their locations.

In Reference [12] Cawley and Adam present a method of detecting damages that represents a loss of local stiffness in an aluminum plate. They use frequency shift ratios f_i/f_j between modes i and j at two stages of the life of a structure. These ratios are compared

with theoretically computed ratios that consider all expected damage locations. The positions with least difference between the two lead to the possible location of the damage. The authors also suggest the use of a damping parameter. This technique of Reference [12] is dependent on the assumptions, the accuracy and use of an analytical model. Multiple damage locations need an extensive amount of computation.

In Reference [14], West presents a first systematic use of the mode shape information for damage location detection on a component using modal assurance criteria between the undamaged and damaged structure modes. A significant amount of analysis of partitioned zones of the structure is required to achieve the modal assurance criteria to reveal the damage location. This technique does not yield the magnitude of the damage.

In Reference [16], Luo and Hanagud present a technique to detect delaminations in a composite beam and disbonds in structures using nonlinear structural dynamic responses. The nonlinear dynamics response due to selected harmonic input, results in superharmonics in the dynamic response signal when the harmonic input is at or slightly below the natural frequency of the damaged structure.

In Reference [18], Gawronski and Sawicki present a technique that uses H2 norms to determine the damage location. They present their results of theoretical studies on a truss type structure. Multiple damages are represented by 20% reduction in stiffness of selected elements. A normalized sensor index based on the difference between the H2 norms of the healthy and damaged stages of the structure is obtained for each of the sensors. The damage location is identified by a significant increase in the sensor index. This technique required a large number of sensor installations to accurately determine the location of damage but without quantitative assessment of the damage.

In Reference [19], Modena, Sonda, and Zonta demonstrate that the changes in damping characteristics are much more sensitive to a crack type of damage than the natural frequency change. The damping parameter increases as a result of damage. The damping is modeled as a coulomb friction dissipative mechanism due to a crack. They successfully identify crack type defects in precast reinforced concrete elements using change in the damping parameter.

In Reference [20], Schulze, Naser, Thyagarajan, and Mickens present a theoretical formulation for structural health monitoring that uses the frequency response function to determine only damage locations. The damage represents a 5% reduction in stiffness of one element of a simple beam type structure. Their formulation requires historical data of the healthy structure as a baseline. A damage vector is defined as a force vector given by:

$$D = (H^{-1})^h . x^d - f^d \tag{1}$$

Where 'H' is the measured frequency response function at multiple sensor locations. 'x' represents the measured displacement due to an applied force 'f' located at one of the sensor locations. The superscript h and d represent healthy and damaged states of the structure. The non-zero elements of the vector D relates to the damage locations. The resolution of the damage location is restricted by the spatial measurements of the responses [20].

2.2.1.2 SHM Techniques based on Derivatives of Mode Shapes

Next set of literature survey includes the concepts that are based on higher derivatives of mode shapes to formulate curvature and strain energy information to enable detection of damaged regions. The dynamic responses are still used to identify natural frequencies, mode shapes, and damping ratios. The goal here is to consider indicators that are more sensitive to the damage in the structure. The curvature shapes of the natural modes are related to the strain distribution. The changes in displacement mode shapes due to local abnormalities such as cracks, delamination, or corrosion are not significantly noticeable, however, curvature distribution of some of the mode shapes are shown to be sensitive to local defects. Strain energy distribution in bending is related to the curvature formulation. It is found that a computation of higher order spatial derivatives of the mode shapes is needed for an accurate damage assessment.

In Reference [21], Pandey, Biswas, and Samman demonstrate the use of absolute change in curvature as a good indicator of a damage in a beam type of structure. They used a central difference approximation for the numerical differentiation technique to compute the curvature from the analytical displacement mode shapes. It is shown that the absolute

changes in curvature mode shapes are localized in the region of damages. Using a finite element model of a beam, the changes in curvature mode shape are used for identifying damage location and the magnitude of the damage in a beam type structure.

In Reference [22], Luo and Hanagud uniquely formulate an integral equation to model a structure with notch type damage and successfully demonstrate a solution technique using perturbation method. The change in curvature mode shape due to a damage distinctly identify the damage location. Their observations show that the influence of a damage on the curvature modes is concentrated near the damage while the influence on the displacement mode shape is more global on the overall structure. Their mathematical treatment of the damaged structures is considered a significant achievement since it offers a theoretical means to perform the parametric studies on the damage location and size. These studies prove to be paramount to the development of new experimental techniques.

In Reference [23], Ma and Asundi demonstrate that it is possible to compute the curvature mode shapes through the use of longitudinal strains at the surface. Fiber optics based gages are utilized for the strain measurements. It is feasible to embed these gages in the structure for on-board health monitoring systems. Salawu and Williams [24] demonstrate that not all curvature mode shapes are sensitive to damages. Luo and Hanagud [13] show that it is possible to use Poli-Vinyl-Diene-Floride (PVDF) sensors directly to obtain a signals that are proportional to the curvature.

In Reference [25], Ho and Ewins formulate a "Damage Index" defined as the quotient squared of the corresponding modal curvatures of the undamaged and damaged structure. The Damage Index is observed to be highly susceptible to noise in the measurement data. The measurement errors are amplified due to 2nd derivative computations based on numerical techniques. They also demonstrate that spatially sparse measurements adversely affect the performance of Damage Index. In Reference [26], Ho and Ewins show that oscillations in the slope computations are minimized by use of a polynomial fit through the measured displacement mode shape as compared to the use of finite difference approximation. They also report the higher derivatives to be more sensitive to damage, but are subject to more errors due to numerical techniques of computing the derivatives. Additional significant problems

result from false damage indication at the mode shape nodal points due to relatively insufficient instrumentation or poor measurement quality. The regions near the boundaries produce false damage indication. Their studies are limited to 1-D beams.

In Reference [27], Wang, Xu, and Lloyd propose a Damage index that is related to an energy criterion. They successfully demonstrate it through the use of a finite element model of a bridge. This method is most successful for damage locations away from the boundaries. The Damage Index formulation requires a full knowledge of the dynamic response of the undamaged structure which is not easy to obtain. In Reference [28], Kim, Ryu, Lee, and Choi formulate a Damage Index without requiring the knowledge of the dynamic response of the undamaged structure. Instead of measurement data on the undamaged structure, they utilize a finite element model of the undamaged structure and the current damaged structure modal test data. This approach depends on the accuracy of the undamaged model and its relationship to the current state of the structure. They define a norm of the fractional changes in the eigenvalues between the finite element model of the undamaged structure and the test data from the damaged structure. They test this method on a steel frame bridge with several repairs and reported good correlation with the existing conditions.

In Reference [29] Shi, Law, and Zhang formulate a distributed parameter, Modal Strain Energy Change Ratio (MSECR), based on the ratio of the change in strain energy of each element to the original strain energy of that element. This distributed parameter (MSECR_ij; i=element#, j=mode#) is obtained for each mode. The stiffness of the element is kept the same for the undamaged as well as damaged structure for strain energy computations of both states of the structure. The damage is assumed to affect only the local stiffness thus causing a change in the mode shape in the localized region. Therefore, MSECR is proposed as an indicator of the damage location. The quality of this indicator is improved by summing the contributions of multiple modes in a normalized fashion. The authors demonstrate the success of the proposed technique on a 2-D truss type structure with a single and multiple damages. It is noted that 40% to 50% damage in the truss elements is imposed during the demonstrations of this technique.

In Reference [30] Choi and Stubbs formulate a damage index based on strain energy

ratios. A ratio of strain energy of each element with respect to all elements in the structure is formulated for the undamaged as well as the damaged structure. The distributed damage index is then formulated as the ratios of these indices for the damaged to the undamaged structure. It is noted that the strain energies are computed using second order derivatives of the mode shapes. This formulation is demonstrated for 1-D beam and 2-D plate applications.

All existing techniques use sensors that are physically placed on the structure under investigation. With the advent of Scanning Laser Doppler Vibrometer (SLDV), it is now possible to obtain these modal parameters using laser sensors with out making any physical contact with the structure. Literature search on the next category pertains to wavefield studies to detect damages in the structure.

2.2.2 SHM Techniques based on Interaction of Elastic Waves with Defects

The second category of damage detection technique is based on elastic wave propagation. In practice, the guided waves are introduced through an ultrasonic device such as a piezoceramic actuator and a sensor.

In Reference [9, 10, 31, 32], Staszewski, et al present a comprehensive discussion on modeling Lamb waves and structural health monitoring. Their analytical results are validated using a 1-D beam. The piezoceramic discs are used both as actuators and sensors. The reflection and refraction patterns of Lamb waves with the damage are discussed. In [31, 32] they use a scanning LDV to acquire data on the Lamb wavefield in an aluminum plate. They report difficulties with noise in the measured data and propose several techniques to filter out the noise. In reference [31] they use 256 averages at each measurement location and also implement extensive data filtering techniques to improve the signal to noise ratio. A significant conclusion from their experiments is that anti-symmetric Lamb waves show a higher sensitivity to damage than the symmetric waves. This is the first reported use of SLDV as a sensor on a structure for a Lamb wave excited in a structure by piezoceramic actuators [9, 10, 31, 32].

Kaczmarek in Reference [46] report the use of an air-coupled transducer to excite the

fundamental anti-symmetric Lamb wave in a composite plate with an excitation frequency of 370 KHz and frequency-thickness product 0.74 MHz mm for a 2mm thick carbon-epoxy composite laminate

The Laser Doppler Vibrometer is a non-contact sensor system with total flexibility in providing a sensor grid selection that can be rapidly increased in the size of the array and the locations of the array can be changed with ease. However, in its current form, it is perceived as a substitution for an accelerometer or a piezoceramic sensor with a finer 'point' location. There have been two very significant developments in Laser Doppler Vibrometry that would revolutionize the use of SLDV. In References [34, 35] Sriram and Hanagud report successful demonstration of a concept of continuously scanning Laser Doppler Vibrometer in 1988. Then in 2001, Marterelli [36] report further improvement on this concept. The significance of these developments is realized in the use of SLDV devices for a distributed structural response data acquisition in an expeditious manner. Despite the promises it holds, there is still a significant development that is needed to prove the practical application of their research.

A new emerging technique called Time Reversal Acoustics (TRA) Analysis pertains to high frequency wave propagation between a set of sending and receiving acoustic transducers. This technique is used for medical application to detect kidney stones [37, 38]. This technique is based on the fact that a wave propagating through an intact region is not abruptly altered. However, the wave pattern is significantly changed if it encounters discontinuities such as cracks, delaminations, or disbonds as studied by Shah, et al. [39, 40, 41]. The procedure of testing TRA has been described in detail by Fink, et al. in References [37, 38]. In Reference [42] Sohn, et al report the application of TRA to detect impact damage in a composite plate. They use a spatially located pair of piezoelectric transducers to span the region of interest. Each device is a sensor as well as an actuator. A high frequency ultrasound wave pattern is sent from the first actuator and is received by the second piezoelectric device which acts as a listener. The received waveform is simply reversed in time and sent back towards the first actuator location. The received signal at the first location is compared and scaled with respect to the original signal that is transmitted from

its location. If the transmitted and received signals are identical in waveform shape within a specified tolerance, it is concluded that there has been no abnormality along the pathway of the wave traveling between the two locations. Here, the magnitude of received signal is scaled-up to match the maximum of the transmitted signal. This technique is useful in sensing a damage only along the path between the set of transducers. Recent advances as reported in [43] include use of Lamb waves in time reversal acoustics analysis for health monitoring of a composite plate. A major problem with noise in the use of Lamb wave is reported by the authors. They use a wavelet-based filtering technique to enhance the time reversibility by taking advantage of temporal and spectral differences between the signal of interest and background noise. All time reversal acoustics developments are around a network of actuator/sensor package. These sensor/actuator arrangements are shown to work only [43] if the damage is along a path within this network. In Reference [43], the authors use 16 piezoceramic actuator/sensor installation on a composite plate of 24"x24". This hardware requirement imposes difficulty in a practical application as each of the channels must be recorded at a high sample rate.

The literature search has revealed the existence of a respectable amount of knowledge in the field of damage detection in structures and it continues to be developed at a fast pace. The robustness of a damage detection technique lies in its insensitivity to the test environment variables and its ability to detect the damage of significance without failure. It is less desirable if one has to carry historical information to assess the future status because that historical information is not always accurate. The techniques proposed and studied in this literature survey is mostly limited to artificially induced damage or disbond. The practical application of these techniques is still in its infancy.

Chapter III

RESEARCH ISSUES AND THE SCOPE OF THE THESIS

3.1 Research Issues

An ideal scenario of structural health monitoring is where the existence of damages and damage locations are identified accurately and then the magnitude of damage is quantified in a short period of time, without requiring the baseline data on the undamaged structure. This information is used in the estimation of the prognosis of the structure. Current state of the art in structural health monitoring is well short of this target.

Literature survey has revealed a vast amount of fundamental building block formulations of scientific and engineering approaches to all forms of known damages such as fatigue cracks, disbonds, delaminations, impact damages, and corrosion effects in structures. Most techniques that are based on low frequency vibration modes require a baseline data on undamaged structure. In practice, the baseline data on undamaged structure are not available. Some of the reasons are due to structural changes that are caused by repairs or environmental changes. In practice, it is desirable to be able to develop a structural health monitoring procedure that relies only on the data currently acquired on the structure, in its current state of health.

Low frequency Vibration modes involve response of the overall structure and these modes have traditionally been measured by physical placement of the sensors like accelerometers or piezoelectric sensors at locations of interest on a structure. It is noted that the sensor grid locations must be adequately populated to capture local changes in the mode shapes due to the local damages. This becomes an expensive proposition and a very difficult concept to implement on a flying platform. With commercially available Scanning Laser Doppler Vibrometer (SLDV), now it is possible to obtain the desired data using a laser sensor. The following benefits of an SLDV are immediately realized in support of vibration tests:

1. Elimination of physically placed sensors and their associated electrical network
2. Measurements using non-contact sensors, with improved accuracy since there is no added mass associated with the sensors
3. Automation of SLDV scan for test efficiency
4. A large sensor grid pattern that can be dynamically changed during a test

Lamb wave propagation in structures has the potential to identify any defects through:

1. interference or
2. reflections and refractions or
3. scattering as observed on the surface

A Scanning Laser Doppler Vibrometer is a practical means of studying the complete wavefield pattern over a range of low to high ultrasonic frequencies. The piezoceramic ultrasonic transducers are used to excite Lamb waves in the structure. The SLDV is used as a sensor to detect the response of the wave propagation on the surface as a surface sensor. An opportunity exists to formulate a unified approach where the benefits of low frequency vibration mode tests are merged with those of the high frequency wavefield observations to achieve a robust structural health monitoring procedures.

The excitation source for low frequency vibration mode tests has traditionally been through an electrodynamic shaker and impact hammer while piezoceramic actuators are used for high frequency wavefield studies. It is also possible to use piezoceramic actuators for both the low frequency vibration mode and the high frequency wave excitations.

Another opportunity exists to improve upon the use of SLDV sensors. Current LDV products require measurement of responses at discrete locations for a finite duration of time in order to perform FFT computations. In essence the SLDV replaces an accelerometer but with a lot of flexibility such as dynamic selection of sensor array. The laser traces at the speed of light. It is realized that there is a lot of room for improvement upon the current state of the art in Scanning Laser Doppler Vibrometery.

A significant subject of study is the analytical model formulation of a structure with damage and seek analytical solutions. This analysis capabilities will allow parametric studies for interpretation of the measured data and also to develop and validate new methods of detection.

3.2 Research Program

Thus the following research program is studied in this thesis:

1. First study consists of formulation of Damage Measures or Damage Indices for SHM technique that are based on Vibration-based SHM and Guided wave-based SHM.

2. Development of techniques to estimate the dynamic response data of the corresponding undamaged structure from measurements on damaged structure. Two techniques known as Spatial Decimation and frequency/wavenumber filtering are developed.

3. Analytical solutions for a study of the vibration characteristics of damaged structures (plates) by the use of perturbation techniques are obtained and the solutions are used in analyzing the measured SHM data.

4. A unified approach for low frequency vibration and modes and high frequency wave-field studies using a combination of piezoceramic actuators and SLDV for localization and quantification of damage are formulated to improve the accuracy and the speed of SHM

5. The next study consists of the development of preliminary automation concepts for useful technology to enhance safety and reduce cost of maintaining advanced structures.

6. The final item of the proposed research program is to take the developed concepts to the field through application of Damage Measure concepts and SLDV for SHM to practical aerospace structures.

3.3 Outline of the Thesis

Early studies on SHM evaluated the changes in the natural frequencies due to a stiffness reduction caused by the damage. These investigations used natural frequencies as damage indicators. For small damage these indicators have a low sensitivity, and they do not allow the determination of the location of damage. In later studies, the effects of damage on mode shapes are used. The displacement mode shapes and corresponding modal curvatures are used. The detection of small changes in the mode shapes of a structure is used to localize damage and potentially estimate its severity. In particular, small variations of mode shapes due to changes from an undamaged state is highlighted by successive spatial differentiations of the deflections, which are typically required in the estimation of curvature modes.

This approach has been pursued by Kim and Stubbs [93] to formulate a damage index based on the comparison of strain energy distributions in damaged and undamaged structures. In [93] and in subsequent papers by the same authors, the technique is applied to beam structures using mode shapes or time-domain data to obtain information on both damage location and extent. The same technique has then been extended to plate structures by Cornwell, Doebling,and Farrar [[94]], where accelerometers are used to measure the deflections to be interpolated for successive differentiation. The results presented in [93] [94], show the effectiveness of the technique. However, in References [93] [94], the calculations of Damage Index needed data from the corresponding undamaged structure. In their paper, laboratory specimens are prepared and undamaged plate or beam is used to obtain the information. In practical application of SHM such information on the undamaged structure is not available.

1. Thus in this thesis, techniques are developed to estimate the dynamic response data on the corresponding undamaged structure by using only the measurements on the current state of the structure that has damage. This technique is named as "decimation" technique in this thesis. This is the first new contribution in this thesis and is described in Chapter 4.

2. Dynamics of damaged beams and plates are analytically studies using perturbations

methods. The notch type of damages are studied here. The analytical methods are useful in validation of the experimental techniques and further evaluation of their limits on damage size and orientation. These studies are presented in Chapter 5.

3. Next, the concept of the strain energy based Damage Measure is extended to the SHM techniques that are based on the propagation of elastic waves in a damaged structure. Discussions on the Damage Measure in time domain using elastic wave propagation are presented in Chapter 6.

4. The fourth new contribution is to use a non-contact Scanning Laser Doppler Vibrometer (SLDV) sensor for measurements on a damaged structure, estimate the response on the corresponding undamaged structure, calculate the Damage Measure, and interpret the results in terms of "Damage on the structure". The application of Scanning Laser Doppler Vibrometer is discussed though out this thesis.

5. The fifth new contribution is the development and demonstration of the concept of automation in structural health monitoring. This automation concept is described in Chapter 7.

6. Finally, a significant contribution is to use these new developments for application to practical structures such as the F-15 aircraft vertical tail, and turbine blade, and graphite composite test panels instead of restricting only to the laboratory test specimens as in previous references [93] [94]. These applications are presented in Chapter 8.

This research effort is based on the use of a Scanning Laser Doppler Vibrometer (SLDV) to measure the dynamic behavior of a test structure. The SLDV allows non-contact vibration measurements which replaces the physical placement of an accelerometer at a particular location of interest. The laser beam placement is controlled by a user-defined set of grid points on the structure, which offers the possibility of accurately estimating deflection derivatives of various orders and in turn allows the estimation of curvatures and strain energy distributions. Such detailed measurement refinement is difficult to obtain in a timely manner using accelerometers and/or strain gauges.

Chapter IV

DAMAGE MEASURE IN STRUCTURAL HEALTH MONITORING

4.1 Strain Energy Based Damage Measures and their Estimation from Measurements only on the Damage Structure

The Damage Measure is formulated on the basis of the distribution of a strain energy functional over the monitored surface. The ratio of the measured strain energy distribution to a reference, baseline value is considered as the damage indicator. This formulation follows the developments presented for example in [93, 94]. The innovations are pursued in the computations of the distributed strain energy and the formulation of the baseline data for the undamaged structure.

4.1.1 Damage Measure for beams: Discrete Element Formulation

4.1.1.1 Statement of the problem

Given: A beam with a crack or notch type of defect is excited by an actuator. The objective is to obtain the strain energy of the beam with the defect, compare this strain energy with the strain energy of the same beam without defect. Use this comparison to formulate a damage measure.

4.1.1.2 Euler-Bernoulli Beam Theory assumptions

1. The beam material is isotropic which implies that the material possesses uniform elastic properties in all directions.

2. The cross-section of a beam remains plane after deformation and is infinitely rigid in its own plane.

3. The cross-section remains normal to the deformed axis of the beam.

4. The stress at the centroid of each cross-section is zero and varies linearly across the cross-section in the direction of bending.

These assumptions imply that each cross-section of the beam undergoes a linearly varying axial displacement across the smallest dimension, also referred to as thickness of the beam. These assumptions further lead to the fact that the bending moment at a cross-section is proportional to second derivative of the transverse deflection at that cross-section.

4.1.1.3 Damage Measure formulation using strain energy

The strain energy for an Euler-Bernoulli beam is given by [82]:

$$U = \frac{1}{2}\int_0^L EI(x)w(x)^2_{,xx}dx \tag{2}$$

where $EI(x)$ is the flexural rigidity of the beam, w is the beam transverse deflection, and $m(x)$ is the distributed mass per unit length, and L is the beam length with the notation $()_{,x} = \frac{\partial}{\partial x}$ adopted to indicate partial derivatives with respect to the spatial coordinates.

At a selected time the amplitude of the beam deflection is $\phi_i(x)$ [in general it can be $a_i\phi_i(x)$] when excited at its i-th natural frequency. In the literature, $\phi_i(x)$ is also known as the displacement mode shape at the i-th natural frequency. The strain energy associated with the beam deflection $\phi_i(x)$ and Euler-Bernoulli beam approximation is expressed as:

$$U_i = \frac{1}{2}\int_0^L EI(x)\phi_i^2(x)_{,xx}dx \tag{3}$$

This expression is approximated by a summation of $\phi_i(x)$ at N discrete locations of x. The purpose is to accumulate later measurements at N discrete locations. Then, the total strain energy of the beam is expressed as [94] follows:

$$\begin{aligned} U_i &= \frac{1}{2}\sum_{k=1}^{N} EI_k \int_{x_k}^{x_{k+1}} \phi_i^2(x)_{,xx}dx \\ U_i &= \sum_{k=1}^{N} U_{i_k}; U_{i_k} = EI_k \int_x^{x} {}_{k}{}_{k+1}\phi_{i,xx}^2 dx \end{aligned} \tag{4}$$

It is assumed that the damage is small and the neutral axis of the beam does not change due to the damage and flexural rigidity of the beam over each discrete region is constant. In addition, it is assumed that damage is localized in a single region $p < x < p + 1$, and that at the damage location:

$$\frac{U_{i_p}}{U_i} \approx \frac{U^*_{i_p}}{U^*_i} \tag{5}$$

so that an estimation of the reduction in the stiffness is obtained as:

$$\frac{EI^*_p}{EI_p} \approx \frac{U^*_i}{U_i} \frac{\int_{x_p}^{x_{p+1}} \phi^{*^2}_i(x)_{,xx} dx}{\int_{x_p}^{x_{p+1}} \phi^{*^2}_i(x)_{,xx} dx} = f_{i_p} \tag{6}$$

where $\phi^*_i(x)_{,xx}$ is the curvature corresponding to the displacement mode shape of the damaged beam, and where the strain energy ratio f_{i_p} is denoted as the Damage Measure (DM). The DM provides indications of both damage location, as well as its extent. Specifically, it is expected to be equal to one over the undamaged regions, and typically higher than one over the damage region. It is well known how damage affects the strain energy distribution when it is located near, or in regions of maximum strain energy for a given deflected shape. Hence, the visibility of a damage is affected by the mode shapes in consideration. For this reason, it is convenient to combine information obtained from the analysis of several modes (I) and therefore to consider a cumulative strain energy ratio, defined as

$$f_k = \frac{1}{I} \sum_{i=1}^{I} f_{i_k} \tag{7}$$

This cumulative index provides a single piece of information which combines the results from the excitation of the beam at several of its natural frequencies. Modes not affected by damage because its particular location do not contribute, i.e. they give unit contributions, whereas the index for modes altered by the defect are combined to provide a robust indication of damage. This cumulative index is conveniently referred to as cumulative Damage Measure. Researchers in References [30, 94] use similar summation of Damage indices of several modes but do not discuss the significance of the cumulative quantity.

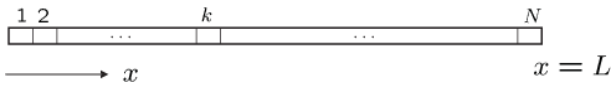

(a) Beam divisions

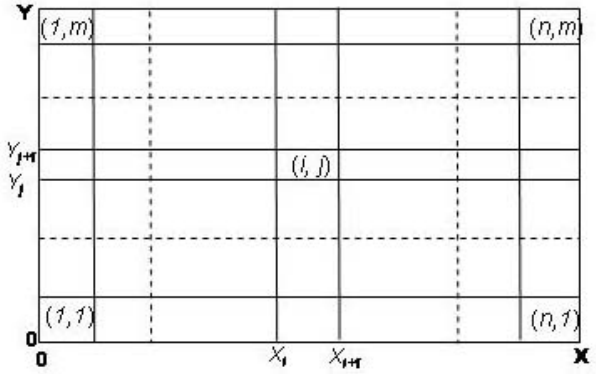

(b) Plate divisions

Figure 3: Schematic of beam and plate divisions

4.1.2 Damage Measure for plates

4.1.2.1 Statement of the problem

The statement of the problem is similar to that of the beam problem except it is for two dimensional plate structure. The focus here is to determine distributed strain energy in a vibrating plate using its out-of-plane defection shape that is identified at a selected time. Formulation of Damage Measure for a plate is based on the strain energy ratios between the damaged and undamaged plate. The out-of plane deflection shapes of a vibrating plate at a selected time are determined for the measured velocity responses using a Laser Doppler Vibrometer.

4.1.2.2 Kirchhoff Plate Theory assumptions

The formulation is with the assumptions of Kirchhoff plate theory. The following assumptions dictate how the normal lines at a plate cross-section behave [82]:

1. The normal lines remain as straight lines even after deformation.

2. The normal lines remain infinitely rigid along its own length.

3. The normal lines remain perpendicular to the deformed mid-plane of the plate.

Following these assumptions, the out-of-plane displacements are defined as a function of in-plane coordinates which is valid for thin plates of homogeneous and isotropic materials. The strain energy for a plate, assuming Kirchhoff plate approximation, is expressed as [45]:

$$U_{_i} = \frac{1}{2}\int_Y \int_X D[\phi_{i,xx}^2 + \phi_{i,yy}^2 + 2\nu\phi_{i,yy}\phi_{i,xx} + 2(1-\nu)\phi_{i,xy}^2]dxdy \tag{8}$$

where $\phi_i = \phi_i(x,y)$ [or $a_i\phi_i(x,y)$] defines the plate displacement corresponding to the i-th mode shape when it is excited harmonically at its i-th natural frequency. It is assumed that small amount of damping does not change the natural frequencies and mode shapes significantly, yet the response is finite. The variable A denotes the plate surface, $D = D(x,y) = Eh^3/12(1-\nu^2)$ is the plate rigidity, with $h = h(x,y)$ denoting the plate thickness, while E and ν are the Young's modulus and the Poisson's ratio of the plate material. The plate is subdivided into an $N \times M$ grid, so that the strain energy associated to the n,m area can be expressed as shown in Figure. 3.b:

$$U_{_{i_{nm}}} = \frac{1}{2}D_{nm}\int_{A_{nm}} [\phi_{i,xx}^2 + \phi_{i,yy}^2 + 2\nu\phi_{i,yy}\phi_{i,xx} + 2(1-\nu)\phi_{i,xy}^2]dA \tag{9}$$

where it is assumed that the plate rigidity is constant over each region. Following the procedure outlined for beams, we define

$$\frac{D_{nm}^*}{D_{nm}} \approx \frac{U_{nm}^*}{U_{nm}} \frac{\int_{A_{nm}} [\phi_{i,xx}^{*^2} + \phi_{i,yy}^{*^2} + 2\nu\phi_{i,yy}^*\phi_{i,xx}^* + 2(1-\nu)\phi_{i,xy}^{*^2}]dA}{\int_{A_{nm}} [\phi_{i,xx}^2 + \phi_{i,yy}^2 + 2\nu\phi_{i,yy}\phi_{i,xx} + 2(1-\nu)\phi_{i,xy}^2]dA} = f_{i_{nm}} \tag{10}$$

where D_{nm}^* and ϕ_i^* are respectively the rigidity and the mode shape of the damaged plate. A cumulative DM can be again defined by combining the contributions from the DM obtained at several excitation frequencies (I) to obtain, for region nm

$$f_{nm} = \frac{1}{I}\sum_{i=1}^{I} f_{i_{nm}} \tag{11}$$

This cumulative DM for a 2-D plate is once again referred to as cumulative Damage Measure, same as defined for the 1-D beam case.

4.1.3 Estimation of Baseline Data on the Damaged Structure

The DM provides a comparison between the strain energy of the damaged and undamaged plate over selected discrete elements on the regions of the structure. In practice however, it is difficult to have or to obtain strain energy of the corresponding undamaged structure. For this reason, a new technique is proposed to estimate the information on strain energy of the corresponding undamaged structure directly from the measured response on the current state of the damaged structure. In the proposed approach, the mode shapes are measured at several locations over the structure, so that spatial derivatives required for the evaluation of DM are accurately estimated. This is done by performing spline interpolations of the measured data. Based on the procedure outlined in [49], the mode shape $\phi(x, y)$ for a plate structure is for example approximated as:

$$\phi(x, y) \cong \sum_{p,q} h_p(x) h_q(y) \Phi_{p,q} \tag{12}$$

where $\Phi_{p,q}$ defines the value of the mode shape at location p, q over the plate, while $h_p(x), h_q(y)$ are spline basis function [100]. The value of $\Phi_{p,q}$ is the quantity measured experimentally at the sensor location, or at the location of a grid point using the SLDV. Alternatively, in numerical simulations using finite elements, it represents the value of the nodal displacement at the considered location. The spline interpolation of the plate deflection at discrete locations is used for accurate prediction of the derivative of the deflection. The curvature estimations are obtained by taking derivatives of the spline functions, while keeping the nodal or measured values as weighting parameters. This concept is described in a concise manner by expressing the plate curvatures as:

$$\begin{aligned} \phi_{,xx}(x, y) &\cong \sum_{p,q} h_{p,_{xx}}(x) h_q(y) \Phi_{p,q} \\ \phi_{,yy}(x, y) &\cong \sum_{p,q} h_p(x) h_{q,_{yy}}(y) \Phi_{p,q} \\ \phi_{,xy}(x, y) &\cong \sum_{p,q} h_{p,_x}(x) h_{q,_y}(y) \Phi_{p,q} \end{aligned} \tag{13}$$

In particular, the interpolation procedure briefly described above offers the opportunity

of calculating DM, without the need for baseline data. The baseline data is approximately obtained by maintaining the size of the discrete element lager than the flaw dimensions. The availability of measurements on a supposedly undamaged structure to be directly compared with those on a damaged structure is an assumption upon which many damage detection techniques rely heavily [5],[93]. In a real test scenario, however, it is very unlikely that historical data are available, and/or that such data can be considered reliable for damage detection purposes. Changes in fact result from a number of uncontrollable sources, such as temperature variations, operating conditions, boundary conditions, etc. A technique is presented whereby damage or anomalies are obtained from a single measurement. Baseline information is estimated by using a subset of the measurement points where the grid spacing is larger than the size of defect that is being identified by the DM. The baseline interpolated deflection is expressed as:

$$\phi^*(x,y) \cong \sum_{r,s} h_r(x) h_s(y) \Phi_{r,s} \tag{14}$$

where r, s are a subset of the measurement grid points p, q, such that $r < p, \quad s < q$. The resulting under-sampling of the data has the purpose of intentionally "missing" any discontinuities or anomalies corresponding to damage, which can generally be detected only through a refined measurement grid. The baseline information is differentiated and used for the estimation of the strain energy generically denoted as U^*.

The concept of under-sampling is in essence a spatial decimation where only a subset of the full nodal displacement set is used with an expectation that this subset is less sensitive to the damage. a simple form of decimation implementation is achieved by skipping a selected set of measurement points. The subset remaining after decimation is used for interpolation of the response data at measurement points that corresponds to the original full set. An example of decimation is explained through Figures 4.a and b. A total of 80 grid points are used to define the mode shape for a simply supported beam. The first mode and its second derivative are shown in Figures 4.a and b. The effects of decimation on the curvature for this example are demonstrated in Figures 5.a,c, and d. The decimation factor 50% implies every other grid point is removed from the full set, a 75% decimation

implies that every fourth grid point is kept, and 90% decimation implies that every 10th point is kept for the synthesis of the baseline information. It is observed that with an increasing decimation factor, the curvature information approaches that of the undamaged baseline structure. However, it is noted that excessive decimation leads to error in the strain energy of the corresponding undamaged structure. The decimation is to be defined such that the baseline mode shape becomes insensitive to the damage and yet retain the basic characteristic of the mode shape. There are no single decimation factor that works for all mode shapes and. It is closely related to the number of node lines in the mode of interest. Thus the optimum value of the decimation factor is still an open research area.

4.2 Numerical Results on Beams and Plates

4.2.1 Beam Analysis

The theory and associated procedures that are developed in Section 4.1.3 are validated through numerically simulated testing and actual tests. First the case of a beam structure is considered. The beam is made of steel ($E = 2.1 \times 10^{11}$ MPa, $\rho = 7800$ kg/m^3), it has rectangular cross section of depth $h_0 = 5$ mm and out-of-plane width $b = 1$ cm, and it is 1 m long. Damage in the beam is simulated as a thickness reduction occurring over a single element of the FE mesh. The thickness of the damaged element is denoted as h, while h_0 denotes the thickness of the undamaged beam. The beam is simply supported at both ends and loaded by a harmonic unit load of varying frequency. The behavior of the beam is predicted through a FE (Finite Element) model, formulated using classical beam elements. The length of the beam is discretized into 80 elements. This large number of elements is selected to replicate experimental measurement density available with SLDV. The nodal displacements corresponding to a harmonic load at a specified frequency are computed and used for the calculation of beam curvature, and DM computation along the length of the beam. In this case, the nodal displacements are interpolated using cubic spline functions. A subset of the nodal displacements is used to generate reference data. The subset is defined by under-sampling the available nodal displacements, according to a so-called "decimation factor", which is here defined as:

$$d = 100 \times (1 - \frac{N_i}{N_t}) \tag{15}$$

where N_i is the number of nodal displacements used for the interpolation, while N_t is the total number of nodal displacements available from the analysis. For example, in this case the analysis provides $N_t = 80$, and a decimation factor $d = 75\%$ indicates that the under-sampling is performed by considering one out of four nodal displacements.

Example of the mode shape amplitude and related curvature for excitation at the first and second natural frequency of the beam are shown in Figure 4. The plots, obtained for damage at mid-length of the beam with $h/h_0 = 0.9$, confirm the sensitivity of the curvature deflection as opposed to the displacement amplitude. Also, the example demonstrates how the influence of both displacements and curvatures depends upon the location of damage with respect to nodal points of mode shape and curvature. The curvature of the second mode in this case does not reveal the presence of damage, while the first curvature mode clearly highlights it. The selection of the decimation parameter is critical to the formulation of the DM. A low decimation factor in fact does not provide adequate baseline information, as the interpolated mode shape captures all the features associated to damage, while a high decimation factor is not sufficient to provide an appropriate description of the mode shape. The effects of decimation on the accuracy of the damage detection methodology are presented here. Figure 5 illustrates the influence of the decimation parameter on the synthesized data and on the resulting estimated DM. The plots are obtained for a damage at mid-length equal to $h/h_0 = 0.9$. For low decimations ($d = 50\%$), the synthesized baseline data, indicated as $'o'$ in the plots, replicate very closely the interpolation obtained from the full data set. The resulting DM estimation highlights some deviation from the unit value at mid-length, but does not give clear indication of the location of damage. The predictions are significantly improved by decreasing the decimation number, which allows baseline information which resembles very closely the undamaged configuration. A proper selection of the decimation parameters provides a good estimation for the DM, which, in principle, is used to assess both damage location and extent. Figure 6 illustrates how the amplitude of the deviation from unity is in fact proportional to the damage extent. The

plots correspond to the DM for excitation at the first and third natural frequency, and for two damage locations. The cumulative DM value is an effective way to combine the results from the excitation of several modes and to avoid lack of accuracy associated to damage located close to nodal points. The cumulative DM is also proportional to the damage extent, as shown in Figure 7, which presents the results of the combination of the first ten modal DM for both single and multiple damage locations.

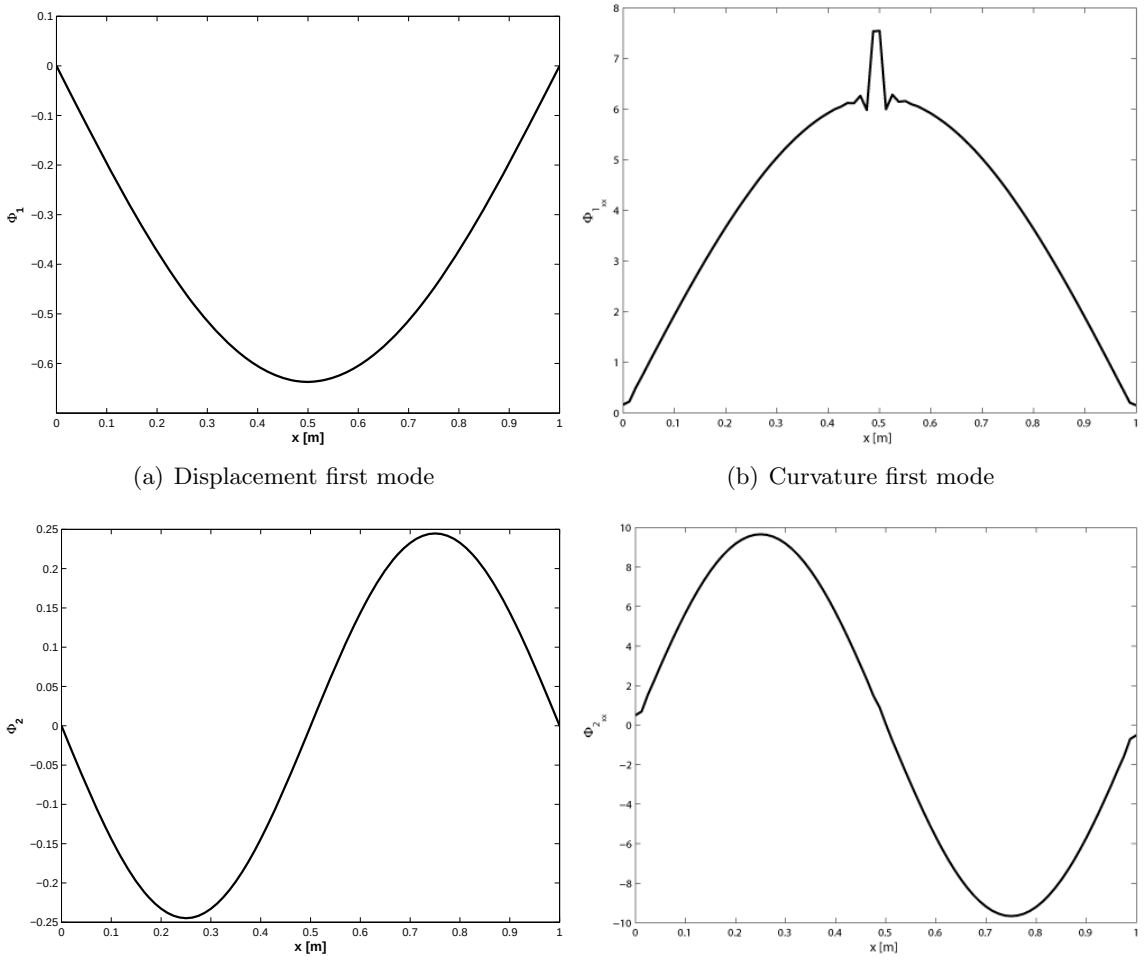

(a) Displacement first mode

(b) Curvature first mode

(c) Displacement second mode

(d) Curvature second mode

Figure 4: Effect of damage @ 50% length on displacement and curvature amplitudes ($h/h_0 = 0.9$)

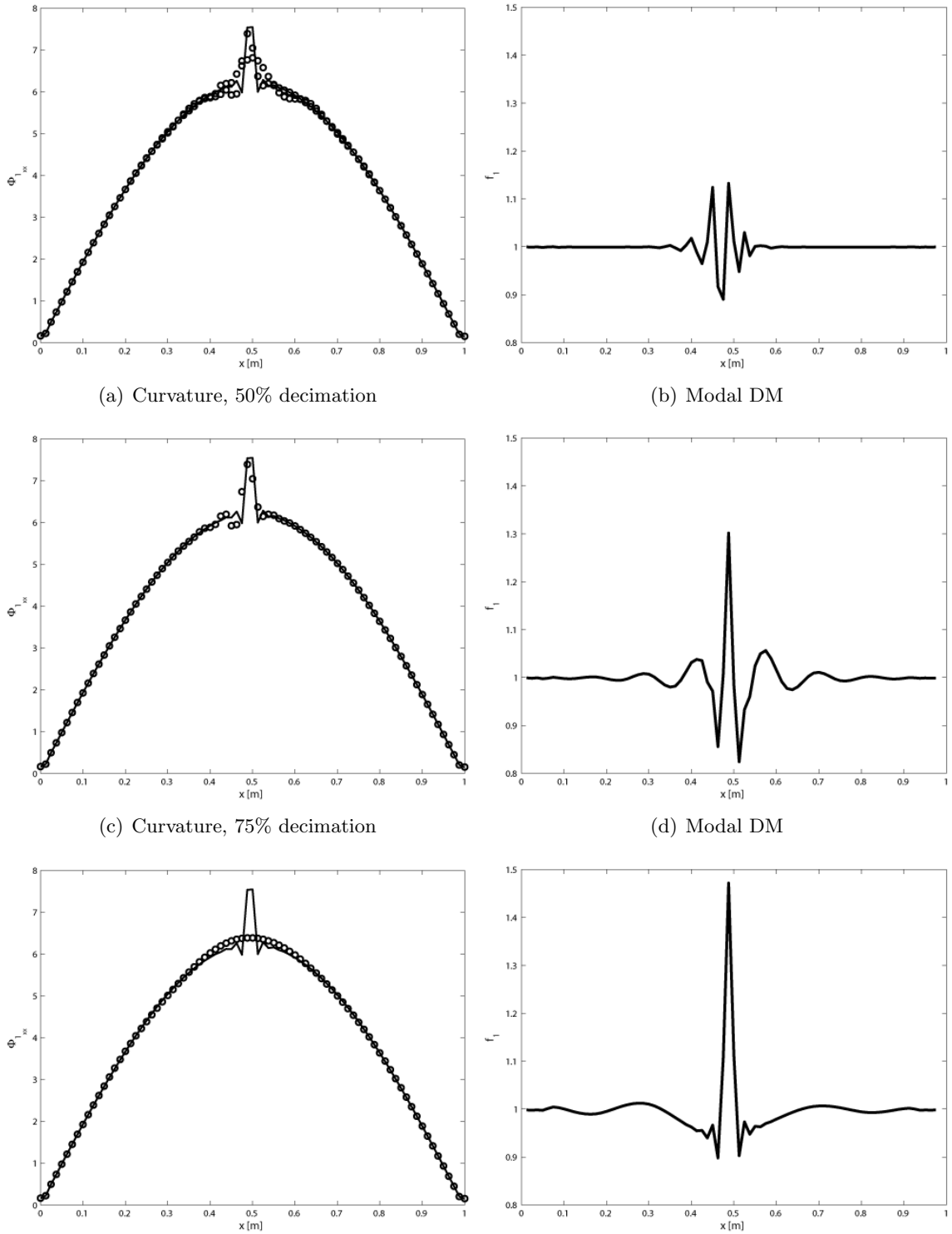

(a) Curvature, 50% decimation

(b) Modal DM

(c) Curvature, 75% decimation

(d) Modal DM

(e) Curvature, 90% decimation

(f) Modal SER

Figure 5: Influence of order of decimation on modal curvature and Damage Measure estimation (first mode)

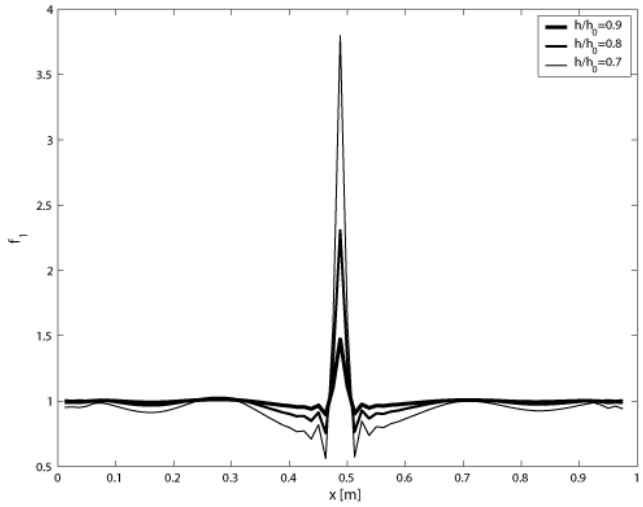

(a) Damage @50% length, first mode

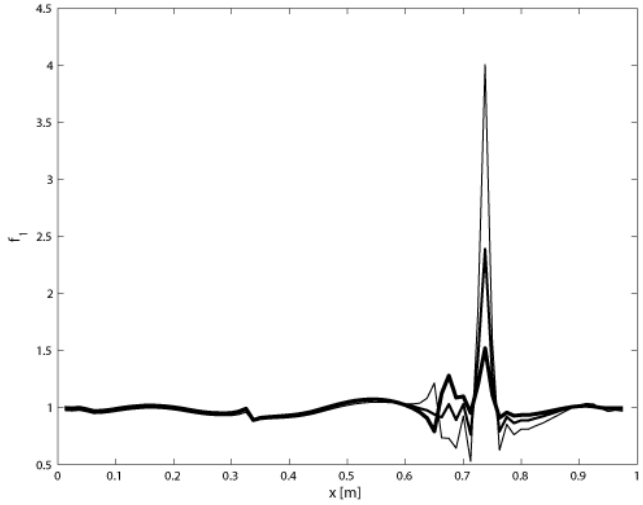

(b) Damage @75% length, first mode

Figure 6: Influence of damage extent on modal DM

4.2.2 Plate analysis

Additional numerical evaluations of the effectiveness of DM are on a plate structure. A finite element model is formulated according to Kirchhoff Plate Theory (KPT) to predict the dynamic behavior of a thin steel plate ($E = 2.1 \times 10^{11}$ MPa, $\rho = 7800$ kg/m^3, $\nu = 0.3$). The plate, which is square and measures 60 cm per side, is discretized using a 40×40 element grid, and it is simply supported on all sides. Damage is simulated again as a thickness reduction over a single element of the considered mesh. The curvatures corresponding to the harmonic excitation of the plate at its natural frequencies are obtained for a concentrated vertical load applied at coordinates $x_l = y_l = 0.16$ m from the lower left corner of the plate. Examples of curvatures for excitation at mode $1, 2$ are shown in Figures. 8, 9. The considered damage corresponds to $h/h_0 = 0.9$ and it is located at coordinates $0.27 \leq x_D \leq 0.32$ m, $0.27 \leq y_D \leq 0.32$ m, which is the location of the element near the plate center. Figures. 8, 9 demonstrate the sensitivity of the curvature mode with respect to damage as opposed to the operational deflection shape, and again indicates how modes with maximum curvature near the damage location are mostly affected. The generation of baseline data through decimation of the available nodal information is also evaluated on simulated plate data. The results of these investigations are shown in Figure 10 which show the influence of the decimation parameter on the first modal DM evaluation. The same damaged configuration is again selected, and the decimation parameter now indicates the reduction of the nodal information along each side of the plate. The curvature plots shown in Figure. 10.a,c,e are obtained by taking a cross section of the curvature surfaces at $y = 0.3$ m. The DM distributions are now represented as contour maps, where the white background corresponds to unit values, and the iso-level colors vary from black, corresponding to values of $f \cong 1.01$, to white again for $f \geq 2$. The DM contours confirm the results obtained from the plate analysis, which indicate how the decimation parameter can be selected to improve the damage sensitivity of the technique. Finally, examples of cumulative DM distribution for various damage locations are shown in Figure 11. The plots, obtained from the superposition of the first 10 modal contributions, indicate the effectiveness of the cumulative DM in identifying the correct location of single or multiple damaged elements.

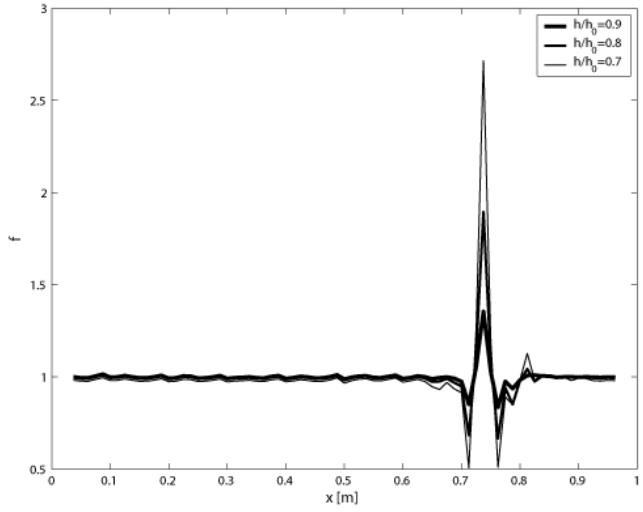

(a) Damage @75% length

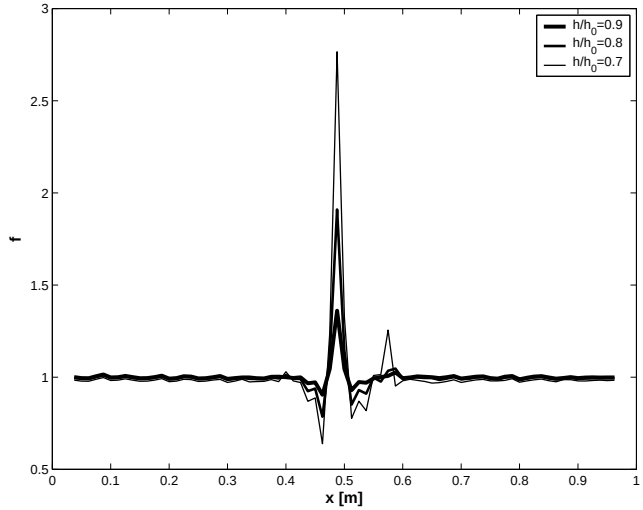

(b) Damage @50% length

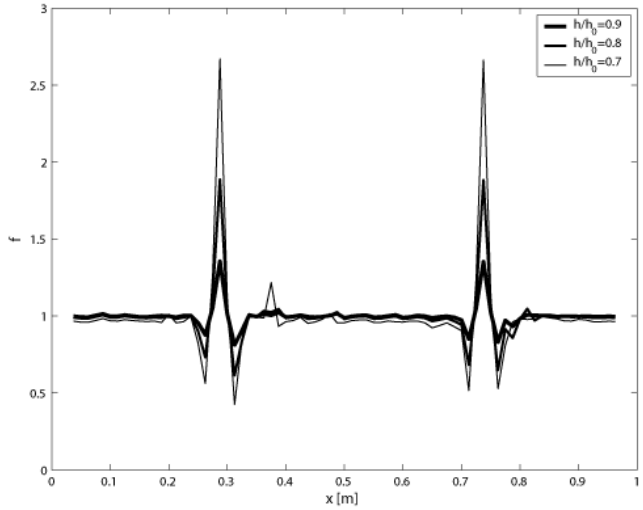

(c) Damage @75 & 30% length

Figure 7: Cumulative DM for different damaged configurations

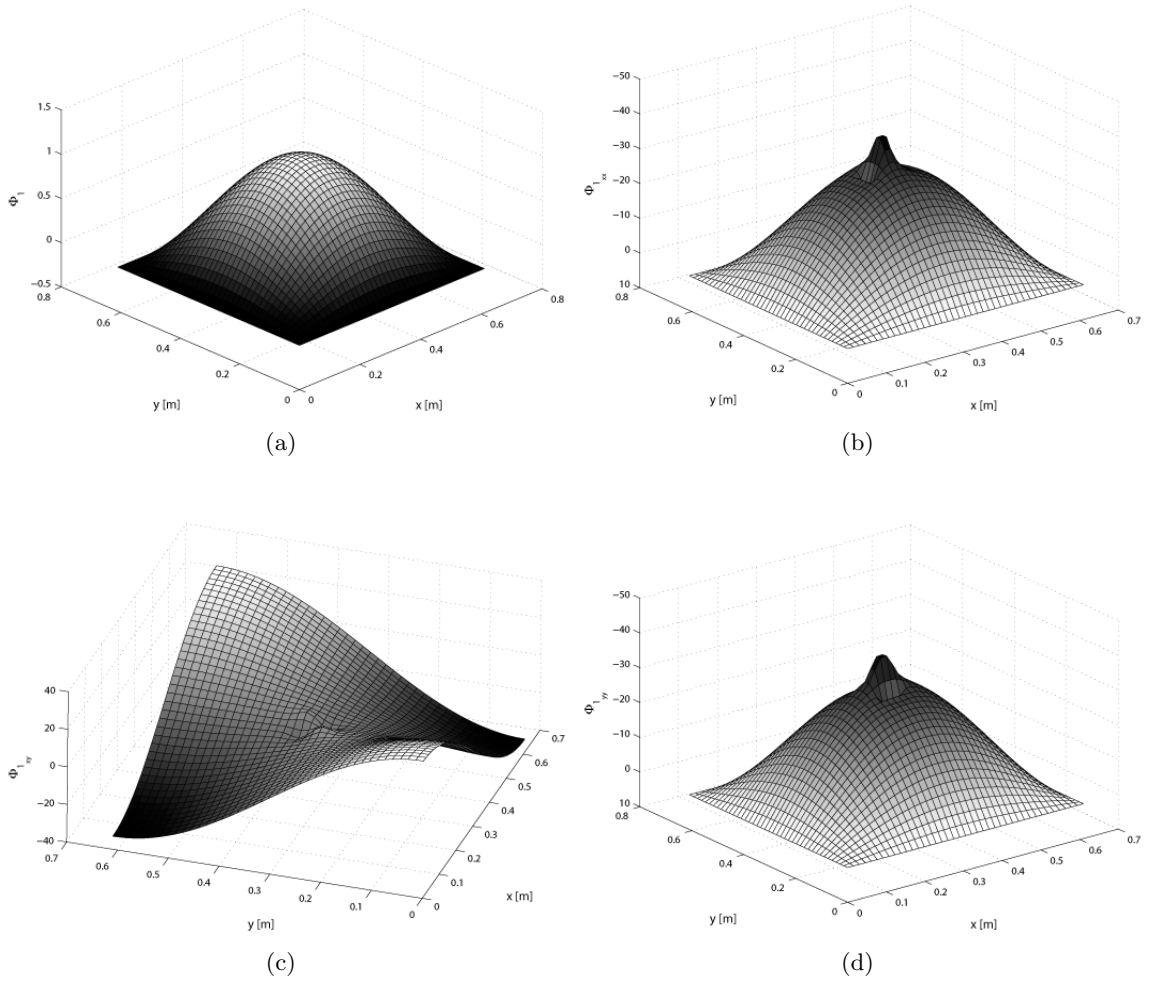

Figure 8: First mode operational deflection shape and curvatures for plate with damage near center ($h/h_0 = 0.9$)

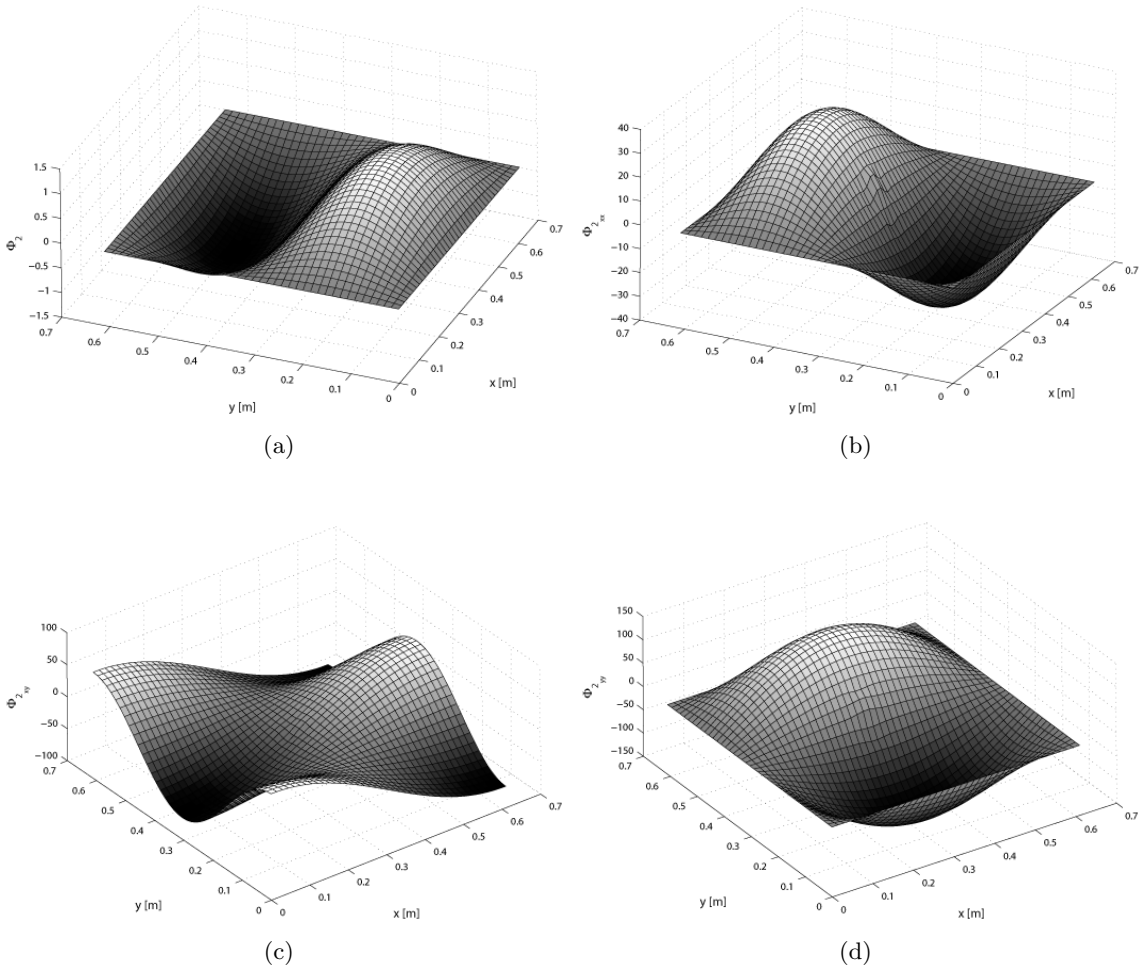

Figure 9: Second mode operational deflection shape and curvatures for plate with damage near center ($h/h_0 = 0.9$)

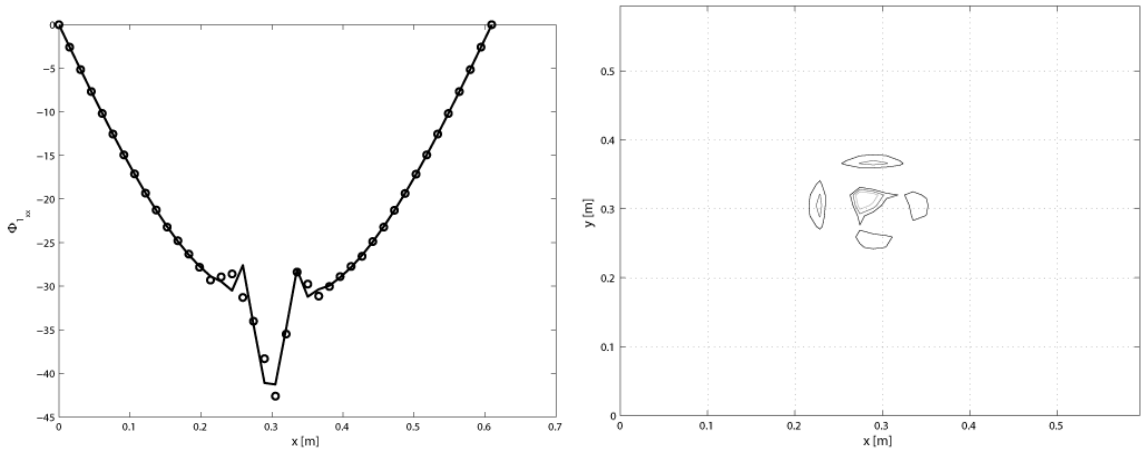

(a) $d = 50\%$, Curvature (b) $d = 50\%$, Modal DM

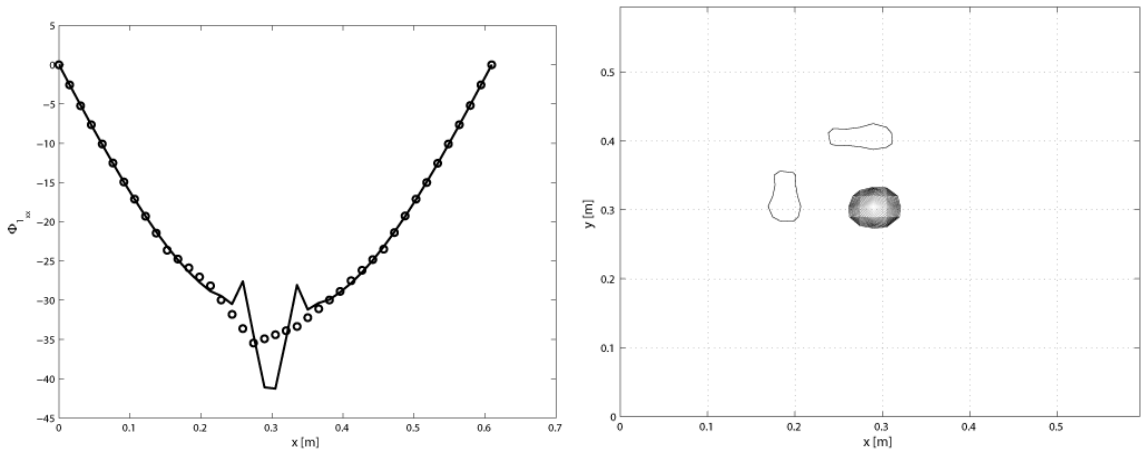

(c) $d = 75\%$, Curvature (d) $d = 75\%$, Modal DM

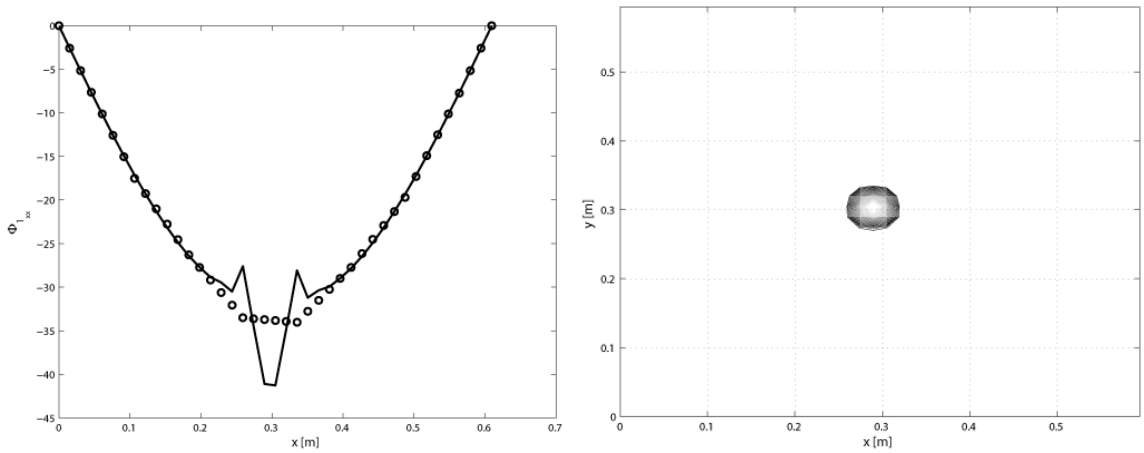

(e) $d = 80\%$, Curvature (f) $d = 80\%$, Modal DM

Figure 10: Influence of order of decimation on first modal curvature and Damage Measure for plate ($h/h_0 = 0.9$)

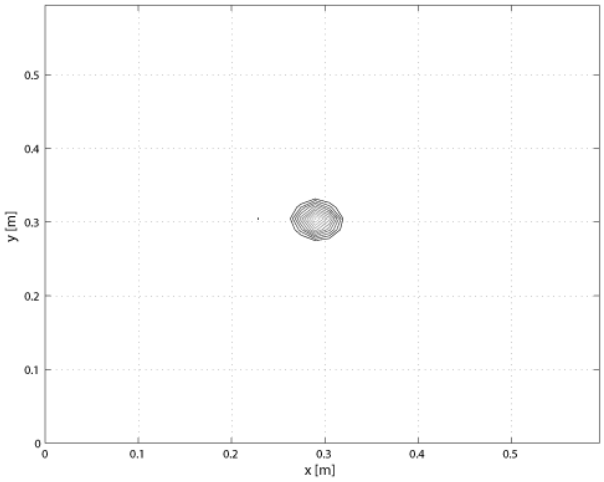

(a) $0.27 \leq x_D \leq 0.32$ m, $0.27 \leq y_D \leq 0.32$ m

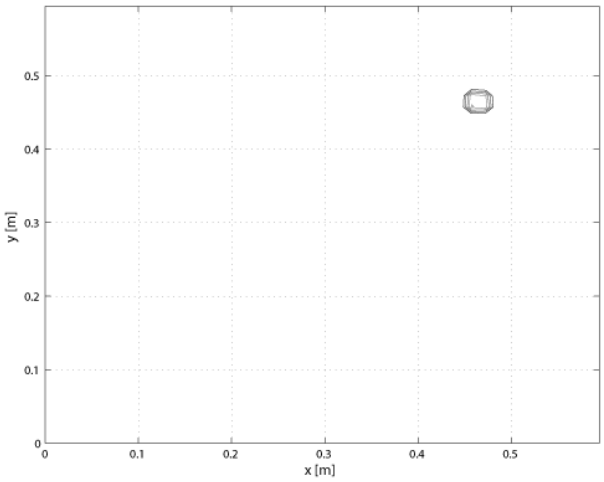

(b) $0.43 \leq x_D \leq 0.46$ m, $0.43 \leq y_D \leq 0.46$ m

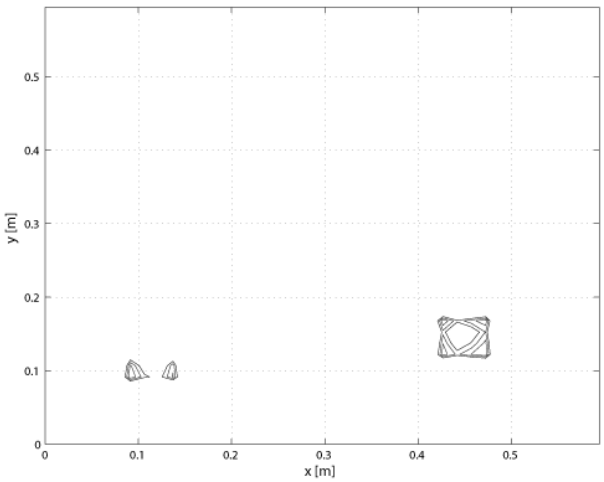

(c) $0.09 \leq x_D \leq 0.15$ m, $0.09 \leq y_D \leq 0.14$ m, $0.43 \leq x_D \leq 0.49$ m, $0.12 \leq y_D \leq 0.18$ m

Figure 11: Plate Cumulative DM for damage $h/h_0 = 0.9$ at various locations

4.3 Experimental results

4.3.1 Beam tests

The theories presented in the sections are now validated experimentally on beam and plate structures. The theories that are developed to formulate DM are for linear and isotropic elastic beam analysis using Euler-Bernoulli theory and for linear and isotropic elastic plate with Kirchhoff theory. The formulations are valid for all plates that are linear, isotropic and of elastic material. The beam analysis is tested on anisotropic fiberglass structure to estimate the limits of the analysis. A simple fiberglass beam was first selected as a stepping stone for application to two-dimensional plate specimens.

4.3.1.1 Beam Configuration and experimental set-up

The beams used in the tests are 1.5" wide and are cut from a plate fabricated with 12 layers of woven cloth with 0 and 90 degrees fiber orientation. The matrix is a polyester resin type. The fiberglass beam used in the tests is shown in Figure 12.a. A cantilevered configuration is chosen for convenience. The beam is excited by an electrodynamic shaker (Ling, Model 102A) shown in the figure, and its response velocity is measured using a SLDV (Polytec PI, Model PSV400M2). Damage is inflicted by cutting rectangular grooves using a hand saw. The measurement grid and the damaged configuration with both cuts are shown in Figure 12.b and Figure 12.c. The first considered cut (♯1) is applied normally to the length of the beam. A second cut ♯2 is inclined with respect to the beam axis to ensure that the effectiveness of the technique is not affected by a particular orientation of the damage. The depth of each cut is kept at approximately 0.050", with tolerance requirements which are not strict, as the objective at this time is to simply detect the presence of the damage in the test specimen. The vibration tests are conducted using pseudo-random excitation over the $0 - 1000$ Hz frequency range. The shaker is driven by the internal function generator available on SLDV. The recorded data are exported and post-processed in MATLAB.

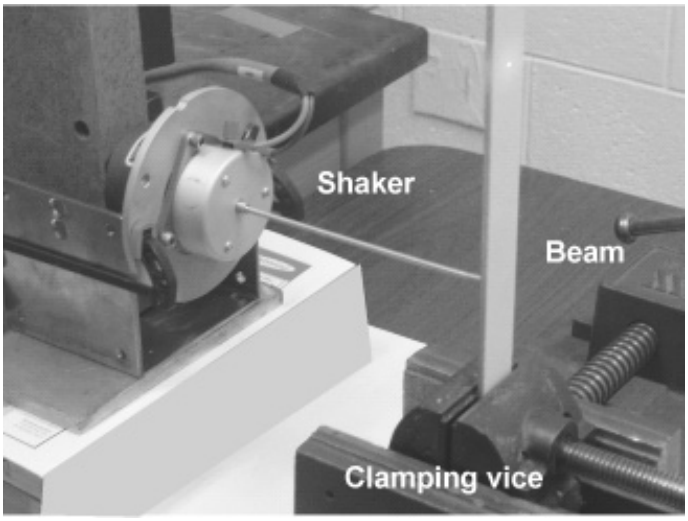

(a) Experimental set-up

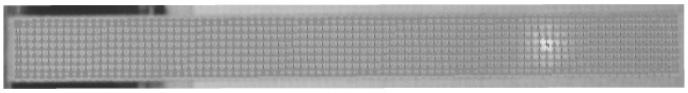

(b) Measurement grid

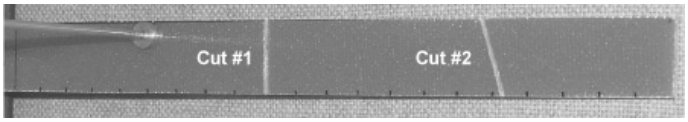

(c) Damaged beam

Figure 12: Experimental set-up and configuration of damaged composite Beam

4.3.1.2 Curvature and DM

The deflections measured along the beam center line are first considered, in order to perform an initial one-dimensional analysis. The measured mode shapes at various resonant frequencies are extracted and then interpolated using splines. The analytical differentiations of the splines functions is used to estimate the beam curvature at the various frequencies. Curvatures and higher derivatives are then evaluated through spline interpolation of the experimental data, according to the procedures described previously.

It is noted that all mode shapes do not show sensitivity to the damages in the test specimen considered here. The mode shape at 657 Hz, shown in Figure 13, is found to respond the most to the damages. The results of the decimation studies are shown in Figure 14 where curvature and Strain Energy Ratio information are compared for 50, 75, and 80 percent decimation. The decimation parameter selection is critical to the formation of the DM. A low decimation parameter does not provide any identification of the damage using curvature data and provides a marginal indication using the DM information. This is similar to what is observed using the analytical simulation data due to the fact that a low decimation parameter does not provide an adequate baseline information. A decimation parameter of 80 percent provided identification of the location correctly for both damages in the beam.

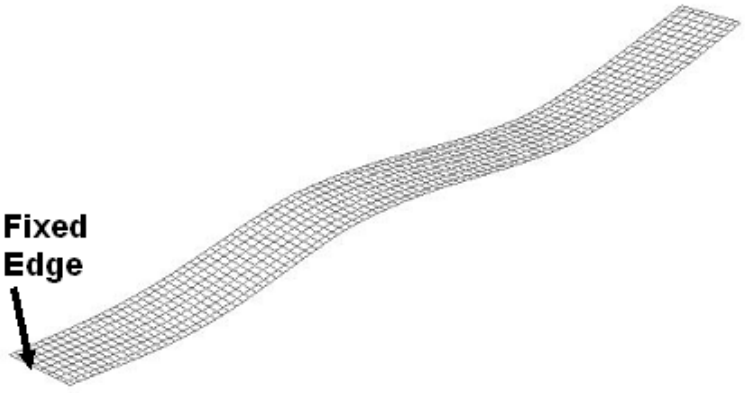

Figure 13: Deflection Shape at 657 Hz Used in Curvature and Strain Energy for decimation study Ratio Estimation

The results of DM formulation for the composite beam are presented in Figure 15. The DM contours are evaluated by superimposing the contribution of the 5 modes of the beam which contribute to the response in the 0-1000 Hz frequency range. Both damages are correctly identified in terms of their location as well as orientation. The advantage of this latter approach is that no expert intervention is required for the selection of the mode to be analyzed, which may facilitate the process of automating the technique. Success of vibration modes analysis to identify damages on a beam specimen provided a strong base to build upon for the next set of experiments on a 2-D plate problem.

4.3.2 Plate Tests

The next step of validation of the damage detection methodology using DM included a thin aluminum plate with artificially induced damage. The strain energy ratio formulation was once again successfully utilized to determine the damage location.

4.3.2.1 Plate Configuration and Experimental Set-up

With improvement in the testing techniques, a piezoceramic disc actuator was then successfully used to excite several vibration modes of the plate test specimen. The piezoceramic actuator is also well suited for introducing high frequency elastic waves such as Lamb waves in the test structure. In these tests a common excitation and sensing system is deployed for all types of damage detection. The second test specimen consisted of an aluminum plate with dimensions 14"x14"x0.040" shown in Figure 16. The plate is cantilevered at its base. A piezoceramic disc of 1.1" diameter and 0.030" thickness is used as an exciter. Placement of the actuator is selected to excite the highest number of modes including symmetric as well as anti-symmetric modes of the structure. The damage is introduced in the form of a 1.4" long and 0.015" deep groove. Plate, with actuator and damage location is shown in Figure 16.

4.3.2.2 Damage Measure

The plate was excited in the 0-500 Hz range using pseudo-random excitation. The scan grid pattern is shown using dots in Figure 17. The mode that contributed the most to the DM

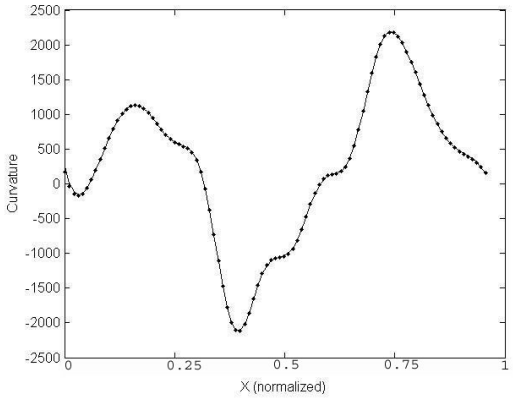

(a) $d = 50\%$, Curvature

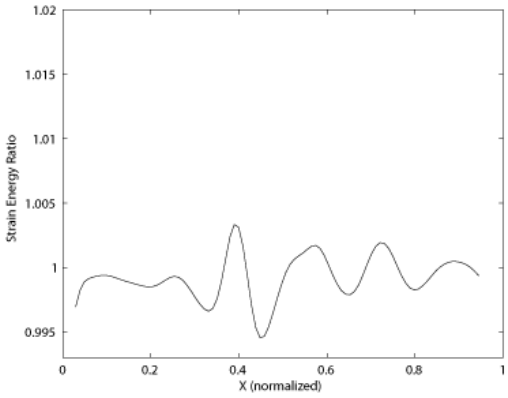

(b) $d = 50\%$, Modal DM

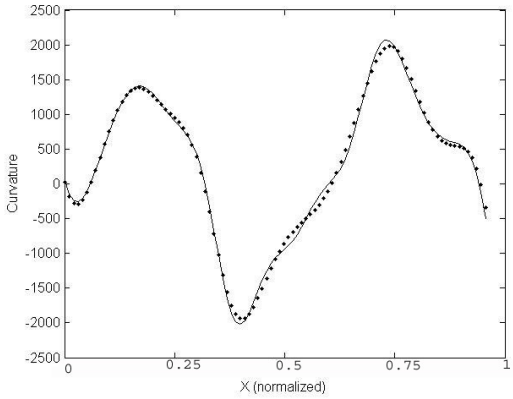

(c) $d = 75\%$, Curvature

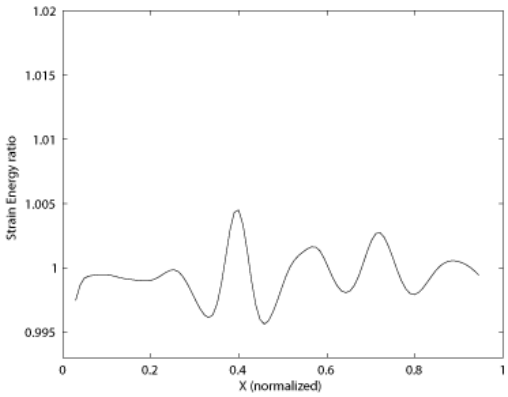

(d) $d = 75\%$, Modal DM

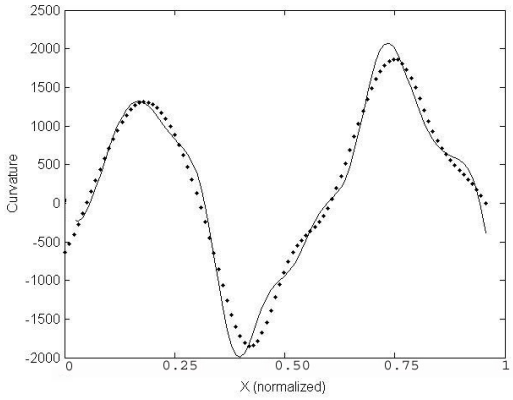

(e) $d = 80\%$, Curvature

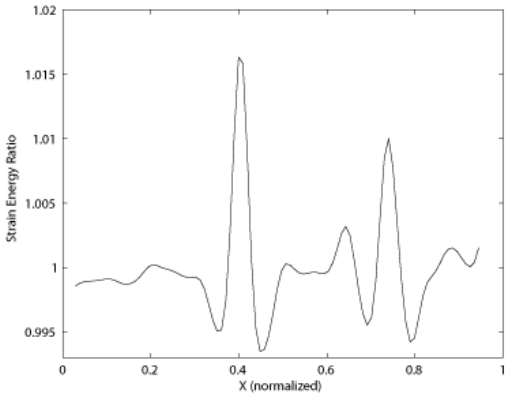

(f) $d = 80\%$, Modal DM

Figure 14: Influence of order of decimation on the 657Hz ODS curvature and DM for composite beam specimen with two damages

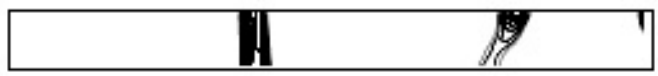

Figure 15: Cumulative Strain Energy Ratio estimation using first five modes of composite beam test specimen with two damages

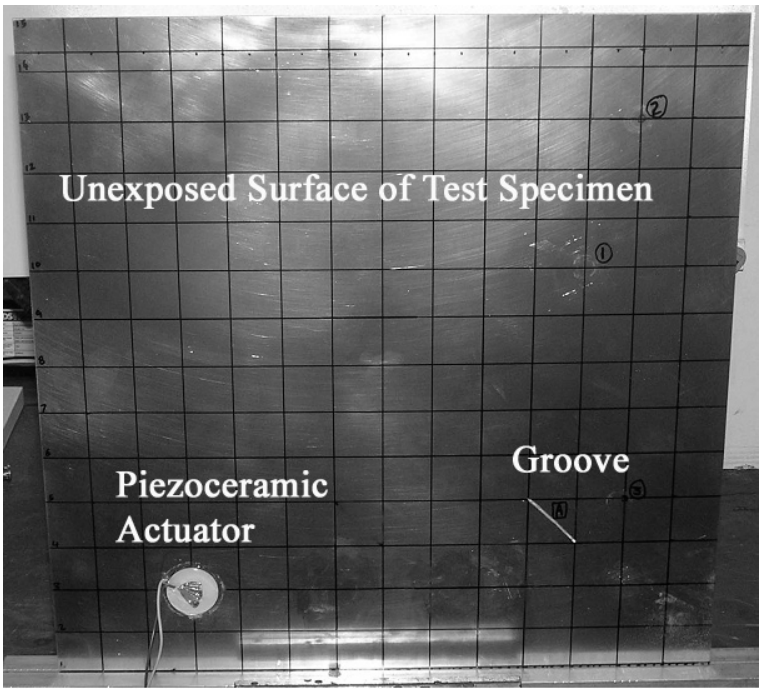

Figure 16: Aluminum Plate (14"x14"x0.040") with Damage and Piezoceramic Exciter

is shown in Figure 18. The DM contour plots of Figure 17 clearly show the location of the damage as well as the excitation point. It is noted that the strain energy ratio analysis is entirely based on an innovation, whereby the baseline DM distribution is synthesized from the test data of the damaged structure through decimation of the data according to the procedure presented earlier in this report. This innovation supports a significant goal of cost effective health monitoring concept by reducing the amount of necessary testing.

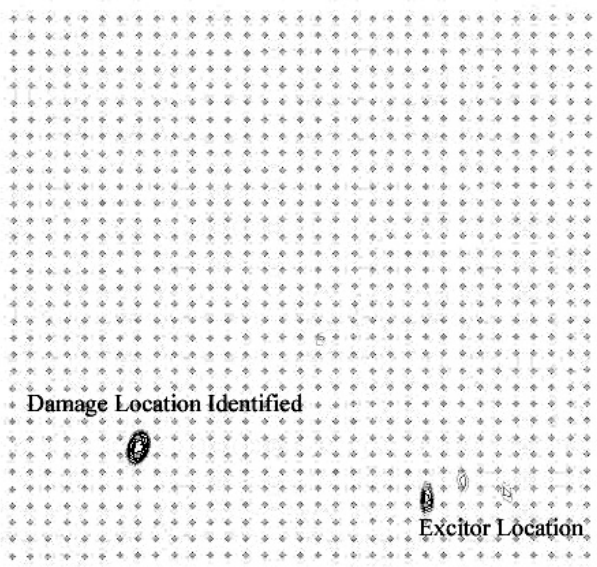

Figure 17: Damage identification using Strain Energy Ratio based detection technique on 294 Hz operational deflection shape

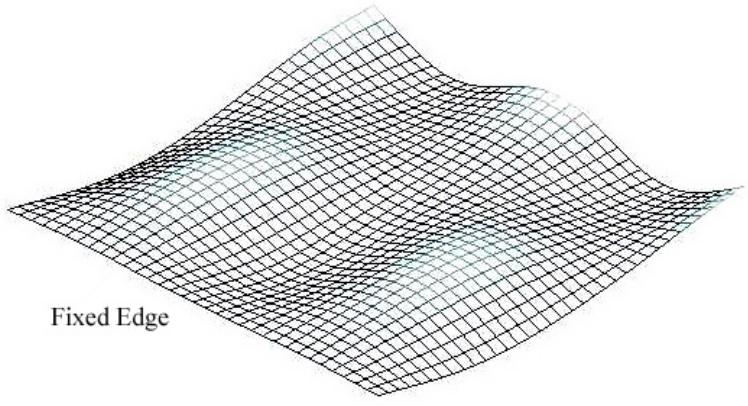

Figure 18: Plate 294 Hz operational deflection shape used in damage detection

4.4 Frequency-Wavenumber Filter for Damage Measure

A new wave propagation-based Damage Measure is presented here, which relies on the evaluation of the strain energy distribution associated with propagating waves. The presence of localized damages typically distorts the wavefield by causing reflections and diffractions. The evaluation of such distortions, in reference to the wavefield corresponding to the undamaged structure, are used as an indicator that locates, quantifies and classifies the damage. The Damage Measure formulation is based on the estimation of the distribution of strain energy associated with propagating and reflected waves. Considering a 1-D linear elastic rod with only axial motion as shown in Figure 19. This rod is of length L, height h and width b. A notch of length Δl and depth h_d is placed at the distance x_d.

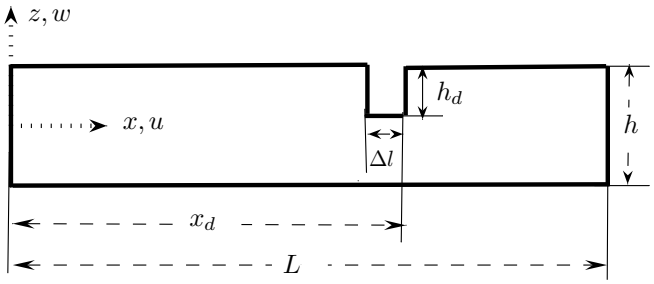

Figure 19: Axial Rod geometry.

The lateral area of the undamaged rod is $A_0 = bh$ whereas the lateral area of the damaged rod is calculated as:

$$\begin{aligned} A(x) &= A_0 \left\{ 1 - \frac{h_d}{h} \left[\mathbf{H}\left(x - (x_d - \Delta l)\right) - \ \mathbf{H}\ \left(x - x_d\right) \right] \right\} \\ &= A_0 \left\{ 1 - \varepsilon \gamma_d(x) \right\} \end{aligned} \tag{16}$$

where $\mathbf{H}$ is the Heaviside step function and $\varepsilon = \frac{h_d}{h}$. If the notch can be approximated with a point defect (which means that value of Δl is very small) then the expression for the damage function, $\gamma_d(x)$ is:

$$\gamma_d(x) = \Delta l \delta(x - x_d) \tag{17}$$

where $\delta\left(x\right)$ is the Dirac-delta function.

Next, the axial displacement of the rod is considered as a perturbation, over the small parameter ε, of the axial displacement of the undamaged rod:

$$u(x,t) = u^{(0)}(x,t) - \varepsilon u^{(1)}(x,t) - \varepsilon^2 u^{(2)}(x,t) - O(\varepsilon^3) \tag{18}$$

The first derivative of the displacement after truncation of second order terms yields the following:

$$u_{,x}(x,t) = u^{(0)}_{,x}(x,t) - \varepsilon u^{(1)}_{,x}(x,t) \tag{19}$$

This rod is divided in to N segments, over which the strain energy is evaluated through the integration of strain energy density over each segment length. At a given instant of time t, the strain energy over segment p, defined by $x \in [x_p, x_{p+1}]$, is obtained by summing contributions from axial deformation:

$$\Delta U_p(t) = U(x_{p+1},t) - U(x_p,t) = \frac{1}{2}\int_{x_p}^{x_{p+1}} \left[EAu^2_{,x}(x,t) \right] dx \tag{20}$$

Substituting the displacement expansions in terms of ε corresponding to the defect and truncating at the second order yields the following approximated expression for the strain energy of the damaged beam:

$$\Delta U_p(t) \approx \Delta U^{(0)}_p(t) - \varepsilon \Delta U^{(1)}_p(t) - O(\varepsilon^2) \tag{21}$$

where

$$\Delta U^{(0)}_p(t) = \frac{1}{2}\int_{x_p}^{x_{p+1}} \left[EAu^{(0)2}_{,x}(x,t)] \right] dx \tag{22}$$

corresponds to the strain energy of the undamaged beam, and where

$$\Delta U^{(1)}_p(t) = \int_{x_p}^{x_{p+1}} \left[EAu^{(0)}_{,x}(x,t) u^{(1)}_{,x}(x,t) \right] dx \tag{23}$$

is the contribution due to damage. Upon calculation of the integrals over each segment. To obtain smooth, continuous results, the segments' strain energies ΔU_p's are interpolated through a set of spline functions. Accordingly, the corresponding strain energy perturbation $\Delta U^{(1)}_p(x,t)$ originates at the damage location, where it reaches its maximum value, to progressively decrease in value as the secondary wave produced by the damage propagates away from the damage. The Damage Measure is thus defined as a ratio between the strain

energies associated with the 1^{st} order perturbation, and therefore corresponding to that of the damaged beam, to the strain energy of the undamaged beam, i.e.:

$$dm(x,t) = \frac{\Delta U(x,t)}{\Delta U^{(0)}(x,t)} \tag{24}$$

The location of damage along the beam length is identified by a peak of the $dm(x,t)$ function occurring at the damage site.

The above Damage Measure is time-dependent, and it is convenient to consider its cumulative value over a selected time interval:

$$dm_c(x) = \int_t |dm(x,t)|dt \tag{25}$$

to obtain a function depending uniquely on the spatial coordinate.

4.4.1 Filtering Procedure for the Estimation of Undamaged Response

The basic concept behind the filtering technique under consideration is illustrated here for the case of propagating waves in a one-dimensional linear elastic rod. The data are obtained based on a Finite Element model of the rod with axial degrees of freedom. It is assumed that the clamped-free rod is excited at its free end by a modulated harmonic load, which generates a wave. The injected wave interacts with the damage located at $x_d = L/2$, again modeled as a thickness area reduction corresponding to $a_d/a = 0.1$, where it is reflected. This thickness reduction for a constant width rod also corresponds to the cross-sectional area reduction. Figure 20(a) presents snapshots of the rod response at instants of time before, during and after the wave interaction with the notch. After the reflection, the rod's displacement is given by:

$$u(x,t) = u^{(i)}(x,t) + u^{(r)}(x,t) \tag{26}$$

The superscripts i and r denote incident and reflected waves respectively. The two-dimensional (2D) Fast Fourier Transform in space and time of the response is also given by the superposition of contributions from incident and reflected waves:

$$\hat{u}(k,\omega) = \hat{u}^{(i)}(k,\omega) + \hat{u}^{(r)}(k,\omega) \tag{27}$$

Its representation in the frequency/wavenumber domain shown in Figure 20(b) highlights the presence of the main pulse propagating along the $x > 0$ direction, and of the reflected pulse propagating in the opposite direction ($x < 0$). As a result, the two corresponding peaks of the 2D FFT appear centered at $\omega = \omega_0, k = \pm k_0$. In particular, the reflected pulse has lower amplitude, it is characterized by the same frequency, and appears in the $k > 0$ region of the wavenumber/frequency domain. The 2D representation hence effectively separates incident and reflected wave components. This allows the application of simple filtering strategies which remove the reflected wave from the recorder signal, thus providing an approximation of the response of the structure in the absence of the damage. For example, a 2D Hanning window is used to eliminate the reflected wave, and to obtain the frequency/wavenumber spectrum shown in Figure 21(a). Mathematically, the windowing process can be simply expressed as a function product between the wave's 2D Fast Fourier Transform and a 2D window function:

$$\hat{u}^{(i)}(k, \omega) \approx [1 - H(k - k_0, \omega - \omega_0)]\hat{u}(k, \omega) \tag{28}$$

where $H(k - k_0, \omega - \omega_0)$ denotes the windowing function centered at k_0, ω_0. The incident space-time domain signal is then reconstructed through inverse Fourier transformation. The incident signal obtained upon filtering at the same instant considered for Figure 20(a) is shown in Figure 21(b), to demonstrate how the windowing procedure removes the reflected propagating pulse, while leaving the response corresponding to the undamaged beam practically unaltered. The separated incident and the total signals are used for the damage index estimation according to the definition provided above. The result in terms of cumulative Damage Measure for the simple case discussed in this section is plotted in Figure 22.

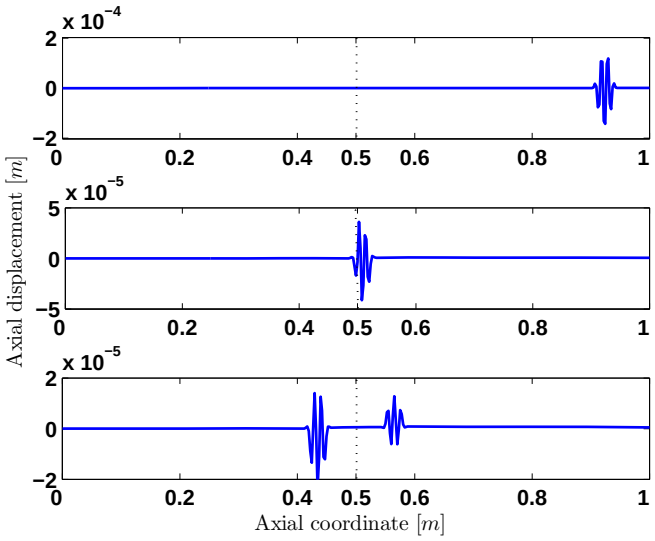

(a)

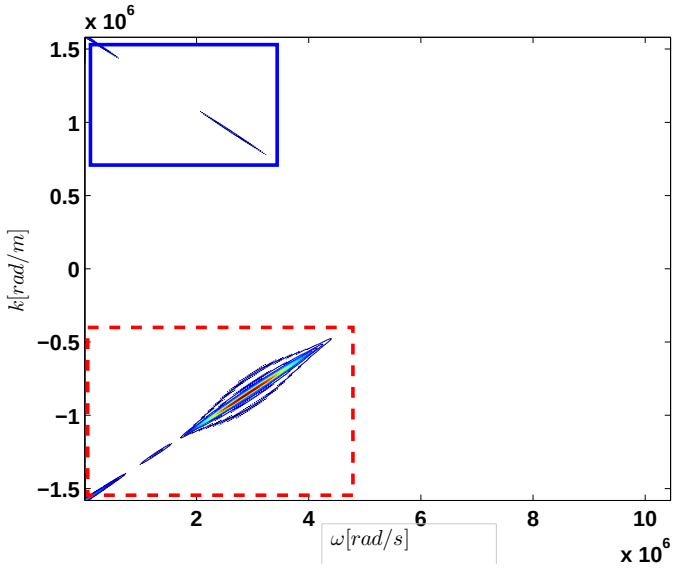

(b)

Figure 20: (a) Snapshots of rod deformed configuration at three instants of time. (b) 2D frequency/wavenumber domain representation (Solid box highlights the reflected component, dashed box highlights the incident component).

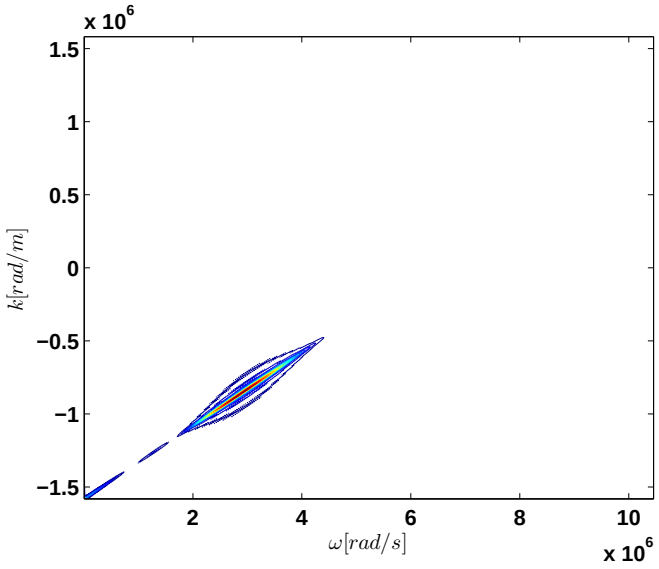

(a)

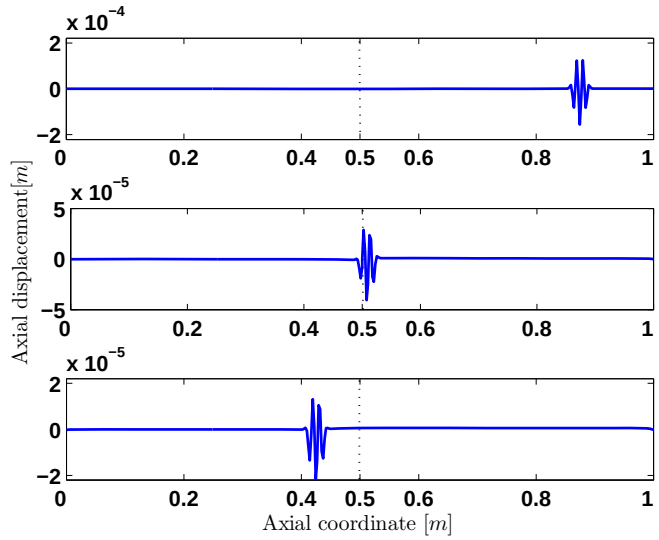

(b)

Figure 21: Representation of filtered (incident) axial displacement (a) in 2D frequency domain, and (b) corresponding deformed configurations at three instants of time.

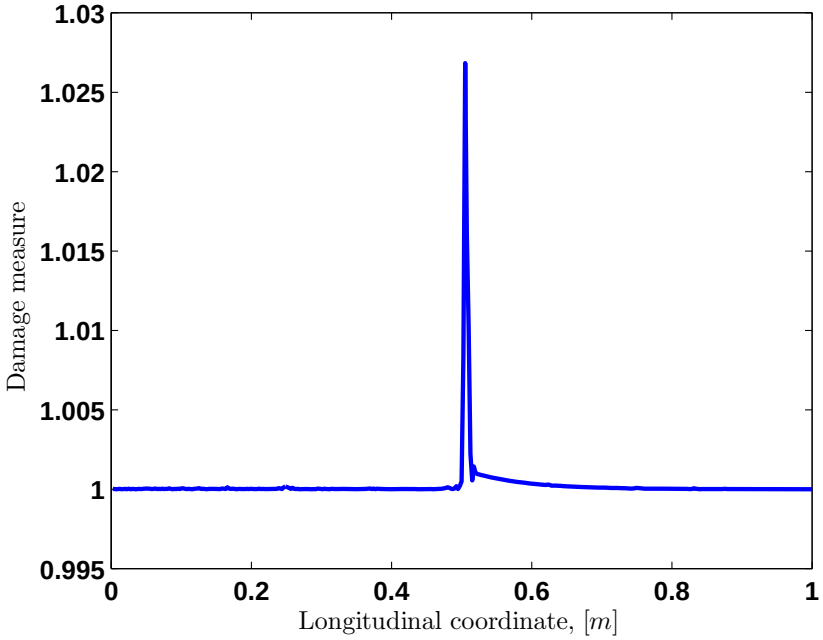

Figure 22: Damage Measure in a rod.

Chapter V

PERTURBATION METHODS FOR THE DYNAMIC RESPONSE OF DAMAGED PLATES AND THEIR APPLICATION TO STRUCTURAL HEALTH MONITORING

The multi-point scanning technology of the SLDV offers the possibility of obtaining detailed velocity information for the structure. Similar amount of information is not available using traditional dynamic sensors such as accelerometers, strain gages or embedded piezoelectric sensor arrays. Measurement of the dynamic response in a refined set of grid points on the structure offers the possibility of accurately estimating deflection derivatives of various orders, which in turn allow the estimation of curvatures and strain energy density. These quantities are significantly more sensitive to damage as opposed to the deflection shapes or the natural frequencies of the structure. The theoretical background in support of the developed vibrations-based damage detection techniques is presented below.

5.1 Perturbation Methods to Analyze Damage in Plates

The analytical evaluation of changes in the curvature of dynamic deflection shapes as a tool for damage detection and location has originally been introduced by Luo and Hanagud [22] where they developed a differential equation. The solution to the differential equation yielded the location and the magnitude of the damages. This was later adapted to a single-mode by Lestari and Hanagud [44]. In their studies theoretical and experimental investigations were performed on simple beam structures. The presented results show the potentials of the technique when applied to the modes of the beam. The limitation to a single mode was mainly dictated by the limited spatial resolution available in the accelerometers-based experiments. Here, the technique is extended to higher order modes which can be

easily and accurately measured using the SLDV. In addition the analysis is extended to plate structures thus increasing the practical relevance of the concept. The perturbation analysis of the effect of notch type damage on curvature modes and natural frequencies of a plate is presented below.

5.2 Dynamics of Damaged Plates

The dynamic behavior of damaged plates without any axial or lateral loads is described by the following equation that is applicable to thin elastic plates of variable thickness using Kirchhoff plate theory [45]:

$$\nabla^2\big(D\nabla^2 w\big) - (1-\nu)\big(\frac{\partial^2 D}{\partial y^2}\frac{\partial^2 w}{\partial x^2} - 2\frac{\partial^2 D}{\partial y \partial x}\frac{\partial^2 w}{\partial y \partial x} + \frac{\partial^2 D}{\partial x^2}\frac{\partial^2 w}{\partial y^2}\big) + m\frac{\partial^2 w}{\partial t^2} = 0 \qquad (29)$$

In this equation, $w = w(x, y)$ is the out-of-plane displacement of the plate in the z-direction, $h = h(x, y)$ is the plate thickness, $D = D(x, y) = Eh^3/12(1-\nu^2)$ is the plate rigidity, and $m = m(x, y) = \rho h(x, y)$ is the mass per unit area of the plate. The quantities E, ρ and ν are the Young's modulus, the density and the Poisson's ratio of the plate material.

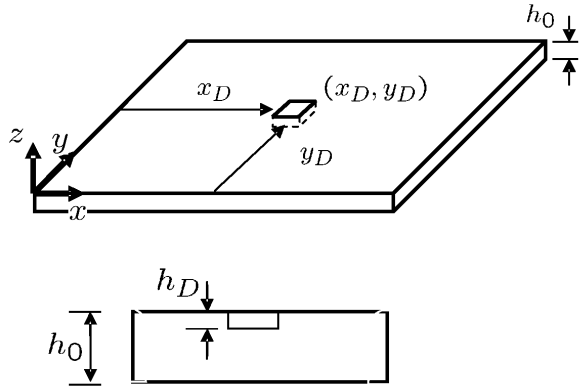

Figure 23: Schematic of plate with notch damage

5.2.1 Modeling of notch and line defects

The defects are described as localized reductions in the plate thickness, notch-type of damage, and line defects along the x and y directions are presented schematically in Figures 23

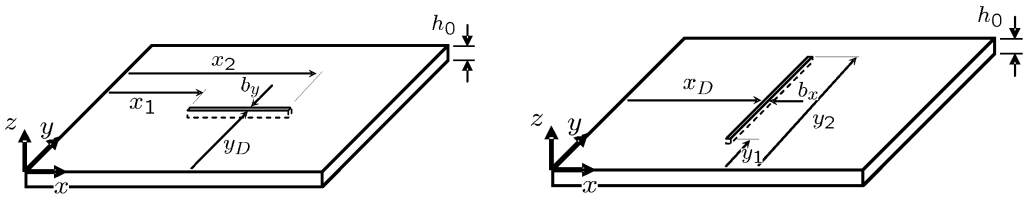

(a) Line defect along x-axis

(b) Line defect along y-axis

Figure 24: Schematic of plates with considered line defects

and 24.

Damage is described by expressing the plate thickness at the defect location as:

$$h_d = h_0 - h_D \tag{30}$$

where h_0 is the thickness of the undamaged plate and h_D is the thickness of the plate at the damage location. Accordingly, the plate rigidity at the defect site is expressed as:

$$\begin{aligned} D_d &= \frac{E h_d^3}{12(1-\nu^2)} \\ &= D_0\Big(1 - \frac{h_D}{h_0}\Big)^3 \end{aligned} \tag{31}$$

$$D_0 = E h_0^3 / 12(1-\nu^2) \tag{32}$$

where D_0 is the rigidity of the undamaged plate. For a relatively small damage, i.e. for $h_D << h_0$, Equation (31) is approximated as:

$$D_d \simeq D_0\Big(1 - 3\frac{h_D}{h_0}\Big) = D_0(1-\epsilon) \tag{33}$$

$$\epsilon = 3h_D/h_0 \tag{34}$$

The perturbation parameter ϵ is defined by Equation (34). Similarly, the mass per unit area of the plate at the defect site is expressed as:

$$m_d = m_0\Big(1 - \frac{h_D}{h_0}\Big) = m_0\Big(1 - \frac{1}{3}\epsilon\Big) \tag{35}$$

where $m_0 = \rho h_0$ is the mass per unit area of the undamaged plate.

The plate rigidity $D(x, y)$ is be described as:

$$D(x, y) = D_0[1 - \epsilon(H(x - x_1) - H(x - x_2))(H(y - y_1) - H(y - y_2))] \tag{36}$$

where x_1, x_2 and y_1, y_2 define the dimensions of the defect in the x, y directions, and H is the Heaviside step function. Equation (36) is conveniently manipulated to describe both notch-type defects, as well as line defects as shown in Figure 24. Equation 36 is now rewritten as:

$$D(x, y) = D_0\Big[1 - \epsilon A_D \frac{(H(x - x_1) - H(x - x_2))}{\Delta l_x} \frac{(H(y - y_1) - H(y - y_2))}{\Delta l_y}\Big] \tag{37}$$

where $b_x = x_2 - x_1$, $b_y = y_2 - y_1$, and $A_D = b_x * b_y$. For a notch defect at x_D, y_D (see figure 23), it is assumed that

$$x_1 \approx x_2 \approx x_D, \;\; y_1 \approx y_2 \approx y_D \tag{38}$$

and Equation (36) becomes:

$$D(x, y) = D_0[1 - \epsilon A_D \delta(x - x_D)\delta(y - y_D)] \tag{39}$$

where

$$\delta(x) = \frac{dH(x)}{dx} \tag{40}$$

is the Dirac delta function. Similar expressions is defined to characterize a line defect. For example, a line defect at location $y = y_D$ and parallel to the x direction (Figure 24.a) is described as:

$$D(x, y) = D_0\Big[1 - \epsilon b_y \delta(y - y_D) \int_{x_1}^{x_2} \delta(x - \xi) d\xi\Big] \tag{41}$$

while a defect at $x = x_D$ along the y direction (Figure 24.b) is expressed as:

$$D(x,y) = D_0\Big[1 - \epsilon b_x \delta(x - x_D) \int_{y_1}^{y_2} \delta(y - \eta) d\eta\Big] \tag{42}$$

where x_1, x_2 and y_1, y_2 define the length of the defect, while ξ, η are dummy integration variables. It is worth observing how in Equations (41,42) the heaviside function is replaced by the integral of the delta function over the extension of the defect. This substitution is to take advantage of properties of the delta function which are very convenient for the the analytical derivations which follow.

A general description of line and notch defects of the kind considered in this thesis are obtained by expressing the plate bending rigidity as:

$$D(x,y) = D_0[1 - \epsilon \gamma_D(x,y)] \tag{43}$$

where $\gamma_D(x,y)$ denotes the function describing the damage configuration in Equations (39, 41, 42). Similarly, the mass per unit area of the damaged plate is described as:

$$m(x,y) = m_0\Big(1 - \frac{h_d}{h_0}\Big) = m_0\Big[1 - \frac{1}{3}\epsilon \gamma_D(x,y)\Big] \tag{44}$$

The expressions for the plate rigidity and mass given in Equations (43, 44) are substituted into Equation (29) to obtain a solution predicting the dynamic behavior of plates with the considered types of damage.

5.2.2 Perturbation solution

A solution for equation Equation (29) is obtained through modal superposition by imposing a solution of the kind:

$$w(x,y) = \sum_{m,n} \phi_{m,n}(x,y) e^{\mathrm{i}\omega_{m,n} t} \tag{45}$$

where $\phi_{m,n}$, $\omega_{m,n}$ are the mode shape and the natural frequency (eigensolutions) of the plate, corresponding to indices m and n while $\mathrm{i} = sqrt(-1)$ is unit. Considering for simplicity the contributions of a single mode m, n and Equations (45) and (29) yields:

$$\nabla^2\big(D\nabla^2\phi\big) - (1-\nu)\big(\frac{\partial^2 D}{\partial y^2}\frac{\partial^2\phi}{\partial x^2} - 2\frac{\partial^2 D}{\partial y\partial x}\frac{\partial^2\phi}{\partial y\partial x} + \frac{\partial^2 D}{\partial x^2}\frac{\partial^2\phi}{\partial y^2}\big) - m\lambda\phi = 0 \tag{46}$$

where $\lambda = \omega^2$, and the subscripts i, j are omitted for simplicity. In this analysis, ϵ is assumed to be a small parameter corresponding to a small damage of depth h_D. Within this assumption, the eigensolutions for the damaged plate is expressed as perturbations from the solution for the intact plate, so that the eigenfunctions and eigenvalues of the damaged plate are respectively expressed as [22]:

$$\phi(x,y) = \phi^{(0)}(x,y) - \epsilon\phi^{(1)}(x,y) + \mathcal{O}(\epsilon^2) \tag{47}$$

and

$$\lambda = \lambda^{(0)} - \epsilon\lambda^{(1)} + \mathcal{O}(\epsilon^2) \tag{48}$$

where $\phi^{(0)}(x,y), \lambda^{(0)}$ are the eigensolutions for the undamaged plate, while $\phi^{(1)}(x,y), \lambda^{(1)}$ are the first order perturbations. Substituting the perturbed eigensolutions into Equation (46), and collecting the coefficients of same power of ϵ gives a set of equations which are then solved:

ϵ^0**:**

$$\nabla^4\phi^{(0)} - \frac{m_0}{D_0}\lambda^{(0)}\phi^{(0)} = 0 \tag{49}$$

ϵ^1**:**

$$\nabla^4\phi^{(1)} + \nabla^2\big[\gamma_D(\phi^{(1)}_{,xx} + \phi^{(1)}_{,yy})\big] = (1-\nu)\big[\phi^{(0)}_{,xx}\gamma_{D,yy} + \phi^{(0)}_{,yy}\gamma_{D,xx} - 2\phi^{(0)}_{,xy}\gamma_{D,xy}\big] + \frac{m_0}{D_0}(\lambda^{(0)}\phi^{(1)} + \lambda^{(1)}\phi^{(0)} + \frac{1}{3}\lambda^{(0)}\phi^{(0)}\gamma_D) \tag{50}$$

In these equations $\gamma_D = \gamma_D(x,y)$ and $(\cdot)_{,\zeta}$ denote partial derivatives with respect to the variable ζ. The equation (49) represents the equation of motion for an undamaged plate, and its solution provides the undamaged modes $\phi^{(0)}(x,y)$ and eigenvalues $\lambda^{(0)}$, which are then substituted in Equation (50) to obtain a solution in terms of the 1st order perturbation modal parameters $\phi^{(1)}(x,y)$ and $\lambda^{(1)}$.

5.2.3 Solution of perturbation equations using Fourier Series

The mn-th eigenfunction and eigenvalue for a plate simply supported on all edges are respectively given by [45]:

$$\phi^{(0)}_{m,n}(x,y) = \sin\frac{m\pi x}{L_x}\sin\frac{n\pi y}{L_y} \tag{51}$$

and

$$\lambda^{(0)}_{m,n} = \frac{D_0}{m_0}\Big[(\frac{m\pi}{L_x})^2 + (\frac{n\pi}{L_y})^2\Big]^2 \tag{52}$$

where L_x, L_y denote the plate dimensions. An approximate solution for Equation (50) is found by imposing a solution of the kind:

$$\phi^{(1)}_{m,n}(x,y) = \sum_p\sum_q \eta_{p,q}\sin\frac{p\pi x}{L_x}\sin\frac{q\pi y}{L_y} \tag{53}$$

which corresponds to the Fourier series expansion of the perturbed mode. Substituting this expansion in Equation (50) gives:

$$\sum_p\sum_q \Big[\Big((\frac{p\pi}{L_x})^2 + (\frac{q\pi}{L_y})^2\Big)^2 - m_0\lambda_0\Big]\eta_{p,q}\sin\frac{p\pi x}{L_x}\sin\frac{q\pi y}{L_y} =$$
$$-(\phi^{(0)}_{,xx} + \phi^{(0)}_{,yy})\nabla^2\gamma_D + (1-\nu)\big[\phi^{(0)}_{,xx}\gamma_{D,yy} + \phi^{(0)}_{,yy}\gamma_{D,xx} - 2\phi^{(0)}_{,xy}\gamma_{D,xy}\big] + \frac{m_0}{D_0}(\lambda^{(1)} + \frac{1}{3}\lambda^{(0)}\gamma_D)\phi^{(0)} \tag{54}$$

where $\phi^{(0)} = \phi^{(0)}_{m,n}(x,y), \lambda^{(0)} = \lambda^{(0)}_{m,n}$ are respectively defined in Equations (51) and (52). The complexity of Equation (54) is substantially reduced by exploiting the orthogonality properties of harmonic functions. Multiplying Equation (54) by $\sin\frac{r\pi x}{L_x}\sin\frac{s\pi y}{L_y}$ and integrating over the plate surface gives:

$$\Big[((\frac{r\pi}{L_x})^2 + (\frac{s\pi}{L_y})^2)^2 - \big((\frac{m\pi}{L_x})^2 + (\frac{n\pi}{L_y})^2\big)^2\Big]\eta_{r,s}\frac{L_xL_y}{4} = \tag{55}$$
$$-\kappa_1 + (1-\nu)\kappa_2 + \frac{m_0}{D_0}\lambda^{(1)}\delta_{rm}\delta_{sn}\frac{L_xL_y}{4} \tag{56}$$

where

$$\kappa_1 = \int_0^{L_x}\int_0^{L_y}\left(\left[\left(\frac{m\pi}{L_x}\right)^2+\left(\frac{n\pi}{L_y}\right)^2\right]\nabla^2\gamma_D-\frac{1}{3}\frac{m_0}{D_0}\lambda^{(0)}\gamma_D\right)\sin\frac{m\pi x}{L_x}\sin\frac{n\pi y}{L_y}\sin\frac{r\pi x}{L_x}\sin\frac{s\pi y}{L_y}dxdy$$

and

$$\begin{aligned}\kappa_2 &= \int_0^{L_x}\int_0^{L_y}\phi^{(0)}_{,xx}\sin\frac{r\pi x_D}{L_x}\sin\frac{s\pi y_D}{L_y}\gamma_{D,_{yy}}dxdy+\\ &+ \int_0^{L_x}\int_0^{L_y}\phi^{(0)}_{,yy}\sin\frac{r\pi x_D}{L_x}\sin\frac{s\pi y_D}{L_y}\gamma_{D,_{xx}}dxdy+\\ &- 2\int_0^{L_x}\int_0^{L_y}\phi^{(0)}_{,xx}\sin\frac{r\pi x_D}{L_x}\sin\frac{s\pi y_D}{L_y}\gamma_{D,_{xy}}dxdy\end{aligned}$$

Also, in Equation (54), $\delta_{k,l}$ is the Kronecker symbol defined as:

$$\delta_{k,l}=\begin{cases}1 & k=l\\ 0 & k\neq l\end{cases}$$

The summation signs in Equation (54) are eliminated by virtue of the well-known orthogonality property of harmonic functions, which reads:

$$\int_0^{L_x}\int_0^{L_y}\sin\frac{p\pi x}{L_x}\sin\frac{q\pi y}{L_y}\sin\frac{r\pi x}{L_x}\sin\frac{s\pi y}{L_y}dxdy=\frac{L_xL_y}{4}\delta_{r,p}\delta_{s,q}$$

and corresponding versions for cosine functions.

Given the considered modes for the undamaged plate, Equation (55) is solved in terms of the unknowns $\eta_{r,s} and \lambda^{(1)}$, using $r=m$ and $s=n$:

$$\lambda^{(1)}_{m,n}=\frac{4D_0}{m_0L_xL_y}[\kappa_1-(1-\nu)\kappa_2] \tag{57}$$

It is worth observing how the integrations required for the evaluation of the constants κ_1, κ_2 are simplified by taking advantage of the following properties of the delta function [89]:

$$f(x)\delta(x-x_0)=f(x_0)\delta(x) \tag{58}$$

and

$$\int f(x)\frac{\partial^n \delta(x)}{\partial x^n}dx = \int \frac{\partial f(x)}{\partial x}\frac{\partial^{n-1}\delta(x)}{\partial x^{n-1}}dx \tag{59}$$

where $f(x)$ is a generic function. A few simple manipulations yield in fact the following expressions κ_1:

$$\kappa_1 = \frac{4D_0\Delta A_D}{L_xL_y}\Big(\Big[\Big(\frac{m\pi}{L_x}\Big)^2+\Big(\frac{n\pi}{L_y}\Big)^2\Big]-\frac{1}{3}\frac{m_0}{D_0}\lambda^{(0)}\Big)\Big(\sin\frac{n\pi y_D}{L_y}\Big)^2\Big(\sin\frac{m\pi x_D}{L_x}\Big)^2,$$

$$\kappa_1 = \frac{4D_0 b_y}{L_xL_y}\Big(\Big[\Big(\frac{m\pi}{L_x}\Big)^2+\Big(\frac{n\pi}{L_y}\Big)^2\Big]-\frac{1}{3}\frac{m_0}{D_0}\lambda^{(0)}\Big)\Big(\sin\frac{n\pi y_D}{L_y}\Big)^2\int_{x_1}^{x_2}\Big(\sin\frac{m\pi\xi}{L_x}\Big)^2 d\xi,$$

and

$$\kappa_1 = \frac{4D_0 b_x}{L_xL_y}\Big(\Big[\Big(\frac{m\pi}{L_x}\Big)^2+\Big(\frac{n\pi}{L_y}\Big)^2\Big]-\frac{1}{3}\frac{m_0}{D_0}\lambda^{(0)}\Big)\Big(\sin\frac{m\pi x_D}{L_x}\Big)^2\int_{y_1}^{y_2}\Big(\sin\frac{n\pi\eta}{L_y}\Big)^2 d\eta.$$

which respectively define the value of κ_1 for a notch damage and for line defects along the x and y directions. Similar expressions are obtained for the parameter κ_2.

The amplitude of the Fourier series coefficients $\eta_{r,s}$ is obtained by letting $r \neq m$ and $s \neq n$ in Equation (54). Summation of the various terms of the Fourier series expansion gives an approximate expression for the first order perturbation eigenvalues and eigenvectors, according to Equations (47,48).

The results obtained from the formulation presented above are here used to assess the influence of various damage levels, at different locations on the plate surface. Natural frequencies (or eigenvalues), modal deflections, as well as modal curvatures are studied as damage indicators to be used in the development of a modal-based damage detection theory. The modal curvatures are easily computed from the perturbation solution, and they are given by:

$$
\begin{aligned}
\phi_{mn,xx} &= -\big(\frac{m\pi}{L_x}\big)^2 \sin\frac{n\pi x}{L_x}\sin\frac{m\pi x}{L_y} - \sum_r\sum_s \eta_{r,s}\big(\frac{r\pi}{L_x}\big)^2 \sin\frac{r\pi x}{L_x}\sin\frac{s\pi x}{L_y} + \mathcal{O}(\epsilon^2) \\
\phi_{mn,yy} &= -\big(\frac{m\pi}{L_y}\big)^2 \sin\frac{m\pi x}{L_x}\sin\frac{n\pi x}{L_y} - \sum_r\sum_s \eta_{r,s}\big(\frac{s\pi}{L_y}\big)^2 \sin\frac{r\pi x}{L_x}\sin\frac{s\pi x}{L_y} + \mathcal{O}(\epsilon^2), \quad (60) \\
\phi_{mn,xy} &= \big(\frac{mn\pi^2}{L_xL_y}\big)\cos\frac{m\pi x}{L_x}\cos\frac{n\pi x}{L_y} + \sum_r\sum_s \eta_{r,s}\frac{rs\pi^2}{L_xL_y}\cos\frac{r\pi x}{L_x}\cos\frac{s\pi x}{L_y} + \mathcal{O}(\epsilon^2).
\end{aligned}
$$

5.2.4 Strain Energy Ratio for Damage Localization

The curvature modes evaluated in the previous section are utilized directly as damage indicators, and their analytical expressions evaluate the extent of damage. Alternatively, the curvature modes are here used for the evaluation of the strain energy of the damaged plate. The strain energy for a rectangular plate vibrating at mode mn is given by [45]:

$$
U_{mn} = \frac{1}{2}D_0\int_0^{L_x}\int_0^{L_y} \phi_{mn,xx}^2 + \phi_{mn,yy}^2 + 2\nu\phi_{mn,xx}\phi_{mn,yy} - 2(1-\nu)\phi_{mn,xy}^2 dxdy \qquad (61)
$$

The evaluation of the strain energy for undamaged and damaged plate are used as an effective strategy for the identification of damage. Furthermore, the location of the defect is also evaluated through the estimation of the strain energy over limited regions of the plate corresponding to its subdivision into a grid. The strain energy associated to the i, j grid of the plate is expressed as:

$$
U_{m,n}(i,j) = \frac{1}{2}D_0\int_{x_i}^{x_{i+1}}\int_{y_j}^{y_{j+1}} \phi_{mn,xx}^2 + \phi_{mn,yy}^2 + 2\nu\phi_{mn,xx}\phi_{mn,yy} - 2(1-\nu)\phi_{mn,xy}^2 dxdy \quad (62)
$$

The term SER is defined as the modal strain energy ratio at location i, j as:

$$
\sigma_{m,n}(i,j) = \frac{U_{m,n}(i,j)}{U_{m,n}^{(0)}(i,j)} \qquad (63)
$$

where $U, U^{(0)}$ respectively denote the strain energies of the damage and undamaged plate at the considered location. The above definition of SER is referred to as DM in chapter 4. The strain energy for the damaged plate is evaluated through the curvatures obtained

from the first order perturbation solution. Imposing Equations (60) in Equation (65) and neglecting higher powers of ϵ allows expressing the strain energy for the damaged plate as:

$$U_{m,n}(i,j) = U^{(0)}_{m,n}(i,j) - \epsilon \Delta U_{m,n}(i,j) \tag{64}$$

where:

$$\Delta U_{m,n}(i,j) = 2D_0 \int_{x_i}^{x_{i+1}} \int_{y_j}^{y_{j+1}} \phi^{(1)}_{mn,xx} \phi^{(0)}_{mn,xx} + \phi^{(1)}_{mn,yy} \phi^{(0)}_{mn,yy}$$
$$+2(1-\nu)\phi^{(1)}_{mn,xy} \phi^{(0)}_{mn,xy} + \tfrac{1}{2}\nu\big(\phi^{(1)}_{mn,xx} \phi^{(0)}_{mn,yy} + \phi^{(1)}_{mn,yy} \phi^{(0)}_{mn,xx}\big) dxdy$$

The Damage measure (DM) is therefore rewritten as:

$$\sigma_{m,n}(i,j) = 1 - \epsilon \frac{\Delta U_{m,n}(i,j)}{U^{(0)}_{m,n}(i,j)} \tag{65}$$

The modal DM provides indications regarding the integrity of the area i, j. Any variation from unity in fact indicates a difference between the curvature modes over the particular area. A similar concept has been proposed in the literature in [47, 48]. The analytical framework of the perturbation analysis of the plate provides a theoretical description of the concept. This analytical study offers the opportunity of quantifying the extent of damage through the value of the DM, which is directly related to the level of damage ϵ.

The definition of strain energy ratio in Equation (65) considers only one mode of the structure. However it is well known how damage mostly affects regions of higher strain energy. It is thus convenient to sum information obtained from the analysis of several modes m, n and to introduce a cumulative strain energy ratio, which is defined as

$$\sigma(i,j) = \sum_{m,n} \sigma_{m,n}(i,j) = 1 - \epsilon \sum_{m,n} \frac{\Delta U_{m,n}(i,j)}{U^{(0)}_{m,n}(i,j)} \tag{66}$$

This cumulative index combines the information from several modes. Modes not affected by damage because of their particular location do not contribute, whereas the index for modes altered by the defect are combined to provide a robust damage indicator.

5.3 Numerical Results for notch damage

5.3.1 Plate geometry and material properties

The perturbation analysis presented in the previous section is applied to evaluate natural frequencies, mode shapes and curvature modes of damaged plates. Initial results consider the effect of notches at various locations, while the investigation of the effects of line defects is presented in the following section. The study is performed on a rectangular plate with $L_x = 1.5$ m and $L_y = 1$ m, simply supported on all edges as assumed in the analytical derivations. The plate has a thickness $h_0 = 5$ mm and it is made of aluminum ($E = 7.1*10^{10}$ Pa, $\rho = 2700$ kg/m^3, $\nu = 0.3$). The extent of damage is varied and is defined by the parameter ϵ.

5.3.2 Natural frequencies

The effect of a notch damage on the plate natural frequencies is first investigated. Various damage locations as well as damage extents are considered for the analysis. The results of the investigations are presented in Table 1. Damage in general tends to reduce the natural frequencies, as a result of the associated stiffness reduction. It is interesting to observe how frequencies remain unchanged when damage is located at the intersection of the nodal lines of the corresponding mode shape as demonstrated for example by the frequency of mode $(2, 2)$ for damage at $x_D = L_x/2, y_D = L_y/2$. Also frequencies corresponding to higher order modes tend to be more affected by the presence of damage, as demonstrated for example by the comparison of the frequency changes in modes $(1, 1)$ and $(1, 3)$.

5.3.3 Modal deflections and curvatures

Modal deflections and curvatures for plates with notch damage are evaluated through the procedure presented above. The perturbation analysis is limited to the first order based on previous results for beams, which have shown how the second order term gives minor contributions [15]. The Fourier series expansions are performed by considering the superposition of 300 terms. This number has been selected after the qualitative analysis of mode shapes and curvatures predicted with increasing number of expansion terms. A sample of

Table 1: Natural frequencies (rad/s) of plates with notch damage

Mode (i,j)	$h_D/h_0 = 0$	$h_D/h_0 = 1\%$	$h_D/h_0 = 2\%$	$h_D/h_0 = 3\%$	$h_D/h_0 = 4\%$
		$x_D = L_x/2$	$y_D = L_y/2$		
1,1	110.6	110.6	110.4	110.2	109.9
1,2	340.3	340.2	339.6	338.8	337.5
2,1	212.7	212.5	212.0	211.1	209.9
2,2	442.5	442.5	442.5	442.5	442.5
1,3	723.2	722.5	720.1	716.2	710.7
		$x_D = L_x/3$	$y_D = L_y/3$		
1,1	110.6	110.5	110.4	110.0	109.6
1,2	340.3	340.1	339.3	338.0	336.1
2,1	212.7	212.6	212.3	211.7	210.9
2,2	442.5	442.2	441.4	440.2	438.4
1,3	723.2	723.0	722.3	721.2	719.5
		$x_D = L_x/5$	$y_D = L_y/5$		
1,1	110.6	110.6	110.4	110.1	109.6
1,2	340.3	340.1	339.4	338.3	336.7
2,1	212.7	212.6	212.1	211.4	210.4
2,2	442.5	442.2	441.6	440.5	439.0
1,3	723.2	722.8	721.3	718.9	715.5

these investigations is shown in Figure 25 , which presents the curvature $\phi_{mn,xx}$ for mode $(1,2)$ estimated with increasing number of terms in the expansion. In the plot, the presence of damage is demonstrated by a peak at the corresponding location. It is easy to observe how 300 terms are able to fully capture the peak and that larger number of terms does not provide additional details on damage. Series expansion with 300 terms are therefore used in this study as a good compromise between accuracy and computational efficiency.

Examples of modal deflections and curvatures are shown in Figures 26 through 30 for several combinations of damage location and damage extent. The results for modes $(1,1)$ and $(1,3)$ are presented in Figures 26,27, which clearly demonstrate how for the considered level of damage, the deflection mode shapes are not affected by the presence of the notch, while the curvature modes highlight its presence through a peak at the corresponding locations. The amplitude of the peak is proportional to the extent of damage as shown in Figure 28, which depicts the curvature mode $\phi_{22,xy}$ for increasing damage ratios h_D/h_0. The effect of damage on the curvature modes also depends on its location with respect to

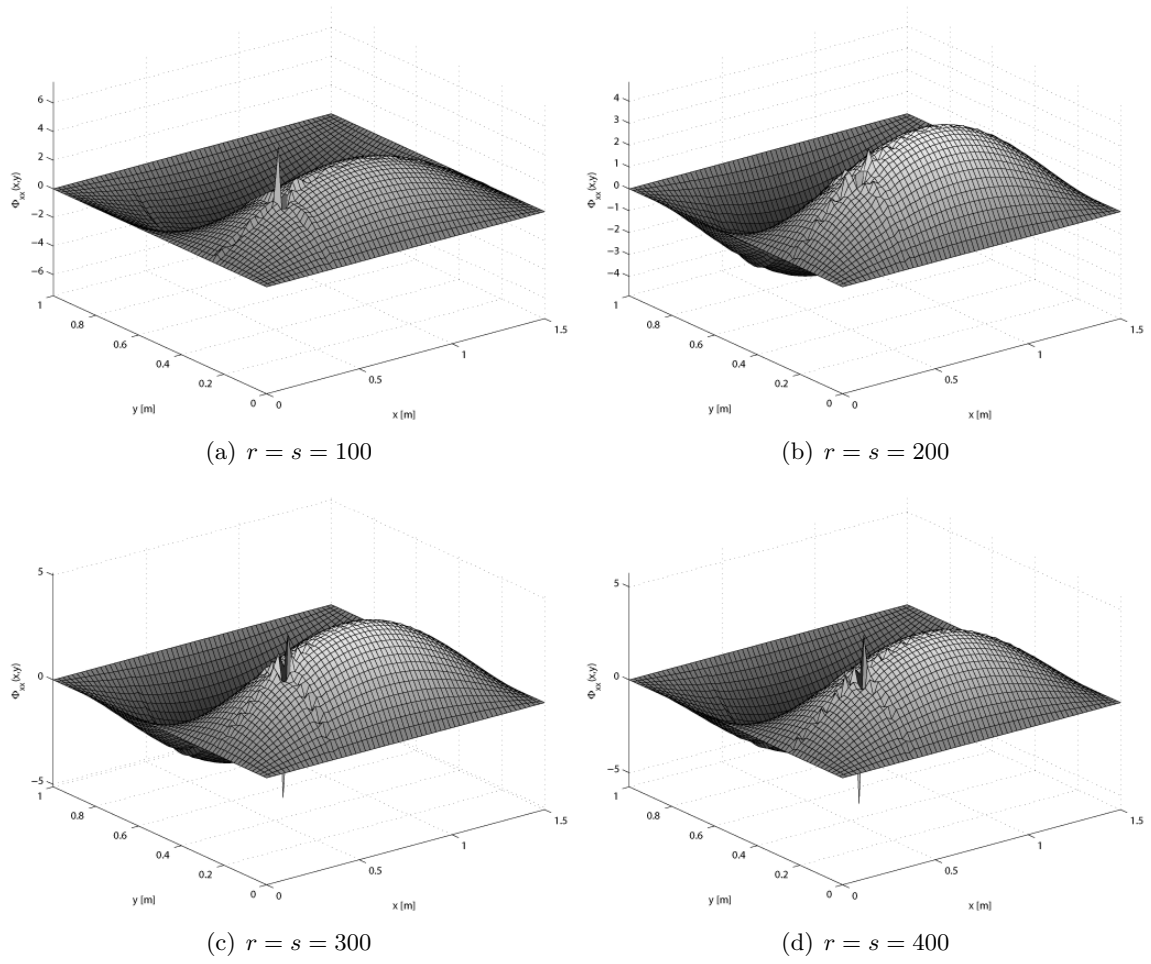

(a) $r = s = 100$ (b) $r = s = 200$

(c) $r = s = 300$ (d) $r = s = 400$

Figure 25: Curvature $\phi_{12,xx}$ estimation using increasing orders of Fourier Series expansion

the nodal lines of the corresponding mode shapes. Figure 29 shows for example how a notch damage with $h_D/h_0 = 2\%$ becomes more evident when it is located close, or at the points of maximum curvature. Finally, Figure 30 compares the effects of a defect of assigned extent on various modes, and demonstrates how the notch tends to affect more significantly higher order modes than lower order modes. This observation confirms the remarks made regarding the natural frequencies of the damaged plates listed in Table 1.

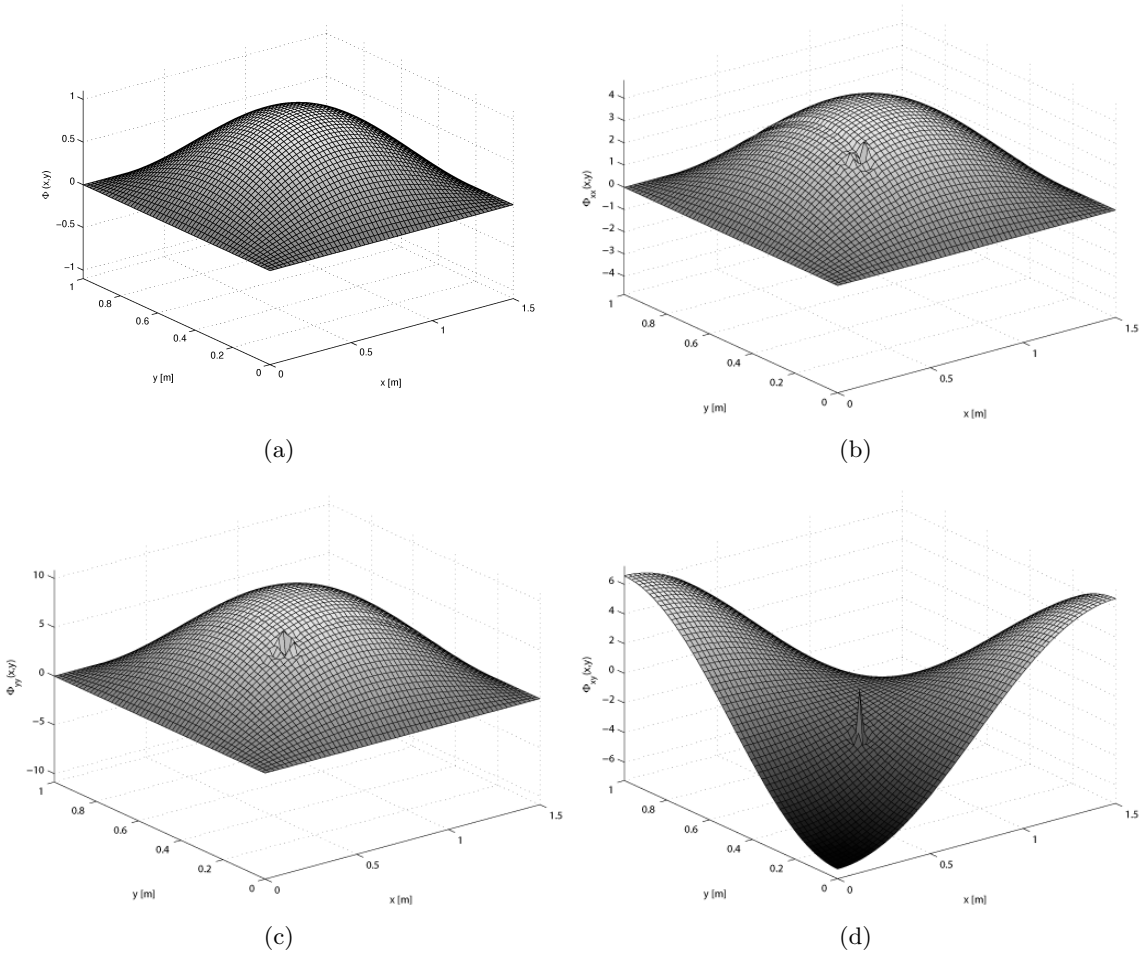

Figure 26: Deflection and curvatures for mode $(1, 1)$ with $h_D/h_0 = 2\%$ and damage located at $x_D = L_x/3$, $y_D = L_y/3$

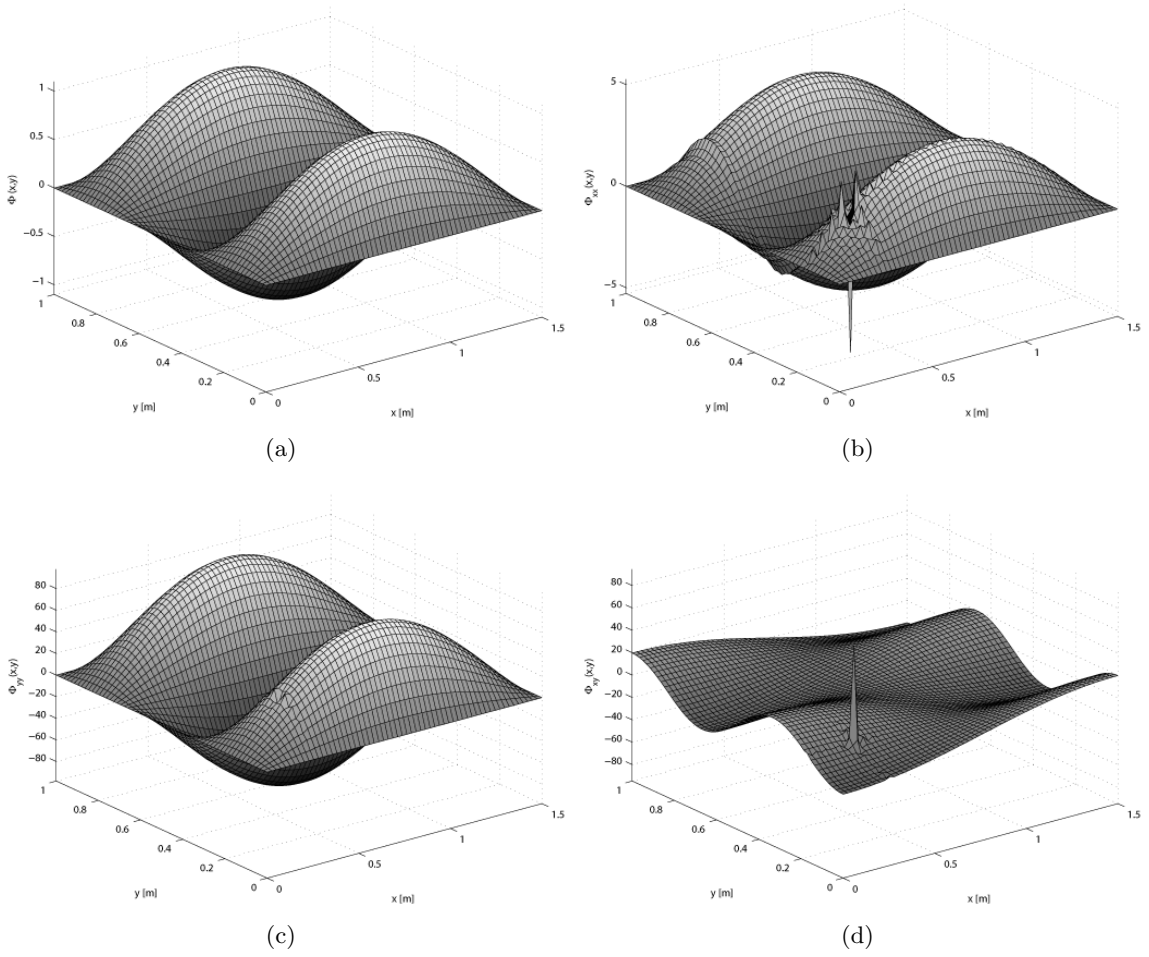

Figure 27: Mode 1,3: Deflection and curvatures for $h_D/h_0 = 2\%$ and damage located at $x_D = L_x/5$, $y_D = L_y/5$

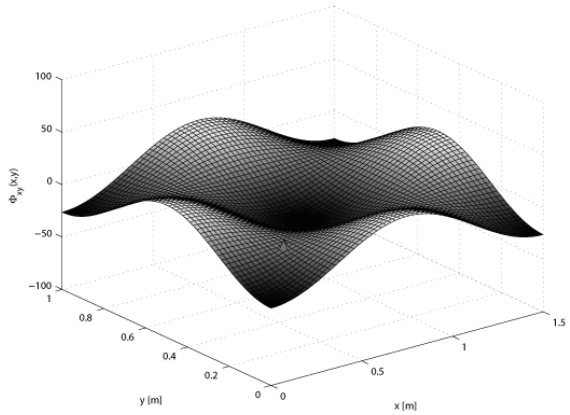

(a) $h_D/h_0 = 1\%$

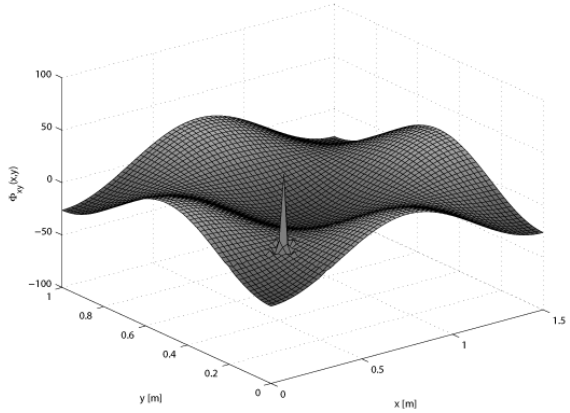

(b) $h_D/h_0 = 2\%$

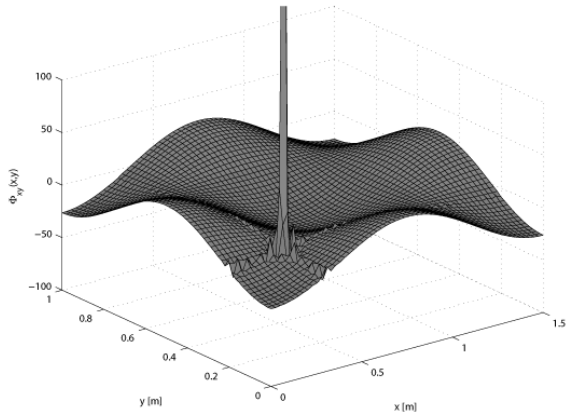

(c) $h_D/h_0 = 4\%$

Figure 28: Influence of increasing damage levels on curvature mode $\phi_{22,xy}$ for notch at $x_D = L_x/5$, $y_D = L_y/5$

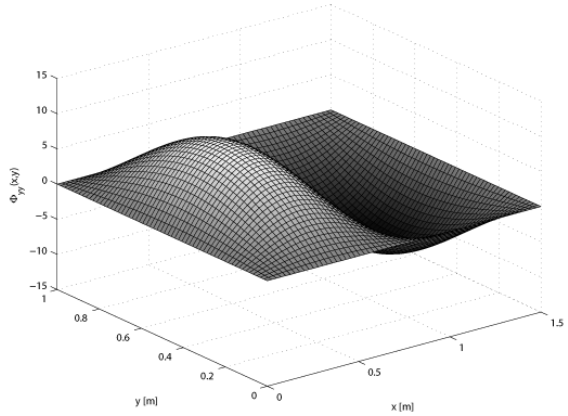

(a) $x_D = L_x/2$, $y_D = L_y/2$

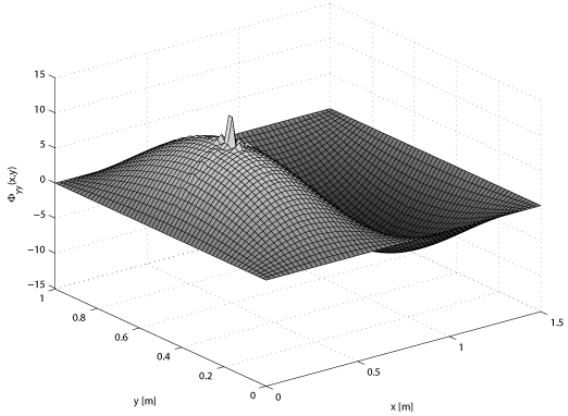

(b) $x_D = L_x/4$, $y_D = L_y/2$

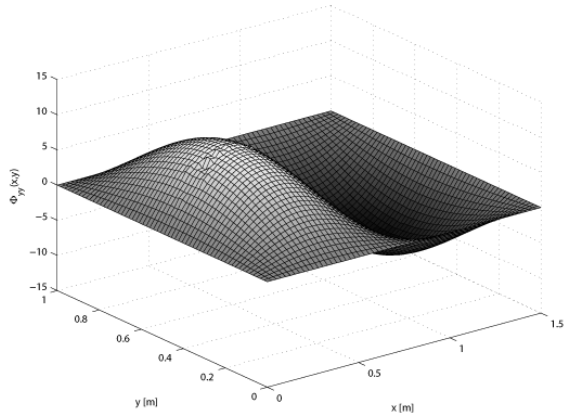

(c) $x_D = L_x/8$, $y_D = L_y/2$

Figure 29: Influence on damage location on curvature mode $\phi_{21,yy}$ for $h_D/h_0 = 2\%$

5.3.4 Strain Energy Ratio for damage localization

The Strain Energy Ratio based DM defined in the previous chapter is here used for the estimation of damage location and extent. The DM is computed by discretizing the plate surface into a 60*60 grid, over which the strain energy and its variation with respect to the undamaged configuration are computed. The integrals in the expression of DM are evaluated analytically through the convenient formulation for the undamaged and damaged curvature modes obtained through the perturbation analysis. Results for notch defects are presented in Figures 31, 32, where the DM distributions are represented as contour plots. The abscissa and ordinates respectively represent the plate length L_x and width L_y, while the magnitude of the DM is indicated by a gray colorscale varying between a minimum of 1.05 (black) to a maximum of 2 (white). The presence of the defect in the presented maps is highlighted by a peak at the corresponding location, which stands out very evidently on the white background imposed on the figure. The extent of the peak and mostly its magnitude are proportional to the damage extent and specifically to the parameter ϵ or to the ratio h_D/h_0 as predicted by Equations (65, 66). The correlation between damage extent and magnitude of the DM is shown in Figure 31, which presents modal DM results for notch defects of different extent and location. The application of the superposition of modal DM distributions to obtain a single damage index is illustrated in Figure 32, which shows modal DM values for an assigned damage configuration and the result of the combinations of the modal contributions according to Equation 66. As discussed above, various modes have in fact different sensitivity to damage at a specific location. For example, it is clear how the damage has very little effect on mode $(3, 1)$, as demonstrated by the corresponding modal DM map shown in Figure 32.d. The combination of the various modal contributions however is able to capture the presence of the defect by combining the information provided by each mode.

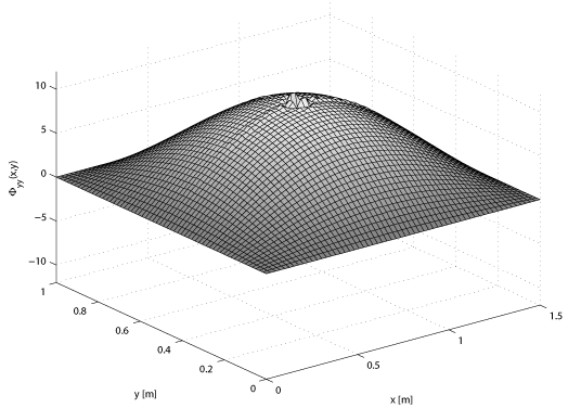

(a) $(1, 1)$

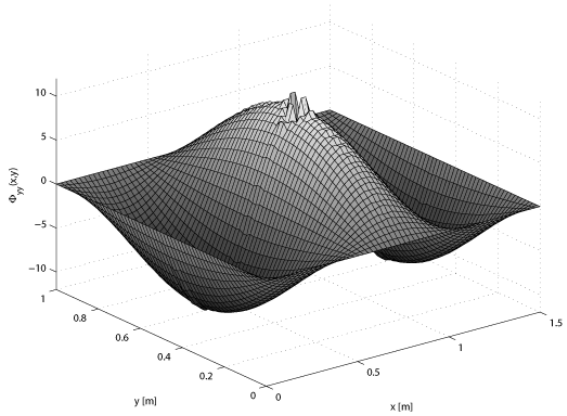

(b) $(3, 1)$

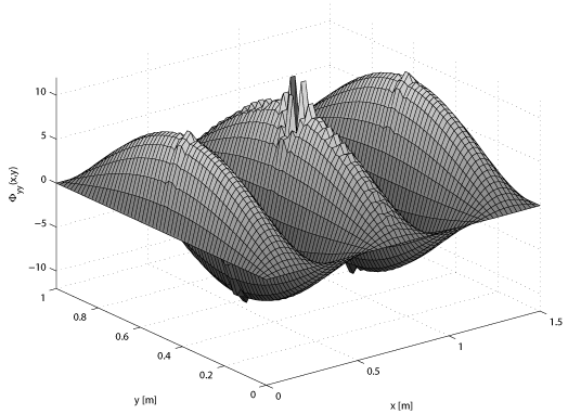

(c) $(5, 1)$

Figure 30: Influence on mode order on curvature mode $\phi_{ij,yy}$ for $h_D/h_0 = 2\%$

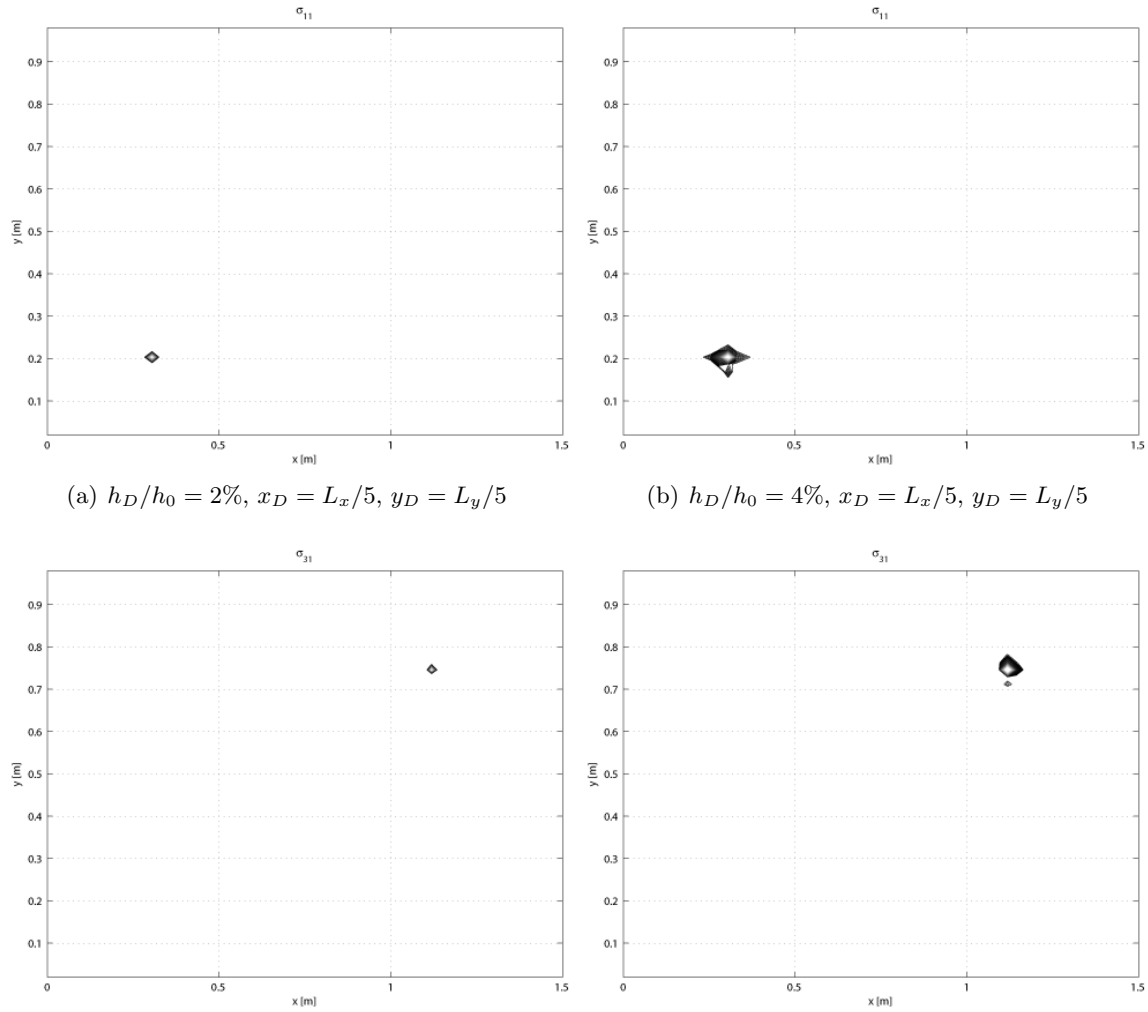

(a) $h_D/h_0 = 2\%$, $x_D = L_x/5$, $y_D = L_y/5$

(b) $h_D/h_0 = 4\%$, $x_D = L_x/5$, $y_D = L_y/5$

(c) $h_D/h_0 = 2\%$, $x_D = 3L_x/4$, $y_D = 3L_y/4$

(d) $h_D/h_0 = 4\%$, $x_D = 3L_x/4$, $y_D = 3L_y/4$

Figure 31: Examples of modal DM for various damage locations and extents

5.4 Results for line defects

The presented analytical procedure is also applied to the analysis of line defects of the kind depicted in Figures 24. Results for various defect lengths, extensions and orientation are presented in Figures 33 through 35. Figure 33 for example displays the influence of damage on the curvature mode $\phi_{11,yy}$. Different defects lengths and orientations are considered to demonstrate how the curvature mode highlights the presence of damage through an evident discontinuity at the damage location. The length and the orientation of the discontinuity correspond to those of the defect. Figure 34 presents results for the curvature mode $\phi_{32,xx}$ of a damaged plate. The plot in Figure 34.a is obtained for the defect located along the nodal line of the curvature mode and therefore no discontinuity is observed. The same damage at a different location however becomes clearly evident as shown in the case presented in Figure 34.b. Moreover, Figures 34.b and 34.c compare damage discontinuities corresponding to damage of increasing lengths to demonstrate the increased sensitivity of the curvature modes. In Figure 35, the influence of damage location and extent is demonstrated for mode $\phi_{12,yy}$.

Strain Energy Ratios are computed also for line defects. Examples of the results are shown in Figures 36 and 37. The maps presented in Figure 36 clearly demonstrate how the DM representation is able to provide information regarding damage extent, length and location. Finally, Figure 37 presents the result of the summation procedure for various modal DM, to obtain a cumulative ratio to be used as a damage index in damage identification routines.

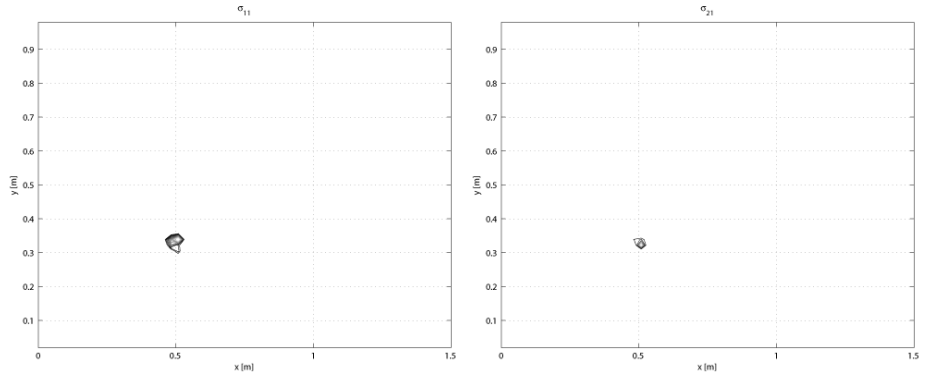

(a) $\sigma_{1,1}$ (b) $\sigma_{2,1}$

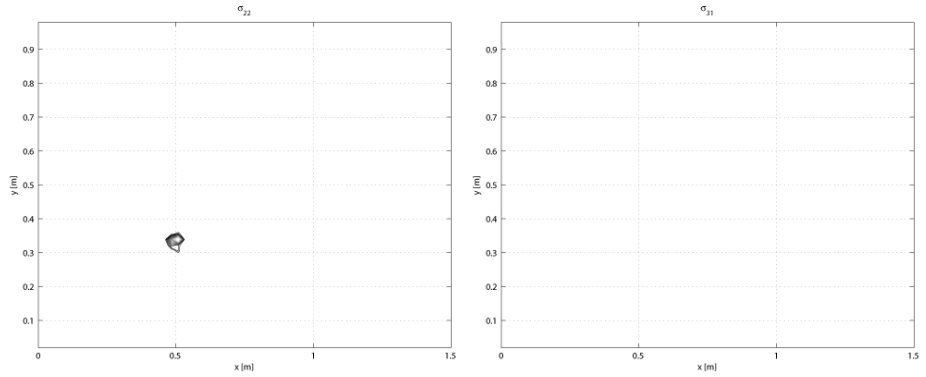

(c) $\sigma_{2,2}$ (d) $\sigma_{3,1}$

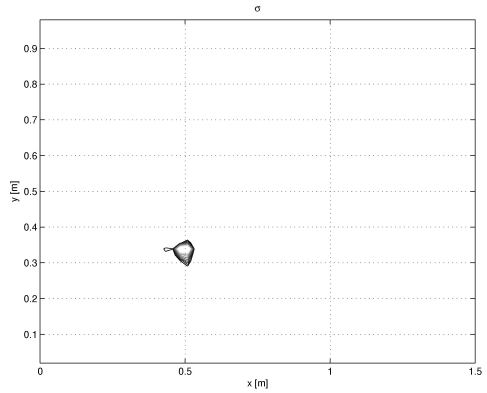

(e) σ

Figure 32: Modal and cumulative DM for $x_D = L_x/3$, $y_D = L_y/3$ and $h_D/h_0 = 4\%$

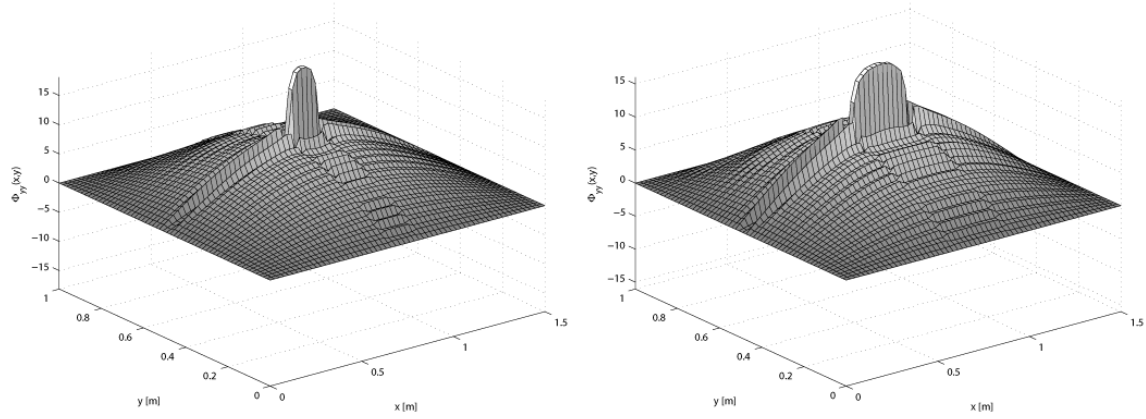

(a) x-line defect, $y_D = L_y/2$, $x_2 - x_1 = 0.15$ m

(b) x-line defect, $y_D = L_y/2$, $x_2 - x_1 = 0.3$ m

(c) y-line defect, $x_D = L_x/2$, $y_2 - y_1 = 0.05$ m

(d) y-line defect, $x_D = L_x/2$, $y_2 - y_1 = 0.1$ m

Figure 33: Curvature mode $\phi_{11,yy}$ for $h_D/h_0 = 4\%$ and line defects of various lengths and orientations

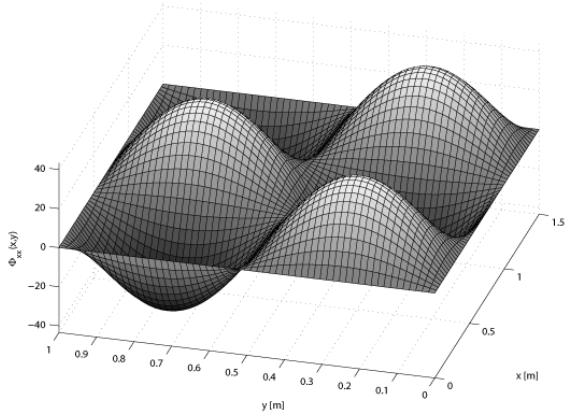

(a) x-line defect, $y_D = L_y/2$, $x_2 - x_1 = 0.15$ m

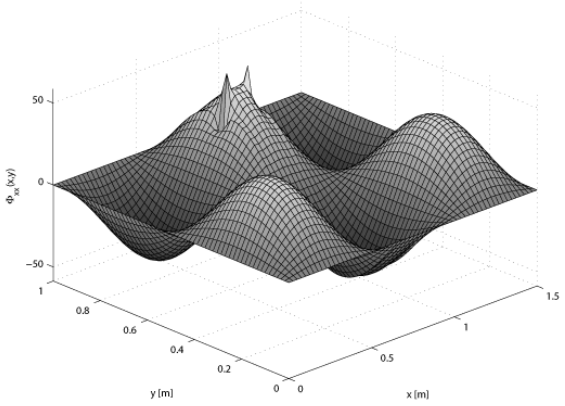

(b) x-line defect, $y_D = 3L_y/4$, $x_2 - x_1 = 0.3$ m

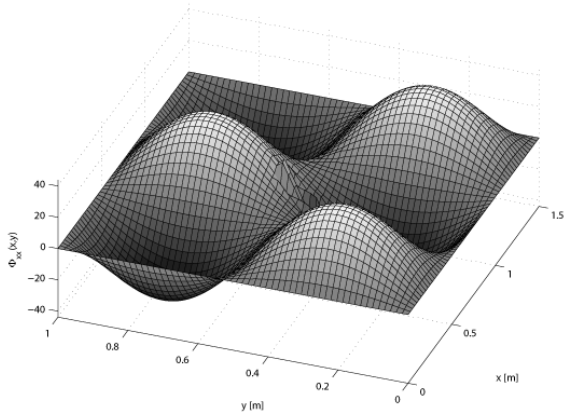

(c) y-line defect, $x_D = L_x/2$, $y_2 - y_1 = 0.05$ m

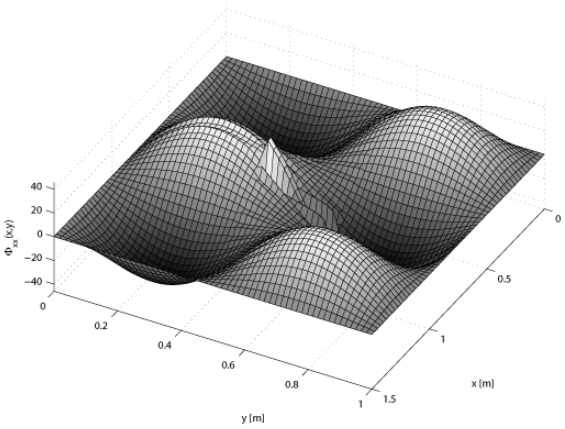

(d) y-line defect, $x_D = L_x/2$, $y_2 - y_1 = 0.1$ m

Figure 34: Curvature mode $\phi_{32,xx}$ for $h_D/h_0 = 4\%$ and line defects of various lengths, locations and orientations

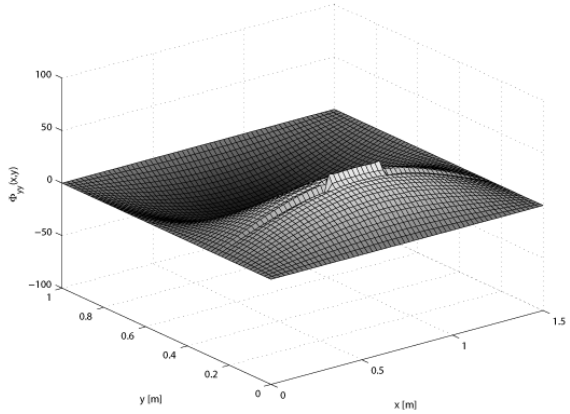

(a) x-line defect, $y_D = L_y/4$, $x_2 - x_1 = 0.3$ m, $h_D/h_0 = 2\%$

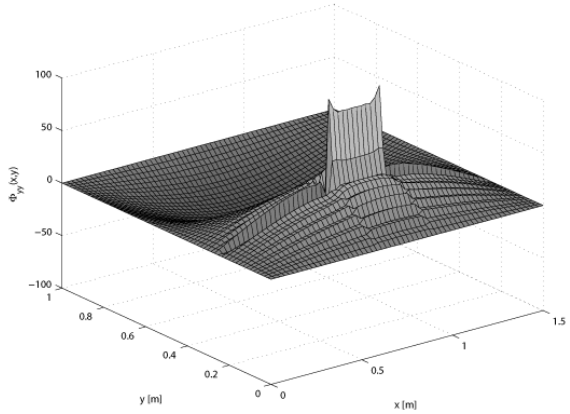

(b) x-line defect, $y_D = L_y/4$, $x_2 - x_1 = 0.3$ m, $h_D/h_0 = 4\%$

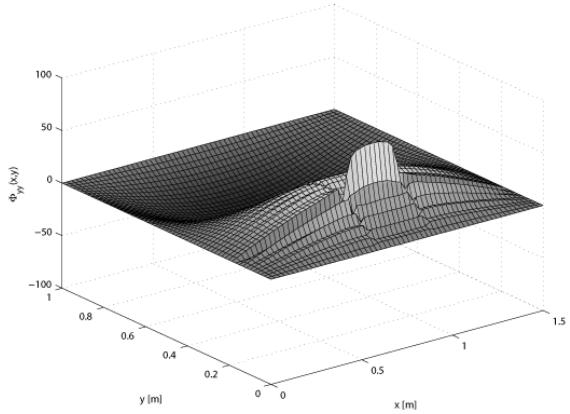

(c) x-line defect, $y_D = L_y/6$, $x_2 - x_1 = 0.3$ m, $h_D/h_0 = 4\%$

Figure 35: Influence of extent and location of damage on curvature mode $\phi_{12,yy}$

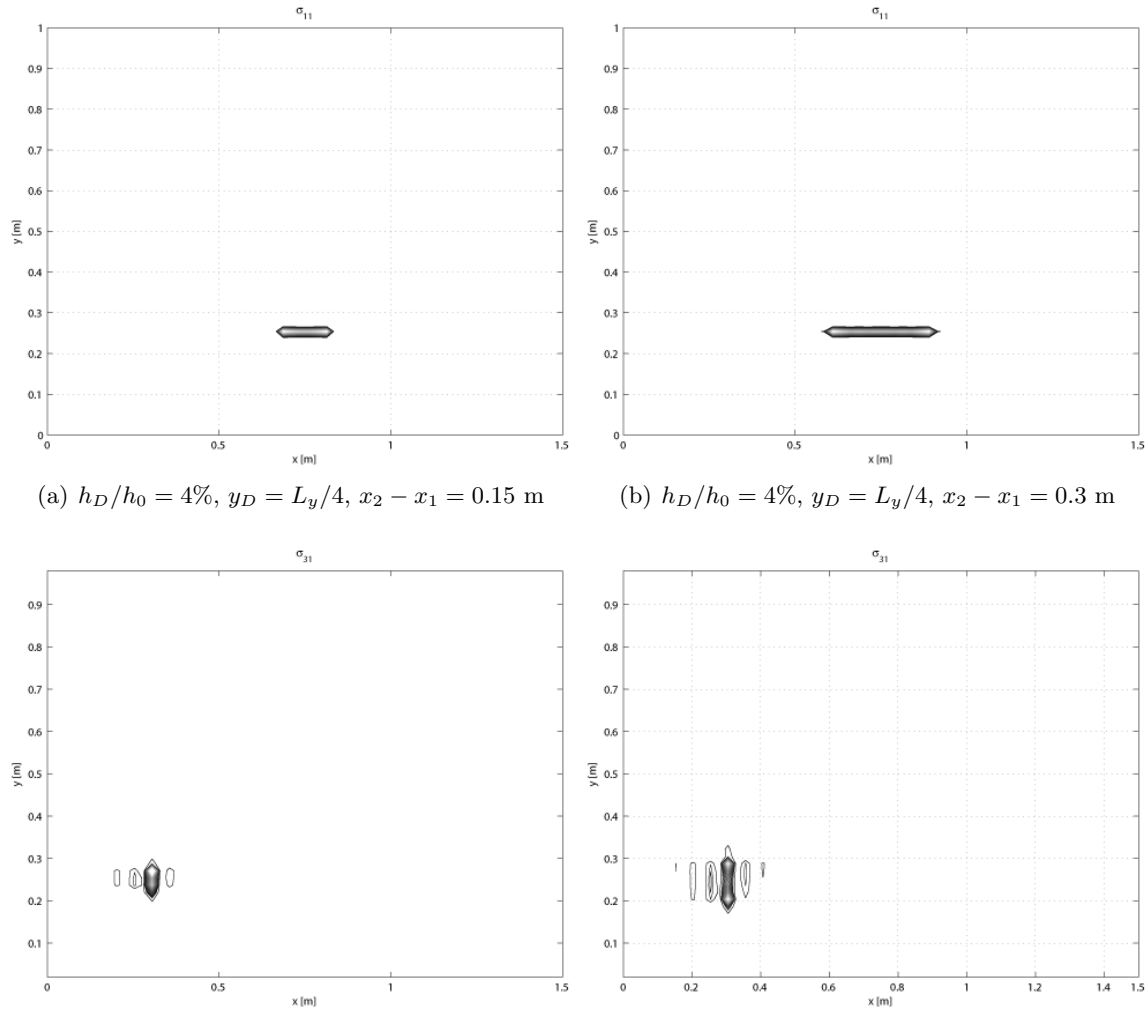

(a) $h_D/h_0 = 4\%$, $y_D = L_y/4$, $x_2 - x_1 = 0.15$ m

(b) $h_D/h_0 = 4\%$, $y_D = L_y/4$, $x_2 - x_1 = 0.3$ m

(c) $h_D/h_0 = 4\%$, $y_2 - y_1 = 0.05$ m, $x_D = L_x/5$

(d) $h_D/h_0 = 4\%$, $y_2 - y_1 = 0.1$ m, $x_D = L_x/5$

Figure 36: Examples of modal DM for various damage locations and extents

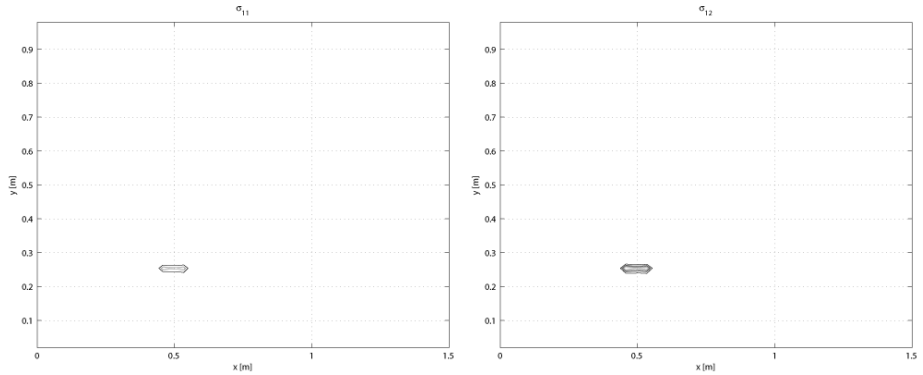

(a) $\sigma_{1,1}$ (b) $\sigma_{1,2}$)

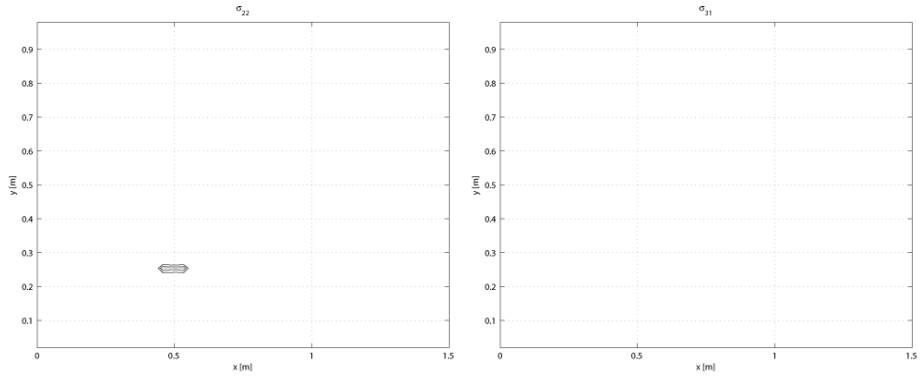

(c) $\sigma_{2,2}$ (d) $\sigma_{3,1}$

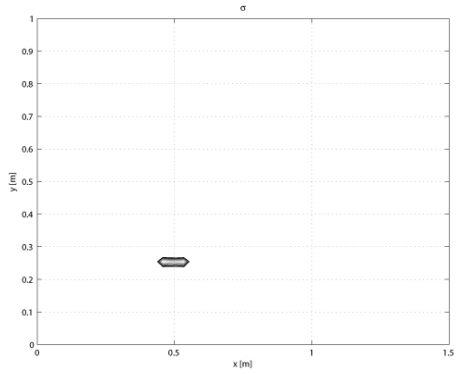

(e) σ

Figure 37: Modal and cumulative DM for line defect with $x_2 - x_1 = 0.15$ m, $y_D = L_y/4$ and $h_D/h_0 = 2\%$

Chapter VI

COMPREHENSIVE DAMAGE DETECTION TECHNIQUE USING LASER DOPPLER VIBROMETER AND A WIDE BAND FREQUENCY EXCITATION

In this chapter, the development of a new comprehensive approach to a non-destructive damage evaluation (NDE) and structural health monitoring (SHM) is presented. The strategy is based on the analysis of the dynamic behavior of the structure over a very wide range of frequencies. The frequency band of investigation spans from the lowest modes of the structure up to the low ultrasonic range, and thus potentially allows the detection of various sizes of defects. The tests are performed using a single actuator/sensor pair: piezoceramic discs are employed as actuators, while a Scanning Laser Doppler Vibrometer (SLDV) is used as a sensing device. The objective is to obtain a comprehensive structural health monitoring methodology able to overcome drawbacks and exploit advantages of various techniques. In the low-to-medium frequency range below 2000 Hz, modal parameters are normally less sensitive to localized defects, but generally provide indications regarding global changes as a result of damage. However, they tend to have limited sensitivity and generally they are not accurate enough to provide detailed account of the damage type and extent. Cornwell, et. al [94] indicate detection of 10% reduction in stiffness of a plate which is equivalent to a 47% reduction in thickness. Lestari in Refenence [44] described detection of 20% reduction in thickness of a beam using modal curvature information. Alleyne and Cawley [7] report detection of 10% reduction in thickness in a beam using the Lamb waves. They also report a relationship between the wavelength and detectable damage size. A notch depth as small as 2.5% of the excitation wave length is shown to be detectable using the Lamb waves. The lack in sensitivity and capability of discriminating damage from

changes in the operating conditions of modal-based methods are overcome by applying ultrasonic inspection techniques [11, 95]. Guided waves such as Lamb or Rayleigh waves in particular have the capacity of traveling relatively long distances within the structure under investigation and show sensitivity to a variety of damage types.

This chapter presents a technique of integrating modal-based and guided waves inspections, in an effort to overcome the drawbacks of the two techniques, while combining their advantages. These two techniques are applied sequentially: vibration-based monitoring first provides indication of potential regions of damage, on which the scanning laser doppler vibrometer is focused to perform high frequency testing and to obtain the precise location and orientation of the damage. It is noted that the modal-based testing must detect the presence of damage first, then the high frequency guided wave investigation is used to define the orientation and length of the damage accurately. Therefore a limitation of the Comprehensive Damage Measure technique is due to the limitations of the modal-based Damage Measure. In all experiments conducted in support of this thesis, the smallest notch type damage size of 20% of the plate thickness has been successfully detected and is considered as a guideline for the minimum damage detection limit. The technique is demonstrated experimentally on a plate structure, and on aircraft components.

6.1 Integration of modal and wave-based inspections

The SLDV identifies the velocity at the user-defined grid points on a structure. It is possible to vary the grid density around any region of interest as quickly as needed because no sensor is hard mounted on the structure. Current limitations on the commercially available SLDV devices allow 512x512 scan points. These scan points are used to cover a large structural component such as a complete vertical tail of a high performance twin tail aircraft for modal test, or a very small region around a critical point of interest such as a fastener hole. The detailed spatial information provided by the SLDV is used to obtain curvature and strain energy distributions over the analyzed structure, following methods similar to those presented in [94, 93, 103]. In addition it is possible to use the SLDV to obtain full wavefield

images of propagating waves to estimate and visualize the strain energy distribution evolution over time. A strain energy-based Damage Measure (DM) is formulated and applied to analyze both steady-state as well as transient structural response. This formulation is part of a two-stage technique, which has the objective of overcoming the drawbacks of various inspection strategies while exploiting their advantages. In the low-to-medium frequency range associated with vibration modes, modal parameters are damage indicators which are normally less sensitive to small defects, but generally provide an indication regarding global changes in the dynamic behavior of the structure. In parallel to the vibrations-based techniques, the SLDV is used for the detection and analysis of transient waveforms propagating in the ultrasonic range, which are locally sensitive to damage.

In the two-stage damage detection process a coarse grid is first considered to monitor large portions of a structural component, and to obtain potential areas of defect through modal-based analyses. Subsequently, high frequency wave propagation inspection is performed around the identified defective regions to obtain confirmation of damage as well as details regarding its orientation and extent. A schematic of the considered strategy for technique integration is shown in Figure 38.

6.2 Time and frequency domain Damage Measure formulation

The detailed theoretical formulation of Damage Measure is presented in Section 4.1. Some descriptions of Damage Measure relevant to this chapter are revisited here. The term Damage Measure defines a normalized form of distributed strain energy ratios between the damaged and undamaged structure. Two versions of Damage Measure are defined depending on the data used for its evaluation. The frequency domain formulation uses the mode shapes obtained at the structure's natural frequencies. The modal DM $f_g^{(i)}$ is defined as the index corresponding to the mode shape at the i-th frequency. It is a fact that damage affects the mode shape when it is located near, or in regions of maximum corresponding strain energy density. Hence, the visibility of damage is affected by the mode shape. For this reason, it is convenient to combine information obtained from the analysis of several

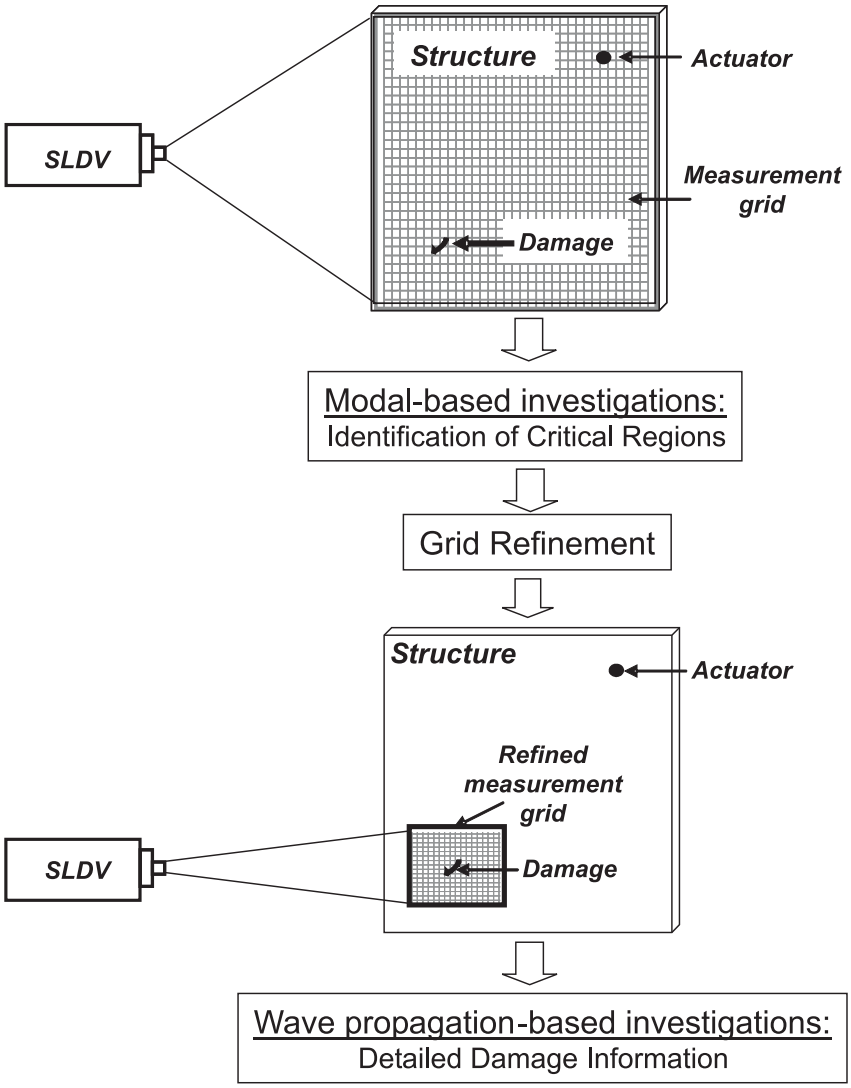

Figure 38: Schematic of the considered strategy for SHM technique integration

modes

$$f_g = \frac{1}{I} \sum_{i=1}^{I} f_g^{(i)} \tag{67}$$

This cumulative index provides a single piece of information which combines the results from several mode shapes and associated energy distributions. The vibration mode shapes that are not affected by damage because its particular location will not contribute, i.e. they give unit contributions, whereas the index for modes altered by the defect are combined.

The DM expression defined in Equation (9) of Chapter 4.1 is also formulated in the time domain, and applied to the analysis of propagating waves. Results from this formulation are DM contour plots that evolve over time as waves propagate within the structure.

6.3 Low and High frequency Experiments

The experiments were designed to validate the developed techniques for detecting damage on simple plate structures and on damaged aircraft components. Both frequency domain tests, as well as wave propagation investigations were performed to implement the integrated approach described in Section 6.1. The two types of dynamic investigations were performed using the same actuator and sensor pair. Piezo-ceramic discs were used as actuators and placed at locations to allow adequate modal excitation, and elastic waves generation suitable for damage detection [91, 97]. The vibration tests were performed simply through broadband excitation of the structure, which allows the extraction of the vibration mode shapes over a selected frequency range.

The SLDV (Polytec PI, Model PSV400M2) allowed high frequency sampling ($\approx$ 2.56 MHz), which enabled ultrasonic waves detection and visualization. In the wave propagation tests, the piezo discs were driven by a sinusoidal burst generated by a signal generator (Stanford Research Mod. SR360). The resulting elastic waves were recorded at the measurement grid points. The operation of the SLDV required a repeatable generation of a pulse for each grid point in order to record the corresponding response. Phase information was appropriately retained by triggering the excitation signal through a low frequency signal (10 Hz), which also defined the scanning rate. Upon completion of measurements at all

grid points, the recorded responses were then processed to obtain full images of the propagating wavefield within the region of inspection. A schematic of the set-up for wavefield measurement was as shown in Figure 39.

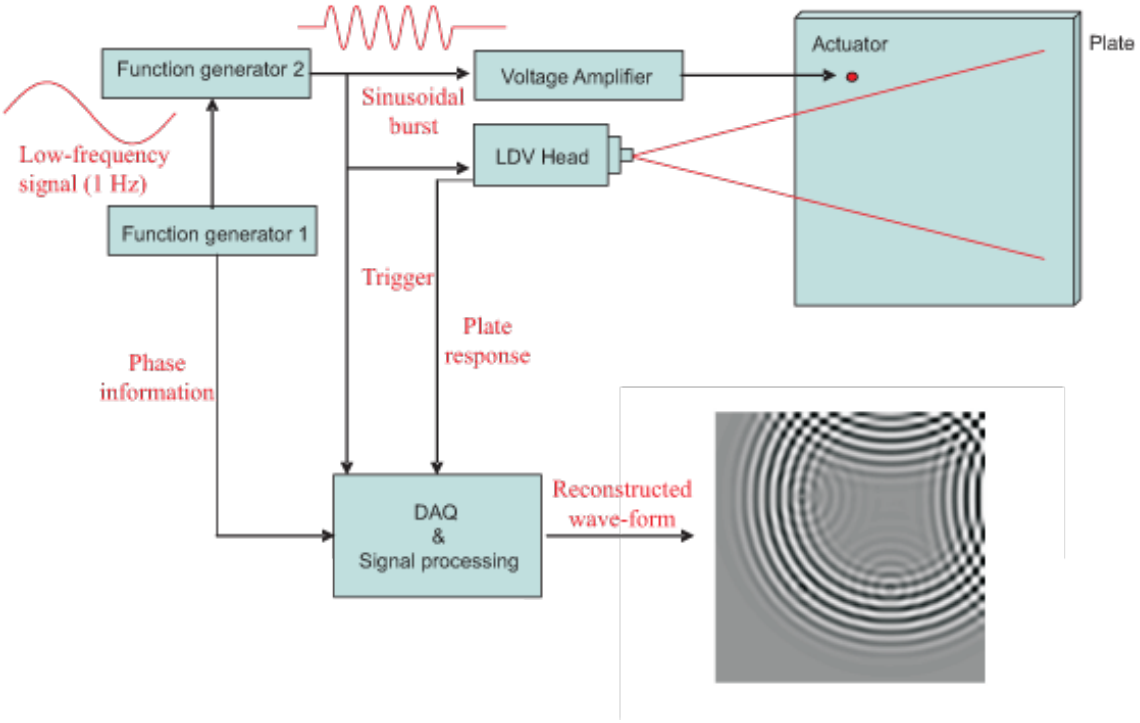

Figure 39: Schematic of experimental set-up for full wavefield detection and visualization

6.3.1 Experiment Setup

In the experiments, a piezoceramic actuator disc was bonded to the structure, and it was driven by a function generator (Stanford Research Model SRS 360) through a voltage amplifier. The considered excitation signals were 5-cycle sinusoidal bursts of varying frequency. The out-of-plane transient response was measured by the SLDV. For each scanning point a pulse was generated by the signal generator. The frequency of pulse generation was defined by a second function generator internal to the SLDV system. The latter is set to produce a low frequency signal (10 Hz) which triggers the pulse on the SRS360 generator, and served as reference for retaining the phase information required for post-processing the time signals. The post-processing tasks for the modal-based test included mode shape extraction and modal Damage Measure computations leading to a cumulative Damage Measure. The

post processing for the guided wave part of the experiment included generation of propagating wave in time domain. A schematic of the experimental set-up is shown in Figure 39. The experimental set-up described above was used to scan the plate and detect its transient response.

6.3.2 Aluminum Plate Test Specimen (wide frequency analysis)

The test specimen of Section 4.3.2.1 was used for the detection of damage using low frequency vibration modes as well as high frequency elastic waves. The test specimen was as shown in Figure 40.a illustrating a piezoceramic actuator disc of 1.1" diameter and one 1.4" long groove type damage. This actuator disc was used as a source of dynamic excitation over the full range of frequency of interest up to 1000 Hz. The measurement grids for the plate tests were as shown in Figure 40.b.

6.3.2.1 Modal-based testing

The plate was first excited in the 0-500 Hz range using pseudo-random excitation. For example the measured mode shape was as shown in Figure 41 at 294 Hz (5^{th} mode), and the corresponding modal DM, which clearly highlighted the location of the damage. Some deviation from unity was observed at other locations, mostly located close to the exciter. This spurious information was effectively filtered out by considering a cumulative DM obtained from the superposition of several modal DMs. The resulting cumulative DM obtained from the superposition of the first 5 modes of the plate was as shown in Figure 42, which provided an unambiguous indication about damage presence and location.

6.3.2.2 Wave propagation tests

Wave propagation tests were subsequently performed using the same actuator used for modal tests as shown in Figure 40. The excitation signal was a 5-cycle sinusoidal burst at 50 kHz. This frequency was selected through a manual sweep over the $20 - 100$ kHz range performed to evaluate the frequency corresponding to the maximum plate response.

A snapshot of the plate time domain response and of the corresponding DM were as shown in Figure 43.b. A qualitative analysis of the time domain signal suggested that the

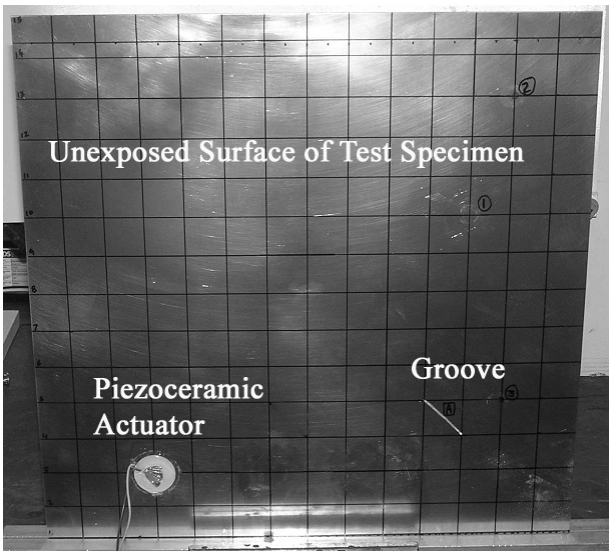

(a)

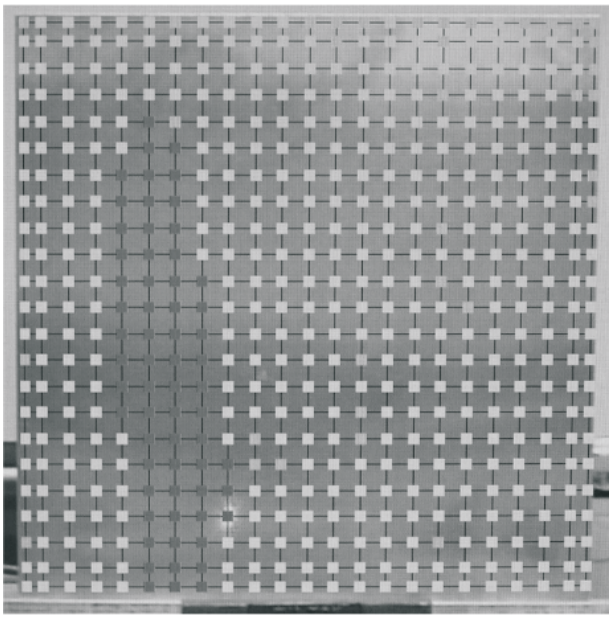

(b)

Figure 40: Cantilevered aluminum plate with detail of actuator and damage locations (a), and measurement grid (b)

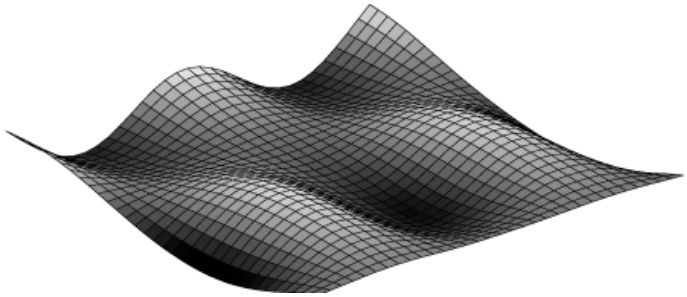

(a) Mode Shape

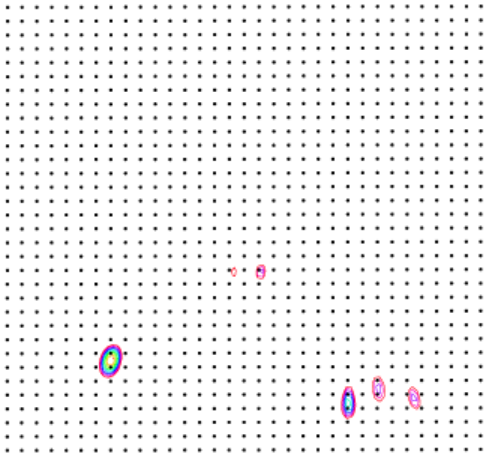

(b) Modal DM

Figure 41: Mode shape and modal DM at 294 Hz (5^{th} mode).

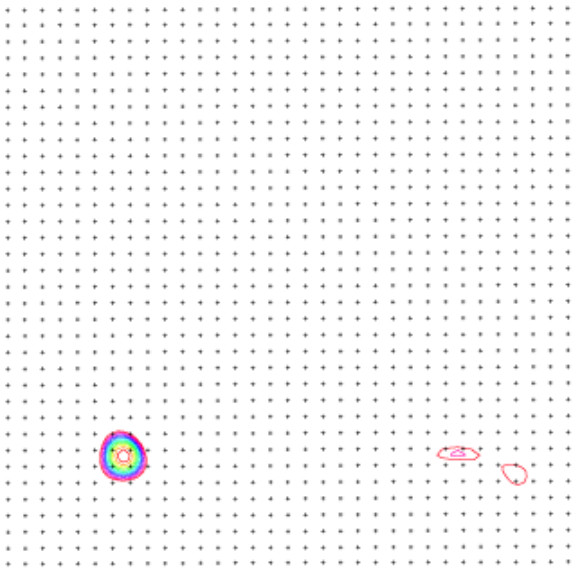

Figure 42: Experimentally evaluated DM through the superposition of first 5 modes.

considered time instant corresponded to the interaction between the symmetric Lamb mode and the defect. The symmmetric mode was faster than the antisymmetric mode, which was the one mostly excited by the considered actuator set-up. The DM shown in Figure 43.b was obtained with a 67% decimation in both directions, and clearly showed orientation and length of the damage.

6.4 Conclusions

An integrated technique for structural health monitoring and damage detection was developed. The technique relied on the evaluation of a damage index, estimated through strain energy function and required knowledge of the structure in its undamaged state. As opposed to similar techniques developed by other researchers, the thesis introduced a procedure whereby the undamaged state was directly synthesized from the measured response on the damaged or the current state of the structure. This was achieved through a decimation process whereby data were purposely under-sampled in order to miss discontinuities due to damage. This procedure was made possible by the use of a scanning laser doppler

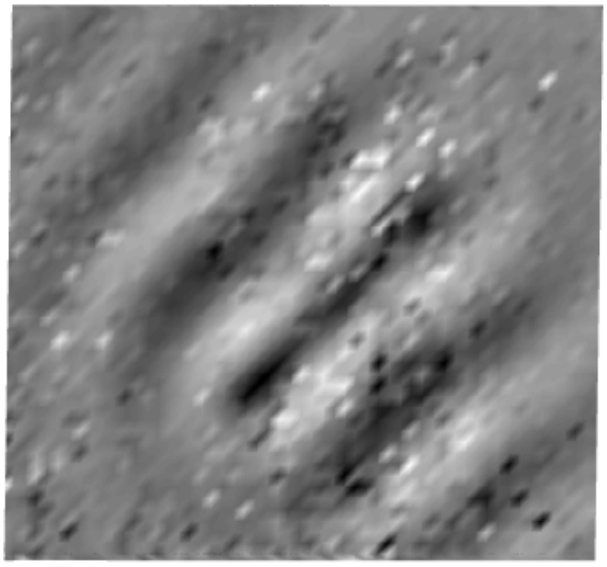

(a) Displacement

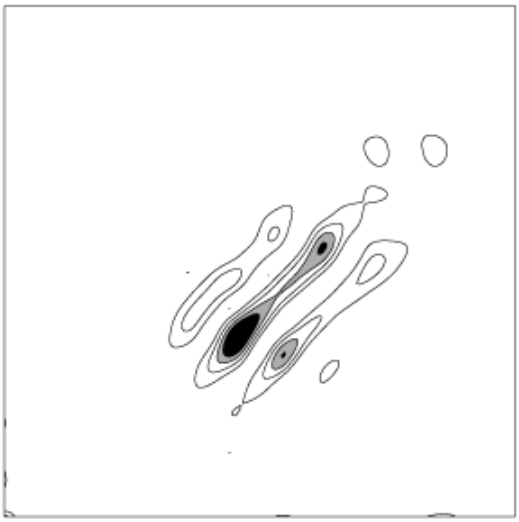

(b) Time domain DM

Figure 43: Snapshot of plate displacement and corresponding DM.

vibrometer which allowed measuring the structure's dynamic response at a large number of points, and over a wide frequency band. Specifically, in the modal frequency range, the frequency domain formulation of the DM was used to obtain general information regarding the location of damage. These tests were then followed by high frequency, wave propagation measurements, which were carried out locally. The objective was to provide detailed and quantitative damage information. This integrated technique and the innovative DM formulation were tested on damaged specimens, which included a simple plate structure, as well as a damaged aircraft component. Successes of the comprehensive damage index formulation sets the stage for implementation of an automation in SHM.

Chapter VII

AUTOMATION IN STRUCTURAL HEALTH MONITORING

An automated structural health monitoring concept is motivated by a need for rapid assessment of the general state of the health of a given structure and to further determine the location and extent of the structural damages with a high degree of confidence, without disassembly of the structure and faster than the present practice of depot inspections. Here, the automation process implies that after initial set up of the experiment, the data acquisition and post-test processing are conducted autonomously such that the damages or defects are identified with a high probability of detection and reported to the executive computer. It is recognized that a computer based decision making process requires numerical representation of the quantity upon which the decision is to be made. The research efforts of this thesis present the concept of Damage Measure who's magnitude is directly related to the extent of the damage. The Damage Measure is formulated as the ratio of the measured strain energy distribution to a reference baseline value. The baseline value corresponds to the strain energy density, at each location, of the corresponding undamaged structure. An innovative technique of obtaining the baseline information is presented in Section 4.1.3 which facilitates the automation process further. This technique requires the use of the measurements of a structure in its current state of damage and synthesize the baseline response data. The strategy for automation and the results of an automated damage detection experiment are presented here.

7.1 Automation Strategy

7.1.1 Modal and Wave-based Inspection

In order to increase the success rate of damage detection, a combined approach of modal and guided wave propagation is pursued. The approach is based on a two-stage process

as depicted in Figure 38 of Chapter 6. The first stage comprises of measuring low to medium frequency vibration modes data using a coarse sensor grid pattern to allow a rapid identification of the suspect regions by the use of strain energy based Damage Measure. These modal-based methods are very attractive as they provide information regarding the general assessment of the structure if any damage or damages exist but not accurate enough to provide precise location or orientation and extent of the damage. This deficiency is overcome in the second stage by applying high frequency guided waves based inspection techniques [References [11, 95]] over each of these suspect regions identified in the first stage of testing. Guided waves such as Lamb waves in particular have the capability of traveling relatively long distances within the structure under investigation and interact with the damages to reveal features such as reflections, refractions, and mode conversion at the discontinuities in the derived quantity such as strain energy over the region of damage. The damage measure is once again applied to the measured wavefield in time domain which leads to full characterization of the damage.

A piezoceramic disk actuator is used as a source of excitation. Placement of this actuator disk is critical to achieving adequate excitation for all modes over a selected frequency range of interest. It is to be located where high curvature is expected such as near the root of a cantilever beam or plate. This actuator disk is also well suited for introducing high frequency elastic waves such as Lamb waves in the test structure. It is also necessary to account for the interference caused by reflected waves from the boundary. Therefore, a spatial separation between the actuator and the nearest edge is necessary. The Scanning Laser Doppler Vibrometer offers tremendous flexibility in measurement point placement since a laser beam can be conveniently controlled by the software. The use of piezoceramic actuator disk and SLDV for low frequency modal test as well as the elastic wave propagation study is a significant achievement in SHM since it supports the goals towards an integrated testing technique where a common excitation and sensing system is deployed for both vibration based SHM and guided wave based SHM.

7.2 Structural Health Monitoring Automation Concept

The analytical formulation of a measure of damage as presented earlier in this thesis provides a significant groundwork for the structural health monitoring technology. The next step is to explore automation for SHM implementations and the decision making process for damage detection. The automation of structural health monitoring concept relies upon a feature that the Laser beam positioning, excitation signal generation, data acquisition, and data processing functions are all controlled by the command of a software architecture. A Polytec PSV-400 Scanning Laser Doppler Vibrometer is used in support of this research. A high level schematic of the automation concept is shown in Figure 44. The details of the flow of information and processing are shown in Figure 45. Initially the user is required to setup the test article and the SLDV. The executive software initiates the SHM process by requiring manual selection of the limits on the overall region of interest on the structural component being investigated. Initial setup information and excitation signal information are recorded on the Executive Computer. The user is required to select parameters for the data acquisition and processing techniques such as type of excitation signal, filters, number of samples, and number of averages. A Pulse excitation is normally selected with user controllable pulse definition. An appropriate pulse shape is selected to excite modal responses over a frequency range of interest. An initial modal test request is issued by the executive to the Test Computer for a coarse measurement grid pattern. All test control parameters such as frequency band width, number of averages, and excitation signal type, are provided to the executive controller. At the completion of the modal test, the frequency response function data are provided to the analysis controller in a Universal File Format for generation of mode deflection shapes. The peak response frequencies are identified using an averaged frequency response function. The averaged frequency response function is obtained by computing a simple average of all frequency response functions. All mode deflection shapes are computed corresponding to each peak magnitude and the processed data are transmitted to the Executive Controller for computation of the distributed Damage Measure over the tested region of the structure. The above described process provides a framework for the automation. However, each of these steps were conducted manually to

establish the proof of the proposed concepts in automation.

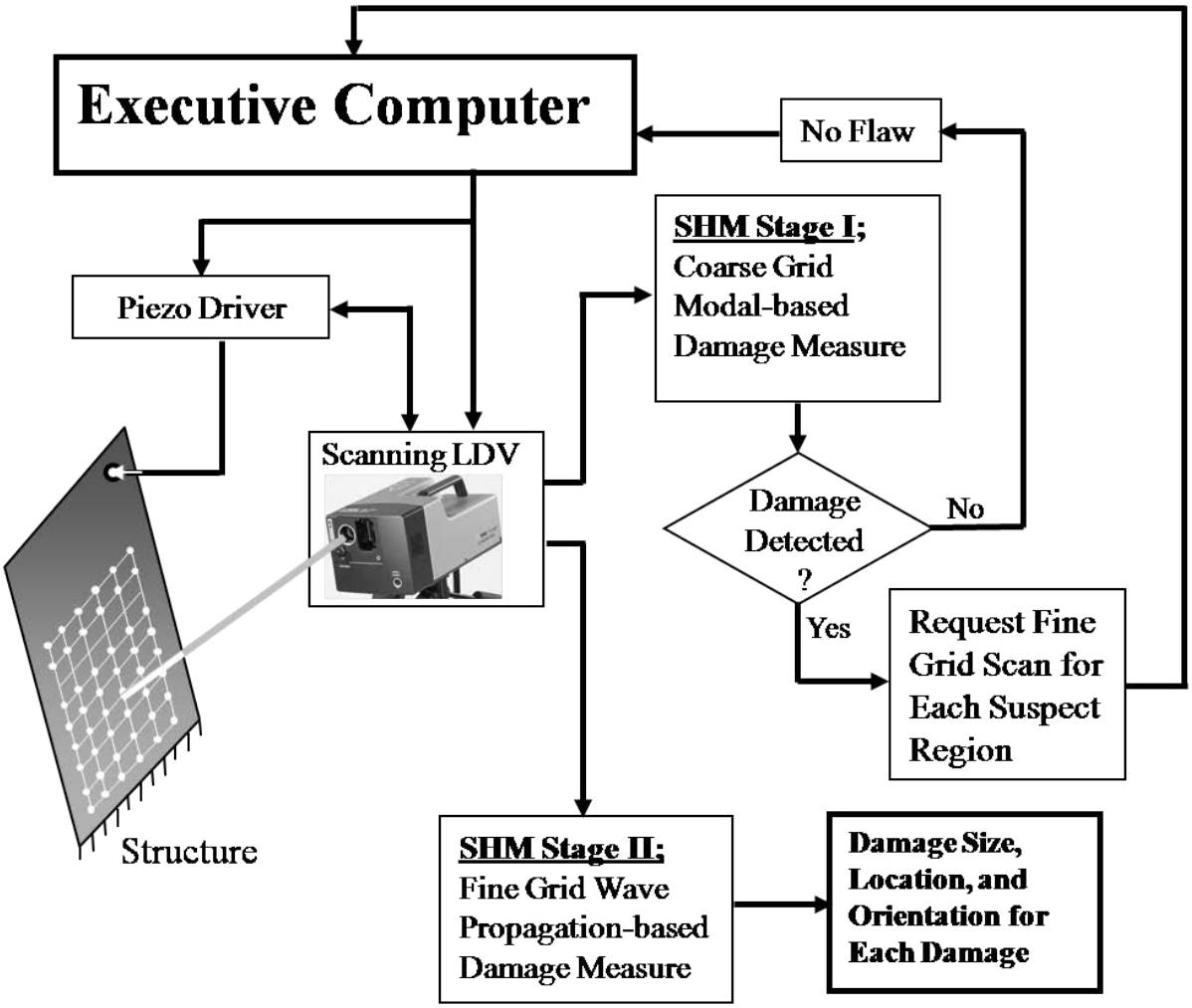

Figure 44: High Level Schematic of Structural Health Monitoring Automation

The Damage Measure is a numerical representation of the state of the structure. A unit value of Damage Measure represents the region with no detectable damage. Any deviations from unit Damage Measure indicates a suspect region with damage. Contour plots of the distributed Damage Measure are automatically scrutinized for non-unit values. The cumulative Damage Measure ensures elimination of spurious values over the tested region. At the end of this first stage of automation, the process identifies likely regions of damage based on a threshold value of Damage Measure. After localization of each suspect region of damage, the Executive Computer directs the Test Computer with coordinates of suspect

regions for guided or elastic wave propagation studies using a finer sensor grid pattern. Once again pulse type excitation signal is used for elastic waves. At the completion of the data acquisition, the time domain elastic wave propagation and geometry data are transmitted back for processing to Controller. The user can intervene the process through a graphical user interface to review the animation of propagating elastic waves and their interaction with the damages along with the computed Damage Measure. The cumulative Damage Measure is finally presented in the form of a contour plot which reveals the orientation, length, and the extent of the damage in the structure under investigation. Such elastic wave propagation data are obtained for each of the suspect regions originally identified in stage 1 of the test procedure.

The programming environment consists of a combination of Visual Basic Application Analysis Controller and MATLAB for data processing along with the Laser Doppler Vibrometer executable control modules that are called by MATLAB software as well as the Analysis Controller. Results concerning the damages are then transferred to the Executive Computer. This thesis presents a showcase of the successful execution of the automatic structural health monitoring concept on a plate-like test structure with one notch type damage. The characterization of damage consists of precise location and orientation along with the quantitative definition of the damage.

7.3 Test Results

The building blocks of the automation in structural health monitoring are demonstrated on an aluminum plate of dimension 14"x14"x0.040". The plate is cantilevered at its base and is excited by a piezoceramic disk of 1.1" diameter and 0.030" thickness (Steminc Model SMD28T07F300). It is necessary to excite a large number of modes with an expectation of capturing local effects through the mode shapes that are affected by the damage. In the demonstration test case the actuator placement is selected so as to excite the symmetric as well as antisymmetric modes of the test specimen. The test plate with the actuator and damage location is shown in Figure 46. The actuator is simply bonded to the plate using Loctite Quick Set epoxy. The disk is also fully encased in a layer of epoxy to provide it with

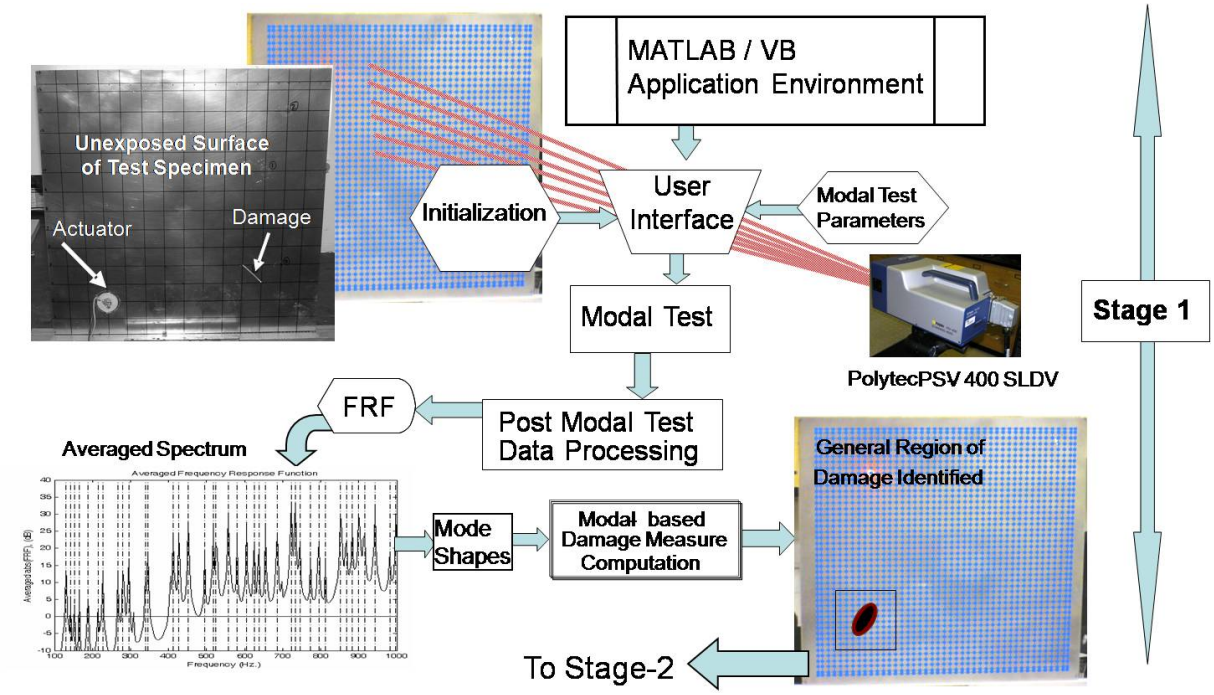

(a)

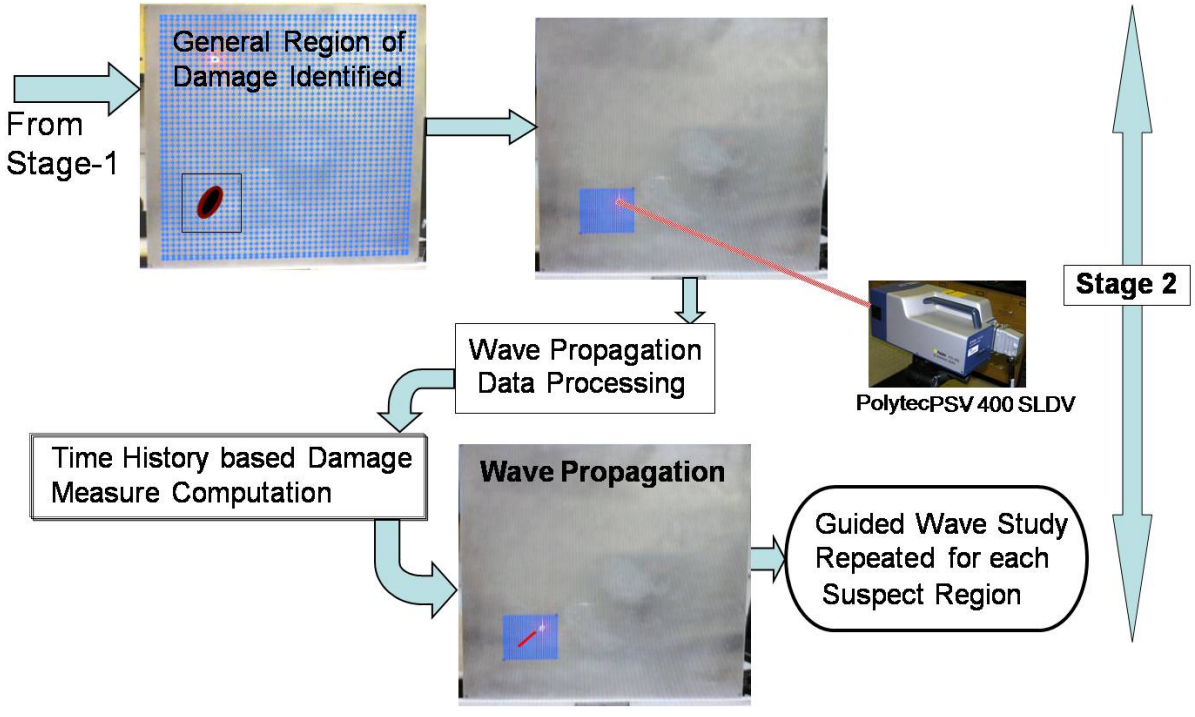

(b)

Figure 45: Flow Diagram of Automated Structural Health Monitoring (a) Stage 1 using modal-based dynamics responses, (b) Stage 2 using wave propagation inspection

adequate backing to impart sufficient force to its base. The considered damage is a 1.41" long, 0.05" wide, and 0.015" deep groove which is cut in the plate at the location shown in Figure 46.

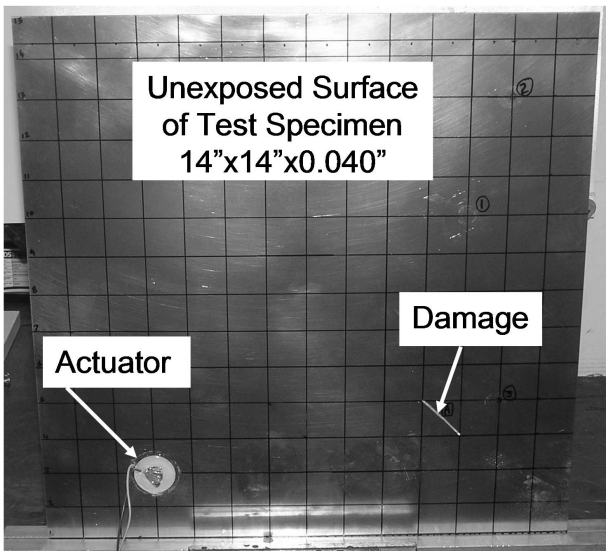

Figure 46: Aluminum plate test structure

A large portion of the plate is selected for modal test data measurement points as shown in Figure 47. All measurements and search for suspect locations are restricted to this region selected by the user initially during the experiment setup . A 30 micro-second pulse is selected to generate the bending and torsional mode responses of the plate up to 2000 Hz. The SLDV is commanded by the Executive Computer to acquire frequency response functions at the measurement grid points using a specified number of averages. At the completion of the modal test, an averaged frequency response function of all measurement grids is computed and is shown in Figure 48. For the sake of clarity, it only shows data up to 1000 Hz. This averaged frequency response function is forwarded to the Analysis Computer for identification of the vibration mode shapes.

The current method of mode selection consists of detecting peaks in the averaged frequency response spectrum and retaining the peaks above a threshold value only. The threshold value is specified by the user during the setup phase of the experiment. A total

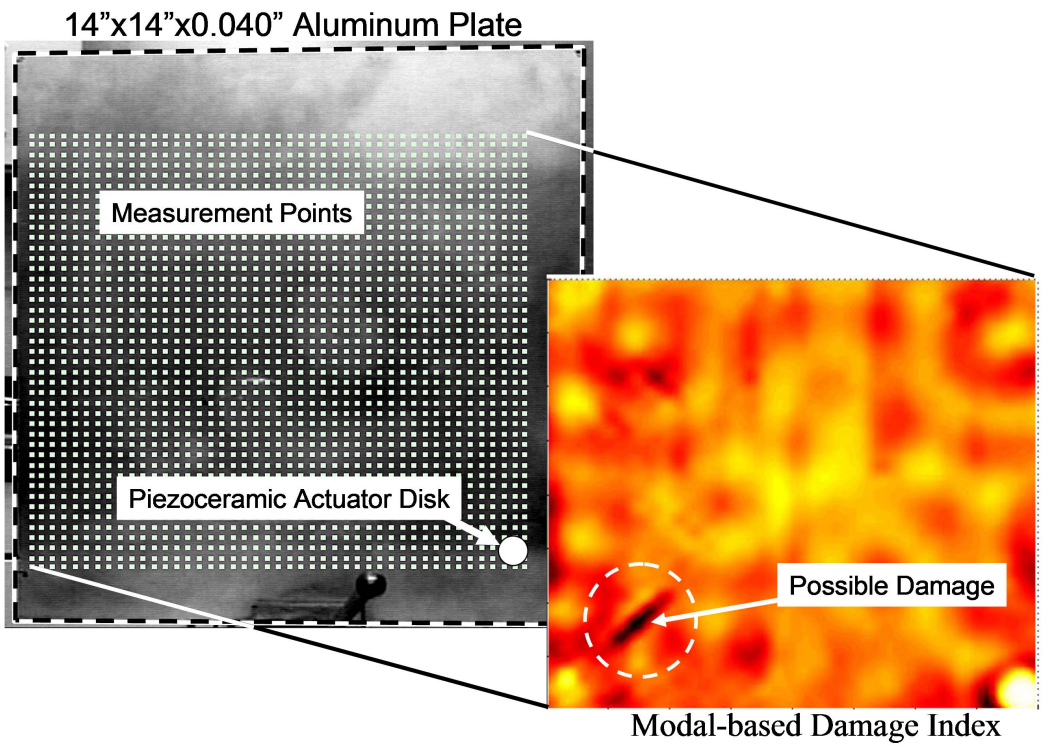

Figure 47: Measurement grid pattern

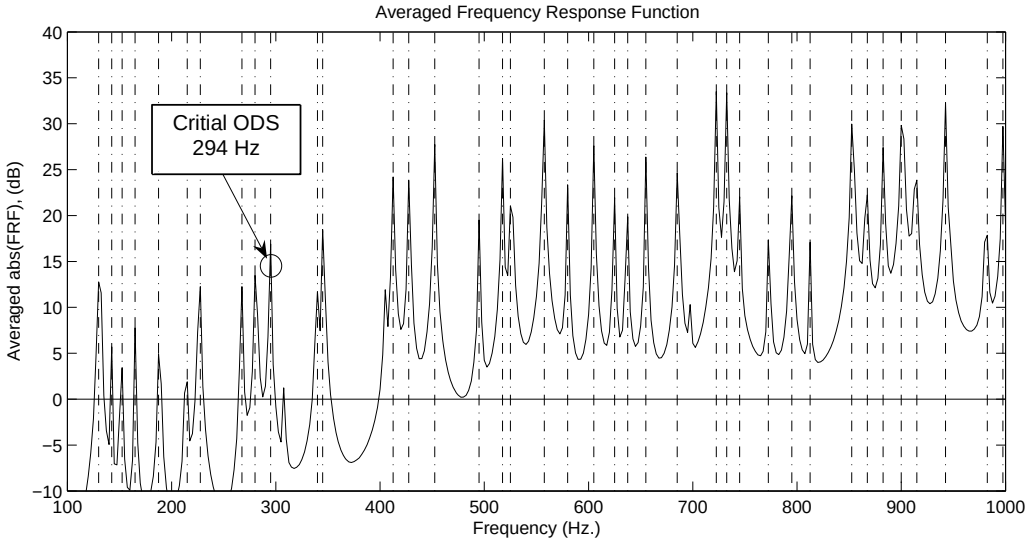

Figure 48: Averaged frequency response function and peaks selection

of 71 peaks are selected from the averaged spectrum. Mode shapes are generated corresponding to each of the peaks. It is noted that each of these operations are conducted in a

sequence per directive from the Executive Computer. Next, a cumulative Damage Measure computations are performed to include all 71 modes. Figure 47 shows the modal measurement grid pattern and the Cumulative Damage Measure. The suspect region of damage is clearly evident from this result. It is observed that the measured displacement shapes at 294 Hz as shown in Figure 49 responds the most to the damage and contributes the most toward the Damage Measure value. Contributions of non-player modes is simply consisting of unit values, thus of no consequence to the computations of Damage Measure. The Cumulative Damage Measure as shown in Figure 47 provides an unambiguous indication of damage presence and its general location.

At the conclusion of modal-based damage detection test, only one suspect region of damage is identified. Wave propagation tests are subsequently performed using the same actuator used for modal test. The excitation pulse width is reduced to only 5 microsecond in order to excite the Lamb waves in the structure. A snapshot of propagating wave measurements surrounding the suspect region identified in the modal-based testing is shown in Figure 50. The mode conversion phenomenon is clearly evident from this snapshot figure. The cumulative Damage Measure shown in Figure 50 clearly defines the shape of the damage along with its length. The magnitude of the Damage Measure is an indicator of the extent of the damage.

7.4 Conclusions of Automation in Structural Health Monitoring

A framework for automation in structural health monitoring is demonstrated. The enabling technology for the success of the automation scheme is the control of the software architecture of a Scanning Laser Doppler Vibrometer. The dynamic selection of sensor grids facilitated the two stage approach as described earlier in this chapter. The formulation of quantitative measure of damage provided a criteria for selection of suspect regions of damage using the modal data. Next, the suspect region is interrogated using guided wave propagation to fully characterize the damage.

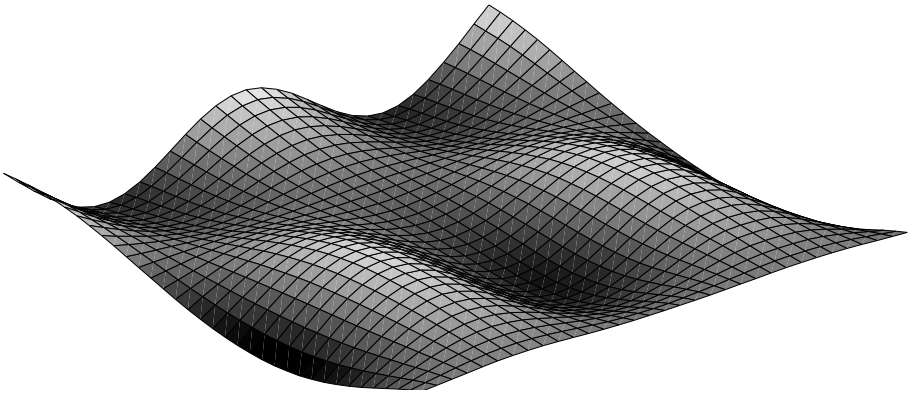

Figure 49: Critical Operational Deflection Shape, 294Hz

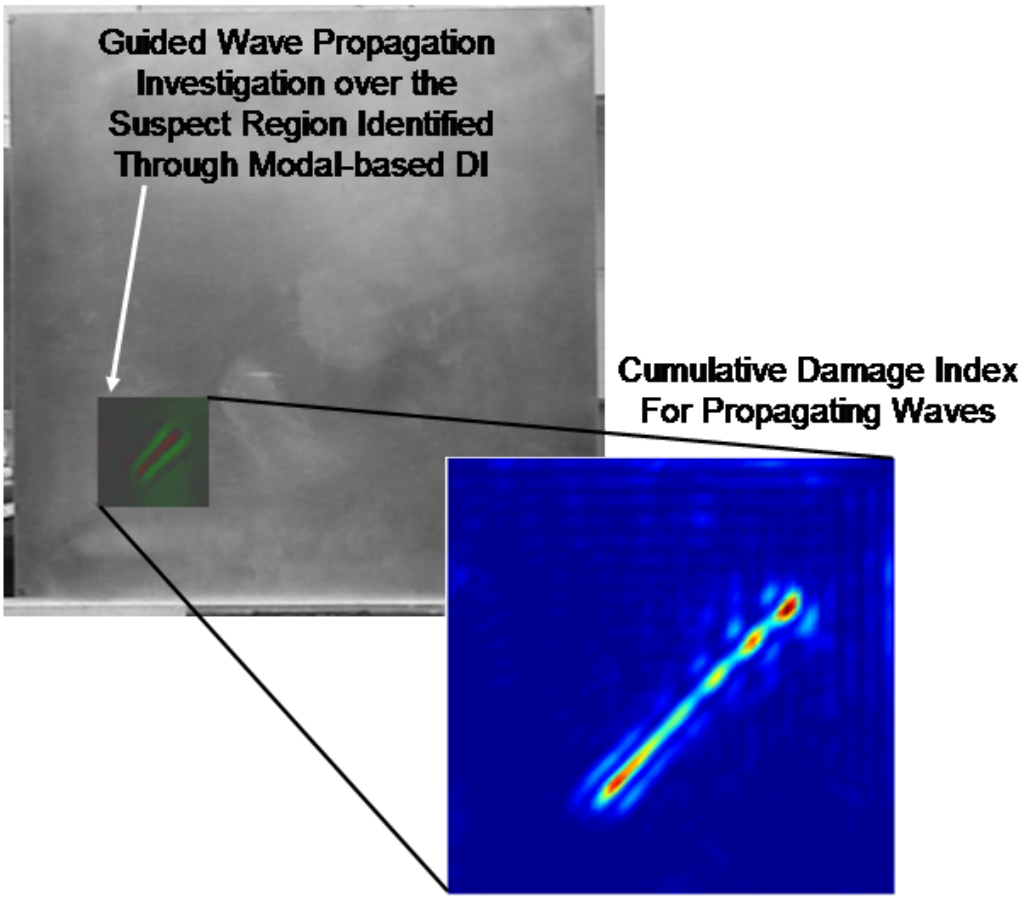

Figure 50: Closer Inspection using guided waves, a) Snapshot of plate displacement, b) Cumulative Damage Index of guided waves response

Chapter VIII

PRACTICAL APPLICATIONS OF THE SHM TECHNOLOGY

There are two major areas of application of the SHM technologies presented in this thesis. The first one relates to manufacturing defect detection while the second application addresses tests on an in-service structure to detect damages attributed to the operating environment. Modern aircraft structures rely heavily on the use of large composite panels. These composite structural components are subject to 100% inspection for voids, porosity, and other manufacturing defects immediately after their fabrication. There are well established practices and procedures of ultrasonic testing for such inspections. The techniques developed in this research effort offer a potential alternative and improvements over the existing ultrasonic test techniques in terms of speed and accuracy. This chapter is a showcase of demonstration of the developed technologies on practical structures. Results of SHM testing on several practical structural components along with a detailed description of the field test on the vertical tail of a high performance twin tail aircraft like F-15 are presented.

8.1 Laboratory Tests

Successful demonstrations of the developed SHM techniques on practical structural components in a laboratory setting are presented here.

8.1.1 Impact damage detection on a Graphite panel

An impact has the potential to cause localized loss of stiffness and a change in acoustic impedance. The affected region interacts with propagating waves and produces reflections and refractions. An experiment was conducted on a graphite composite panel with impact damage. This test specimen was obtained from The Boeing Company for testing purposes. Figure 51 shows the scanned region of the plate with the RMS plot of the wave-field over a

time duration of 200 micro seconds. The excitation signal consisted of a 12.5 micro-second rectangular pulse. The results of the DM and wavenumber/frequency filtering techniques were as presented in Figure 52. Both techniques successfully identified the location and the size of the damage correctly. The DM information was presented as a cumulative measure of damage over the 200 micro second duration. The wavenumber filtering results were presented in the form of an RMS plot over a 200 micro-second duration. Both techniques, Damage Measure and wavenumber/frequency filtering, correctly identified the impact damage location and size of the impact indentation.

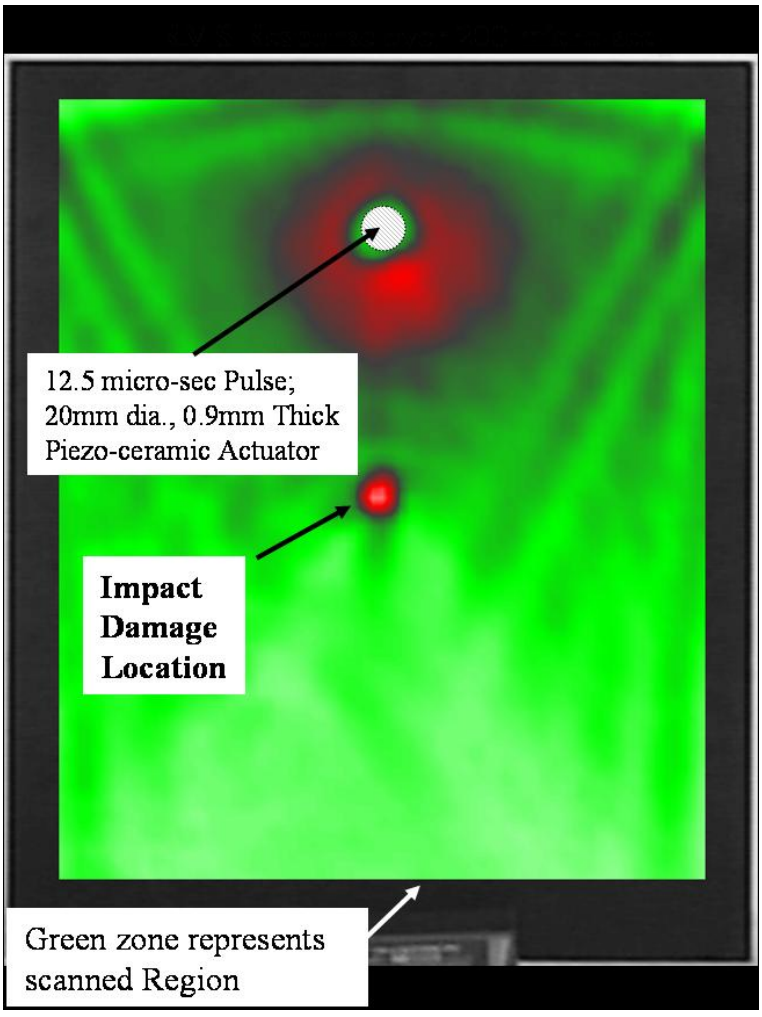

Figure 51: Graphite panel with impact damage; RMS Plot of Dynamics Response over 200 micro-seconds duration

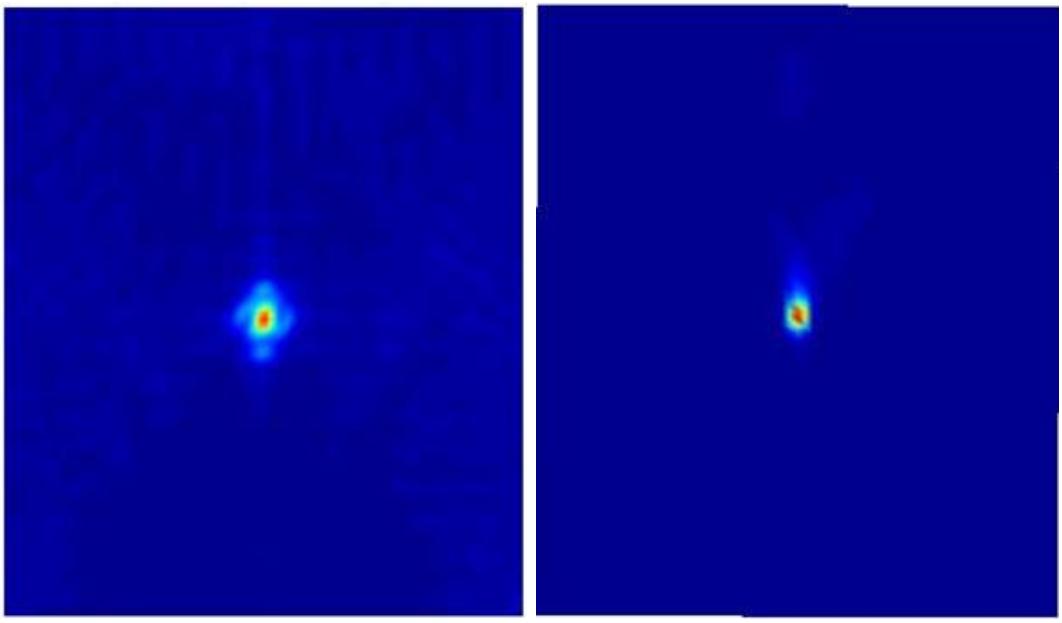

(a) (b)

Figure 52: Impact damage detection in a graphite panel; (a) Cumulative DM, (b) RMS plot of wavenumber/frequency filtered data

8.1.2 Manufacturing defect detection on a Graphite panel with stiffener

Another test specimen of graphite composite was obtained from The Boeing Company. This panel contained manufacturing defects at the interface between stiffener and the panel skin. Figure 53 shows the scanned region of the panel. A rectangular pulse of 17 micro-second width was used as a source of excitation to a 9mm diameter piezo-actuator. The results of cumulative DM computations and RMS Wavenumber/Frequency filtering were as shown in Figure 54. Both techniques proved to be excellent in accurately identifying the location and size of the damage.

8.1.3 Jet Engine Turbine Blade Inspection

A jet engine turbine blade made of nickel alloy was obtained for demonstration of othe developed damage detection techniques. The test specimen had been subjected to high cycle fatigue which caused small cracks on its surface. These cracks were not visible with naked eye. The damages had been confirmed using ultrasonic testing techniques. A 9mm diameter and 0.8mm thick piezoceramic disc was bonded to the turbine blade as shown

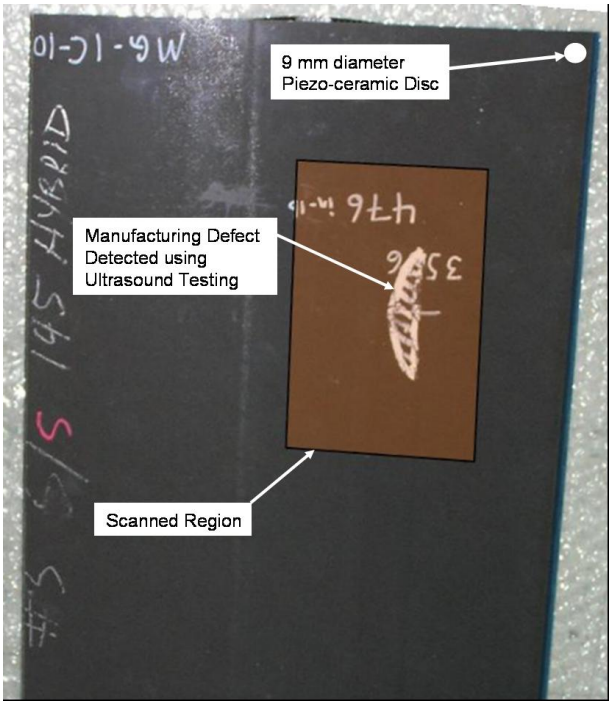

Figure 53: Stiffened graphite composite panel with manufacturing Defects

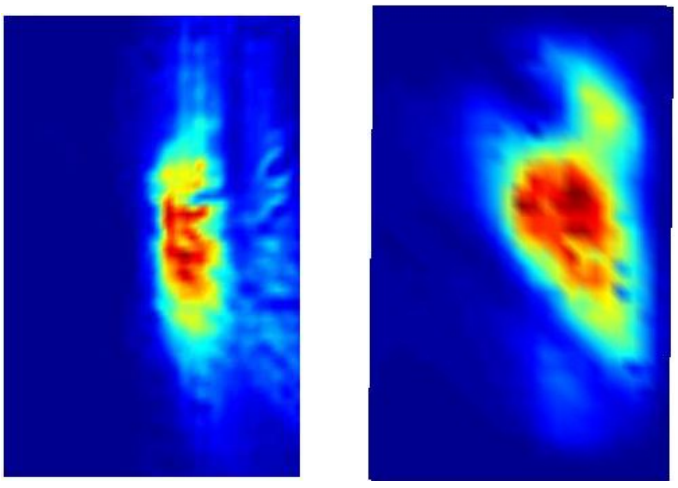

(a) (b)

Figure 54: Manufacturing damage detection in a graphite composite panel; (a) Cumulative DM, (b) RMS plot of wavenumber/frequency filtered data over the scanned region

in Figure 55. A Sine burst of five cycles at 196Khz was used to obtain the elastic wave propagation over the region of interest. It was noted that the frequency of excitation was higher than other tests conducted during this research since the damage size was very small which complied with a fact that the excitation wavelength needed be smaller than the damage size to allow detection of the interference between the waves and the damage.

The resulting cumulative Damage Measure plot was as shown in Figure 55 where the damage location, orientation, and length are correctly identified.

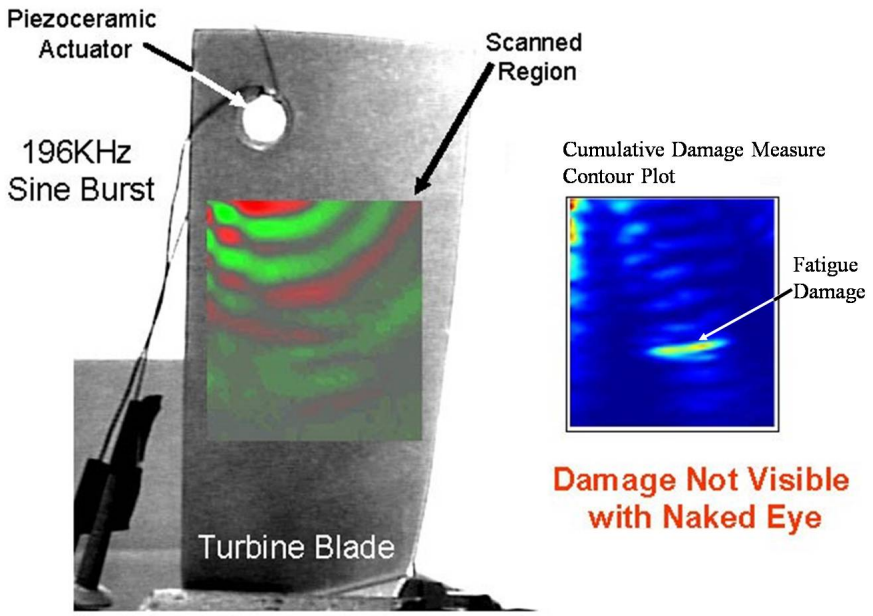

Figure 55: Cumulative Damage Measure for identification of microscopic damages in a turbine blade

8.2 Field Tests

Success of the developed techniques was demonstrated on an operational high performance twin tail aircraft vertical tail in the field. Specifically, the primary objectives of the field tests were to successfully demonstrate the SLDV data measurement procedure under service conditions, and thereby highlight key benefits of the technology:

1. Data recording is achievable while aircraft maintenance is simultaneously performed
2. Non-intrusive and easily adaptable to multiple aircraft components

3. Minimal set-up time and immediate data processing of very large structures

4. Minimal a priori knowledge of structures required for damage investigation

A secondary objective of the field tests was to utilize the wavenumber/frequency filtering to identify structural anomalies in the aircraft immediately following completion of the test, such as:

1. Delaminations and adhesive disbonds

2. Cracks, notches and cut-outs

3. Other structural discontinuities, such as overlap joints, etc.

It was noted that no information regarding damage and general structural health of the airframe was available. Therefore, no baseline for comparisons were available.

8.2.1 Test Procedure

8.2.1.1 General Test Set-Up

The field personnel initially identified critical structural regions on the vertical tail that may require investigation. The general test set-up consisted of positioning the scanning laser head of a Scanning Laser Doppler Vibrometer (SLDV)(Polytec PI, Model PSV400M2) perpendicular to the pre-determined scanning surface, ensuring excellent signal reception. Waves were generated through surface-bonded piezo-disks (Steminc model SMD2021F1000) of 20 mm in diameter and 2.1 mm in thickness. Temporary and non-intrusive adhesive aluminum strips of approximately 3 cm were applied to act as a barrier between the bonded piezo-disks and aircraft surface. The piezo-disc was then driven by wave bursts from a signal generator (Stanford Research Mod. SR360). Mid-range frequency sweeps (from 10 to 100 kHz) were utilized in determining the frequency at which to excite the structure via the piezo-disc, and thereby obtain noise-minimized data. The test techniques and procedures used in this field test were consistent with the rest of the testing throughout this research effort.

The elastic waves were recorded at pre-determined measurement grid points, and then post-processed to obtain full images of the propagating wavefield. The data acquisition

stand consisted of a vibrometer controller, a wave generator that triggered data recording, and a monitor to visualize the grid points. It was noted that no preparation of the scanning surface was required to yield clean wave propagation data. Likewise, the aircraft was scanned where field personnel were performing maintenance checks.

8.2.1.2 F-15 Aircraft Vertical Tail Tests

The first series of tests were conducted on the test aircraft vertical tail. Minimal knowledge of the structure's composition was known a priori, and the Lower torque box region of the left hand side vertical tail was identified for scan. The torque box construction was a Nomex Honeycomb core bonded to Aluminum skins. The edges of the torque box are formed by a continuous frame called 'Picture Frame' Figure 56 shows the test set-up and corresponding representative grid points for the vertical tail.

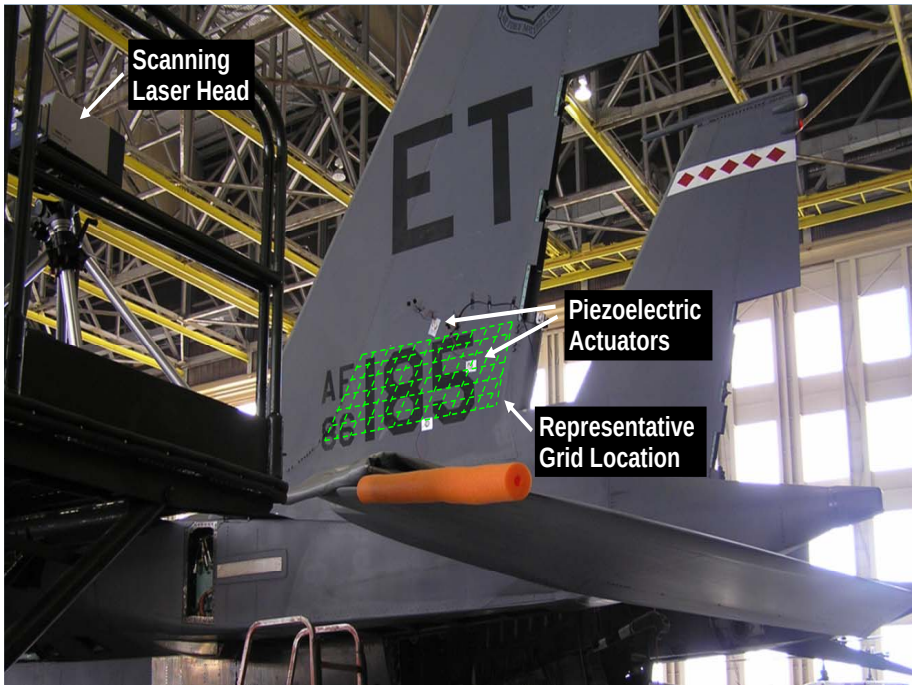

(a)

Figure 56: F-15 Vertical Tail Test Set-up

After performing a rapid frequency sweep on the vertical tail, a frequency of 31.5 KHz was selected to produce optimal wave propagation results. A pulse of 16.5 micro-second was also selected by observing the wave propagation signals at various location over the

selected region of interest.

8.2.2 Wave Propagation and RMS Results

A snapshot of the wave propagation due to pulse excitation is shown in Figure 57.a and the RMS contour plot over 200 micro-second duration is shown in Figure 57.b.

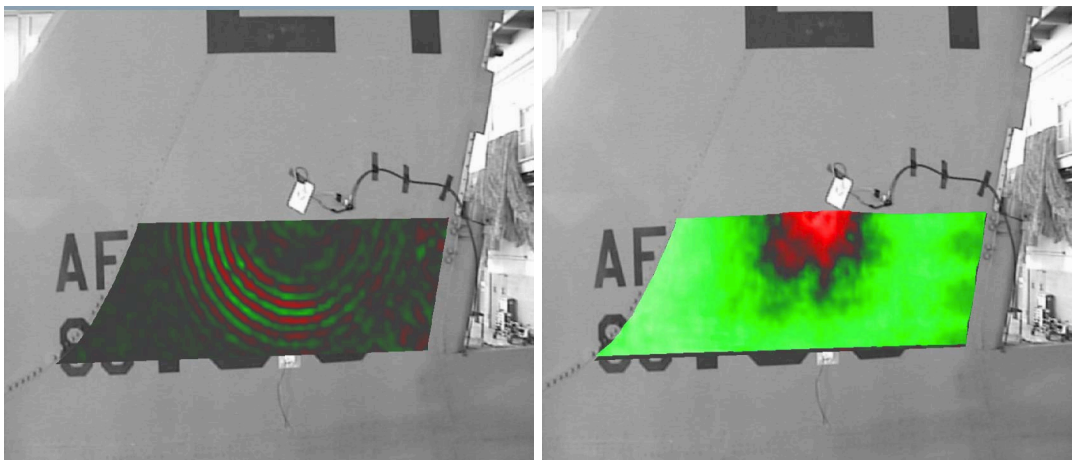

(a) (b)

Figure 57: F-15 Vertical tail-lower base region:; (a) Wavefield propagation (b) RMS of wavefield due to pulse excitation

8.2.3 Wavenumber/Frequency Filtering Results

For demonstration purposes, a case study of the vertical tail-lower base region data was conducted using the wavenumber/frequency filtering techniques. Employing 3-D FFT algorithms, the wavefield results were filtered in the wavenumber/frequency domain and then reconstructed in the spatial domain. The RMS of the filtered signals were computed to identify reflections along the wave path and potential associated damage. In order to evaluate the sensitivity of the results to the excitation signal, the data from the 7-cycle modulated sine wave and the pulse burst wave were compared. Figure 58 shows the wavenumber/frequency filtered results corresponding to the Sine and pulse burst excitation signals.

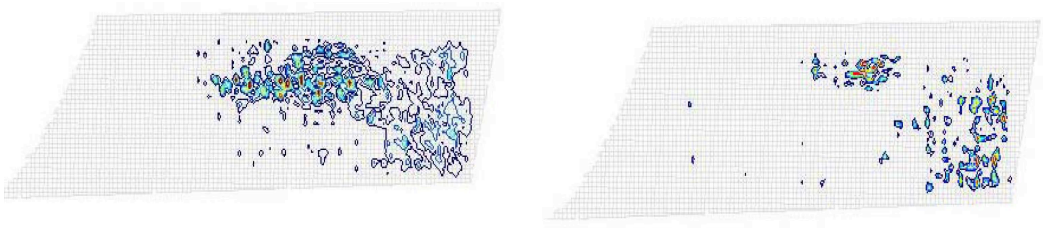

(a) (b)

Figure 58: Filtered RMS spatial results of F-15 vertical tail-lower base region: (a) 7-Cycle modulated sine wave at 31.5 kHz (b)Pulse burst wave at 16.5 μsec

Qualitatively, several key points may be addressed in evaluating the trends from Figure 58.

1. Both sets of data detect the fasteners along the far right-hand edge where the rudder actuator attaches to the vertical tail. This region is known to accumulate fatigue damage due to dynamic loads transmitted from the rudder.

2. Both sets of data demonstrate a common region of high RMS response in the middle top region of the scanned area where no discontinuities, joints, visible rivets, etc. are known to exist.

At this stage in the analysis, refined testing of the suspect areas is necessary to further understand the extent of any damage. No further tests were conducted on the aircraft.

8.2.4 Conclusions of the Field Tests

Several conclusions were drawn from the brief two-day tests in the field:

1. The novel SHM techniques were not sensitive to in-the-field conditions.

2. Wave propagation results compared favorably to those typically obtained in a lab-like environment.

3. Preliminary filtering of the data shows several structural areas that require further testing for damage.

4. Further reduction of the data, coupled with finer dense grids at suspected areas, is necessary to ascertain the degree and extent of any anomalies.

Overall, the SLDV data measurement procedure under service conditions successfully demonstrated its industry-applicable Structural Health Monitoring potential.

Chapter IX

CONCLUSIONS AND RECOMMENDATIONS FOR FUTURE STUDIES

9.1 Contributions

This thesis introduces the following contributions:

1. *Non-contact sensor for Structural Health Monitoring:* A unique contribution of this research is the use of a non-contacting Scanning Laser Doppler Vibrometer sensor for dynamic response measurement. The scanning features allow a capability to dynamically vary the sensor grids to meet the requirements of a test. The sensing limitations due to physical size and mass associated with the conventional sensors are overcome by the Laser beam. The high spatial density of sensor grids is an enabling technology for better quantitative assessment of damage.

2. *Damage Measure and Spatial Filter:* A new definition, 'Damage Measure', is introduced in this thesis. The ratio of measured strain energy distribution to a reference baseline value provides quantifiable measure of damage. The reference baseline represents the structure under consideration in its undamaged state. The information for the undamaged structure is synthesized by sampling the responses at a decimated set of measurement points which are less sensitive to the damage. This under-sampling is equivalent to spatial filter.

   Previous work of ratios of strain energy distribution between the damaged and undamaged structure required measured reference baseline data or historical reference data. This makes it extremely difficult to obtain a new set of measurements that would correspond to the original measurements taken on the structure in its undamaged state. Furthermore, the actual physically measured reference baseline data may not remain useful for any length of time as the operational conditions would result

in changes in the structure during its normal usage. Hence, the Damage Measure formulation without user supplied reference baseline data has a profound implication. It facilitates immediate assessment of the state of a structure without carrying along any historical information.

Representation of propagating waves in the frequency/ wave-number domain conveniently decouples incident from waves reflected by damage. Reconstruction of the incident waves allows formulation of the equivalent undamaged structure responses. Thus, the Damage Measure based on the strain energy ratio of the damaged structure and its undamaged baseline structure is formulated using the elastic wave propagation data.

The innovations include use of a single set of actuator/sensor pair to excite and detect the responses of a structure for low frequency vibration as well as guided wave propagation studies.

3. *Perturbation Methods:* Analytical modeling and solution techniques of perturbation methods are developed to study the dynamic behavior of damaged plates. This analytical framework allows investigating the effect of various types of damage on the plate modal characteristics and formulation of the Damage Measure.

   The analytical formulation and solution techniques of perturbation methods offer a unique opportunity to guide the experimental modal testing in support of SHM. The analytical results provide invaluable insights on the effects of damage on the plate modal parameters. In addition, the curvature modes are used for estimation of plate strain energy and to formulate the Damage Measure, which is used as effective indicator of the damage location and its extent.

4. *Comprehensive Damage Measure:* A cumulative Damage Measure is formulated for application in modal domain as well as elastic wave propagation in time domain. Hence, a comprehensive damage detection technique is introduced where initial assessment of the state of the structure is established using low frequency vibration modes followed by high frequency guided wave propagation to accurately characterize

the damage.

The cumulative damage measure assessment using modal data minimizes subjective judgement of a user in the process of mode selection. All measured modes may be included in the computation of the cumulative Damage Measure. Only those modes that are affected by the damage will contribute toward the Damage Measure.

5. *Automation in SHM:* The comprehensive damage detection concepts using Scanning Laser Doppler Vibrometer provide the enabling technologies for automation of SHM. A proof of concept study of automation in SHM is successfully conducted on a plate with simulated fatigue damage.

   The computer control of a scanning Laser Doppler Vibrometer allows selection of the measurement grids through smart logics and decision making processes. The Damage Measure is a quantitative representation of the damage, thus, allowing identification of suspect regions of damage using a threshold value of Damage Measure. Sub-regions of potential damage are first identified through the modal-based Damage Measure and finally the damage is characterized using guided wave propagation inspection of these suspect regions. Use of only one actuator suitable for both the vibration modes and elastic wave excitation is considered crucial to the success of the current technique of automation in SHM. Use of a non-contacting sensor, executive computer, test and analysis computers and the above described features of the software facilitate implementation of the Comprehensive Damage Measure in support of the automation in SHM. The final result of the automation procedure is to provide a quantitative assessment of damages in a structure under consideration.

9.2 Future Studies Recommendations

Future research effort should be directed towards making the SHM a nondestructive evaluation tool that can significantly reduce the time and cost associated with the inspection and maintenance of aerospace structures. It should be capable of performing detection, diagnosis, and prognosis of damages. The following discussions hold promises for future

directions:

1. *Enhanced filtering techniques:* Filtering techniques in the frequency/ wave-number domain provide decoupled incident from waves reflected by damage. The energy associated with the reflected wave is used to estimate the extent of damage, while the phase can be used to predict its location. Proper design of the filtering window allows in fact the separation of incident and reflected waves as well as the decoupling of different modes propagating at the same frequency. Automated selection of filtering window is an important topic for further studies.

   Spatial decimation of measured responses to generate baseline reference data requires a careful study. The purpose of decimation of the dynamic response data is to synthesis the baseline reference not sensitive to the damage while preserving the baseline characteristics. Hence, a careful investigation of spatial decimation would be of significant value for a robust Structural Health Monitoring technology.

2. *Revisit Damage Measure for better damage characterization:* Damage localization can be obtained based on the phase gradient of propagating waves whereas damage quantification can result from mode conversion analysis. Lamb waves propagate in a multi-modal fashion. At low ultrasonic frequencies, one symmetric S_0 and one antisymmetric mode A_0 typically coexist. The S_0 is predominantly an in-plane mode, while A_0 is mostly out-of-plane. The interaction of the wave with damage causes the partial conversion of the A_0 mode into S_0 and viceversa. The conversion coefficient, defining the amount by which one mode gets converted into the other, can be directly related to the extent of damage, as defined for example by the localized loss of thickness corresponding to a crack. Direct measurement of the conversion coefficient can therefore provide precise information regarding the crack depth and therefore can be used for damage quantification. This topic should be studied further for improved Damage Measure assessment.

3. *Analytical tools:* An emerging field of Spectral Finite Element Analysis, when combined with the perturbation methods, holds a promise of accurate damage detection

analytical formulation. This formulation is good not only for the low to medium frequency vibration modes but also guided waves at ultrasonic frequencies, all using one analytical Spectral Finite Element Model. Use of Spectral Finite Element combined with perturbation techniques and wavenumber/frequency filtering procedures should be explored for application in SHM.

4. *Enhanced modal testing techniques:* The fidelity of the Damage Measure based on low frequency vibration modes is dependent upon the measurement grid density and the size of the damage. Modal based initial detection of the suspect region of damage is critical to the successful characterization of the damage. Future analytical and experimental studies should be conducted to establish the relationship between the probability of detection and damage size and location for a particular structure so as to realize practical applications of the automated techniques.

   Current methods of modal testing may require a significant amount of data acquisition time duration since the conventional frequency response functions are based on Fast Fourier Transform computations of time history signals. A major step toward test time reduction may be achieved through the use of either Continuous Scanning Laser Doppler Vibrometer or holographic modal test. Both of these advanced topic have shown promise in the laboratory environment. However, more research is necessary to realize their application in the field of SHM.

5. *Prognosis:* True benefits of SHM can only be fully realized when the prognosis can be reliably used for safe usage of the structure. Technique should be developed to obtain Stress Intensity Factor to allow better determination of the remaining useful life of the structure.

6. *Technology transition:* Develop integrated software tools and experimental procedures for practical application in the field in support of SHM. The SHM technology holds a promise for detection of manufacturing defects as well as defects related to the aircraft operation.

Chapter X

APPENDIX

10.0.1 Scanning Laser Doppler Vibrometer and Automation in SHM

This research effort is based on use of a Scanning Laser Doppler Vibrometer (SLDV) to measure the dynamic response of a test structure. The SLDV allows non-contact vibration measurements which replaces the physical placement of accelerometer at a particular location of interest. The laser beam placement is controlled by a set of user defined parameters through a software/computer hardware device. This allows accurate positioning and dynamic selection of the measurement locations. Furthermore, the measurement locations can be spaced close enough to meet the requirements of a test. Previous research efforts in References [25, 26, 47, 94] for quantifying the extent of damage have been based on measurements using accelerometer. They demonstrated that spatially sparse measurements adversely affect the performance of damage measure due to a fact that the measurement grid spacing should be of the order of the damage size of interest. These problems are easily overcome by using a SLDV which allows a tremendous flexibility in selection of measurement grid pattern which can be dynamically selected under the control of a software. The SLDV can scan both large surfaces of an entire component (fuselage, wings, control surfaces, etc.), or very small regions around critical spots (holes, joints, etc.). The SLDV measures and records the velocity of the structure at points belonging to either a set defined by the user or a subset that is selected by the software as a result of damage assessment. Computer controlled Laser Doppler Vibrometer provides an enabling technology such that the sensor grid pattern is automatically selected for either a coarse sensor grid over a large region for vibration mode response measurement or zoom-in on a specific region of suspect damage for guided waves propagation investigation using a finer sensor grid pattern. The Damage Measure clearly defines the location, shape, and the extent of the damage. Such process is

to be repeated for each of the suspect regions to fully characterize the damages. Quantitative assessment of the damage through the use of damage measure provides a critical link with the automation in our structural health monitoring concept. The suspect regions are automatically identified through non-unit value of the Damage Measure under the control of the software. A unit magnitude of the Damage Measure implies that the strain energy distribution in the current state of the structure is the same as observed in its baseline, thereby, implying existence of no damage. Any perturbation from unit Damage Measure implies existence of damage. Hence through the use of this quantifiable Damage Measure it is now feasible to identify the suspect regions of damage under the control of a computer software. The Laser beam scanning mechanism under the control of a software facilitates the SHM concepts pursued in this research.

10.0.2 Basic Principles of Laser Doppler Vibrometer

A non-contacting Laser Doppler Vibrometer is an interferometer type device. It is based on the principle of detection of Doppler shift of the Laser light scattered form the vibrating surface. The Laser beam is passed through a beam splitter to create a reference beam and a measurement beam. The measurement beam illuminates a small area on the vibrating surface of interest. The scattered light from the vibrating surface exhibits a shift in frequency due to Doppler effect in response to the motion of the surface. The Vibrometer receives the scattered Laser light and compares its frequency against the reference beam and generates a voltage corresponding to the shift in frequency. This voltage signal is a representative of the surface velocity. A schematic of the Laser Doppler Vibrometer is shown in Figure 59.

The change in frequency due to Doppler shift on scattering is given by [106] $\Delta f = 2v/\Lambda$, where f and Λ are the frequency and wavelength of the reference Laser beam and v is the velocity of the surface. Due to sinusoidal nature of the detector signal, the direction of vibration is ambiguous. The Polytec PSV400 Scanning Laser Doppler Vibrometer used in this research employes a heterodyne type interferometer to address the directional sensitivity. The hetrodyne [106] technique is also called 'optical beating' where two optical beams are mixed to produce a mixed signal modulated by the difference in the two frequencies.

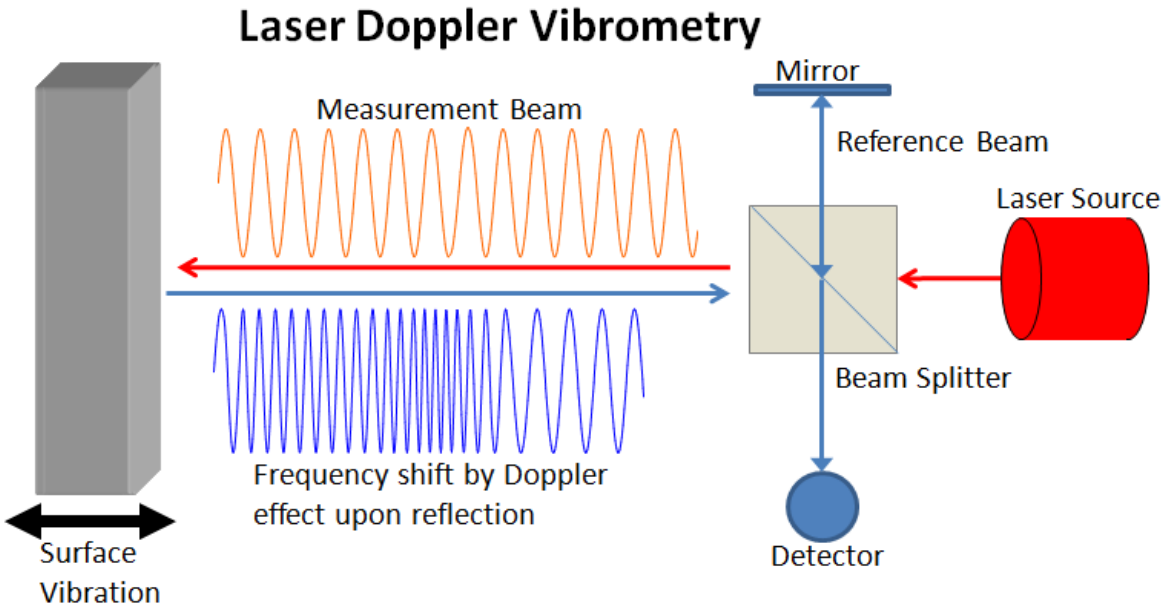

Figure 59: Schematic of Laser Doppler Vibrometer

The implementation of the heterodyning in a Laser Doppler Vibrometer is illustrated in Figure 60. A Bragg cell is introduced into one arm of the interferometer. The Bragg cell is an acousto-optic modulator that is driven at a frequency of 40 MHz or higher. This generates a carrier signal at the drive center frequency. This carrier signal is modulated by the movement of the object. Any deviation from the carrier center frequency is obtained by demodulating this signal thus providing the sign and magnitude of the velocity of the object.

The noise to signal ratio of the output from an LDV depends upon the amount of light scattered back from the surface under investigation. Diffused surfaces scatter the incident light over a large cone thus sending less light back to the Laser head following Lambert's cosine law. The back scatter from a shiny surface is larger than that of a diffused surface. However, a shiny surface, obeying the law: angle of incidence = angle of reflection, may offer a restricted cone from which an adequate signal is returned back to the Laser head. It is feasible to improve the reflectivity of a surface by using retro-reflective tape that is coated with microscopic glass spheres of approximately $50\mu m$ diameter. This tape bonds temporarily to a surface with an adhesive layer which is conveniently removed after use.

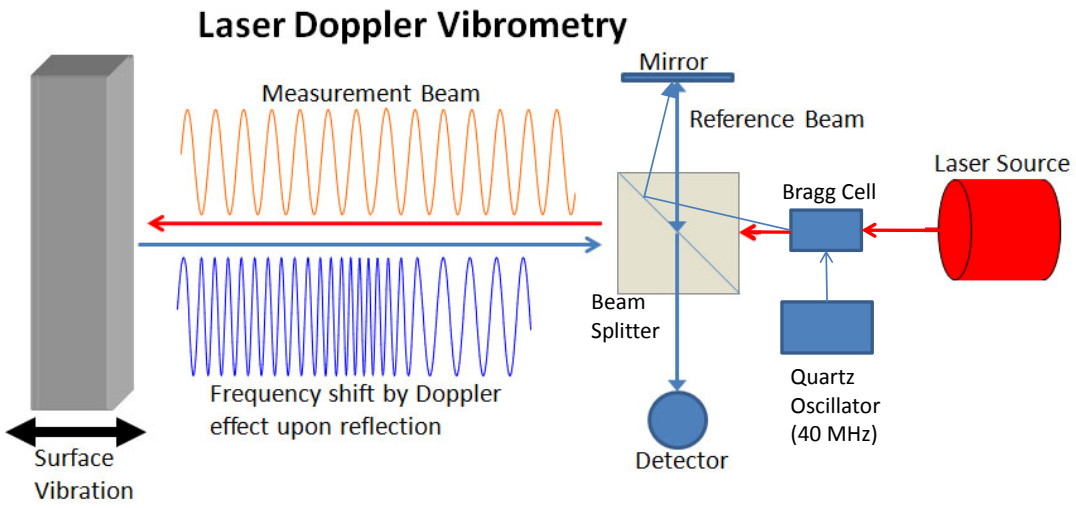

Figure 60: Schematic of Hetrodyne Interferometer-based Laser Doppler Vibrometer

REFERENCES

[1] Colvin, J., (1992), *Stiffness Enhancement Using Bonded Composite Skin Doublers Solved F-15 Vertical Tail Problem*, USAF Structural Integrity Program, December 1992.

[2] Shah, B.M., Cannington, J.C., Ferko, E.J., Kwon, Y.S., Saunders, S.A., Phan, N., and Candela, J.M., (2004), *P-3C Service Life Management*, USAF Aircraft Structural Integrity Program, November 2004.

[3] NTSB/AAR-89/03,*Aircraft Accident Report–Aloha Airlines, Flight 243, Boeiung 737-200, N73711, near Maui, Hawaii*, April 28,1988.

[4] FAA AC 29 MG 15, *Airworthiness Standards, Miscellaneous Guidance*

[5] Hooh Sohn, Charles R. Farrar, Francois M. Hemez, Devin D. Shunk, Daniel W. Stinemates, and Brett R. Nadler,(2003), *A Review of Structural Health Monitoring Literature: 1996-2001*, Los Alamos National Laboratory Report, LA-13976-MS.

[6] Doebling S.W., Farrar C., Prime M.B. and Daniel W.S., *Damage Identification and Health Monitoring of Structural and Mechanical Systems from Changes in Their Vibration Characteristics: A literature Review*, LA-13070-MS, May 1996.

[7] Alleyne, D.N., Cawley, P., *The Interaction of Lamb Waves with Defects*, IEEE Transactions of Ultrasonics, Ferroelectrics, and Frequency Control, Vol 39, No. 3 May 1992.

[8] Alleyne, D., Cawley, P., *A Two-dimensional Fourier Transform Method ofr the Measurement of Propagating Multimode Signals*, Journal of the Acoustical Society of America, Vol. 89, March 1991, pp. 1159-68.

[9] Lee, Staszewski, *Modelling of Lamb waves for damage detection in metallic structures: Part I. Wave propagation*, Smart Materials and Structures 12(2003) 804-814

[10] Lee, Staszewski, *Modelling of Lamb waves for damage detection in metallic structures: Part II. Wave interactions with damage*, Smart Materials and Strcutures 12(2003) 815-824

[11] Staszewski W., Boller, C., Thomlinson, G., (2004),*Health Monitoring of Aerospace Structures; Smart Sensor Technologies and Signal Processing*, John Wiley & Sons, Ltd, 2004.

[12] Cawley, P., and Adams, R.D. (1979) *The Location of Defects in Structures from Measurements of Natural Frequencies*, Journal of Strain Analysis, Vol. 14, No. 2, pp. 49-57

[13] Luo, H. and Hanagud, S., *PVDF Film Sensor and its Application in Damage Detection*, Journal of Aerospace Engineering, Vol. 12, No. 1, pp. 23-30, 1999

[14] West, W.M., (1984), *Illustration of the Use of Modal Assurance Criterion to Detect Structural Changes in an Orbiter Test Specimen*, Proc. Air Force Conference on Aircraft Structural Integrity, 1-6

[15] Luo, H., Hanagud, S., *An Integral Equation for Changes in the Structural Characteristics of Damaged Structures*, International Journal of Solids and Structures, 1997, Vol. 34, No. 35-36, pp.4557-4579.

[16] Luo, H., Hanagud, S., (1997), *Delaminated Beam Nonlinear Dynamic Response Calculation and Visualization*, Processdings of the 38th AIAA/ASME/ASCE/AHS SDM Conference, Vol. 1,1997, pp 490-499.

[17] Luo, H., Hanagud, S., (1998), *Detection of Debonding in Thermal Protective System Titles by Using Nonlinear Structural Dynamic Response*, AIAA-98-1924.

[18] Gawronski, W., and Sawicki, J.T. (2000) *Structural Damage Detection Using Modal Norms*, Journal of Sound and Vibration, Vol. 229, pp. 194-198.

[19] Modena, C., Sonda, D., and Zonta, D. (1999) *Damage Localization in Reinforced Concrete Structures by Using Damping Measurements*, Damage Assessment of Structures, Proceedings of the International Conference on Damage Assessment of Structures (DAMAS 99), Dublin, Ireland, pp. 132141.

[20] Schulz, M.J., Naser, A.S., Thyagarajan, S.K., Mickens, T., and Pai, P.F. (1998), *Structural Health Monitoring Using Frequency Response Functions and Sparse Measurements*, Proceedings of the International Modal Analysis Conference, pp. 760-766.

[21] Pandey, A.K., M. Biswas, and M.M. Samman, 1991, *Damage Detection from Changes in Curvature Mode Shapes*, Journal of Sound and Vibration, 145(2), 321-332.

[22] Luo, H, Hanagud,S., *An Integral Equation for Changes in the Structural Characteristics of Damaged Structures*, International Journal of Solids and Structures, Vol. 34, No. 35-36, pp.4557-4579.

[23] Ma, J., and Asundi, A., 2001, *Structural Health Monitoring Using a Fiber Optic Polarimetric Sensor and a fiber Optic Curvature Sensor - Static and Dynamic Test*, Smart Materials and Structures 10, 181-188.

[24] Salawu, O.S. and C. Williams, 1993, *Structural Damage Detection Using Experimental Modal Analysis-A Comparison of Some Methods*, in Proc. of 11th International Modal Analysis Conference, 254-260.

[25] Ho, Y.K., and Ewins, D.J. (1999) *Numerical Evaluation of the Damage Index*, Structural Health Monitoring 2000, Stanford University, Palo Alto, California, pp. 995-1011.

[26] Ho, Y.K., and Ewins, D.J. (2000) *On the Structural Damage Identification with Mode Shapes*, European COST F3 Conference on System Identification and Structural Health Monitoring, Madrid, Spain, pp. 677-686.

[27] Wang, M.L., Xu, F.L., and Lloyd, G.M. (2000), *A Systematic Numerical Analysis of the Damage Index Method Used for Bridge Diagnostics*, Smart Structures and Materials

2000: Smart Systems for Bridges, Structures, and Highways, Proceedings of SPIE, Vol. 3,988, Newport Beach, California, pp. 154-164.

[28] Kim, K., Ryu, J., Lee, S., and Choi, L. (1997), *In-Situ Monitoring of Sungsan Bridge in Han River with a Optical Fiber Sensor System*, Smart Systems for Bridges, Structures, and Highways, Proceedings of SPIE, Vol. 3,043, pp. 72-76.

[29] Shi, Z.Y., Law, S., Zhang, L.M, (1998), *Structural damage localization from modal strain energy change*, Journal of Sound and Vibration, v 218, n 5, Dec 17, 1998, p 825-844

[30] Choi, S., and Stubbs, N. (1997), *Nondestructive Damage Detection Algorithms for 2D Plates*, Smart Systems for Bridges, Structures, and Highways, Proceedings of SPIE, Vol. 3,043, pp. 193-204.

[31] Staszewski, Lee, Mallet, Scarpa, *Structural health monitoring using scanning laser vibrometery: I. Lamb wave sensing*, Smart Materials and Structures 13(2004) 251-260

[32] Staszewski, Lee, Mallet, Scarpa, *Structural health monitoring using scanning laser vibrometery: II. Lamb wave sensing*, Smart Materials and Structures 13(2004) 261-269

[33] Purekar, A.S., Pines, D.J., Sundararaman,S., and Adams, D.E., (2004), *Directional Piezoelectric Phased Array Filters for Detecting Damage in Isotropic Plates*, Smart Materials and Structures, 13 (2004), 838-850.

[34] P. Sriram, 1988, *Whole Field Optical Methods for Structural Mechanics: Digital Speckle Correlation and Laser Doppler Velocimetery*, PhD Thesis, Georgia Institute of Technology

[35] Sriram, P., Hanagud, S., Craig, J.I., (1992),*Mode Shape Measurement Using a Scanning Laser Doppler Vibrometer*, The International Journal of Analytical and Experimental Modal Analysis, V 7, No 3, p 169-178, July 1992.

[36] Martelli, M., (2001), *Exploiting the Laser Scanning Facility for Vibration Mesaurements*, PhD Thesis , Imperial College of Science, Technology and Medicine, University of London

[37] Fink, M., (1992) *Time Reversal of Ultrasonic Fields - Part I: Basic Principles*, IEEE Transactions on Ultrasonics, Ferroelectrics, and Frequenct Control, Vol. 39, No. 5, September 1992

[38] Wu, Francois, Thomas, Jean-Louis, Mathis, Fink, (1992), *Time Reversal of Ultrasonic Fields - Part II: Experimental Results*, IEEE Transactions on Ultrasonics, Ferroelectrics, and Frequenct Control, Vol. 39, No. 5, September 1992

[39] Paskaramoorthy, R., Datta, S.K., Shah, A.H.,(1988),*Effect of Interface Layers on Scattering of Elastic Waves*, Journal of Applied Mechanics, Vol 55, December 1988.

[40] Zhu, J., Shah, A.H., Datta, S.K., (1998),*Transient Response of a Composite Plate with Delamination*, Transactions of ASME, Vol 65, September 1998.

[41] Datta, S.K.,Ju, T.H., Shah, A.H., (1992),*Scattering of Impact Wave by a Crack in a Composite Plate*, Transactions of ASME Vol 59, September 1992.

[42] Sohn, H., Park,H., Law,K.H., and Farrar, C.R., (2004), *Instantaneous Damage Detection using Time Reversal Process*, 15th International Conference on Adaptive Structures and Technologies, October 2004

[43] Hyun Woo Park, Hoon Sohn, Kincho H. Law, Charles R. Farrar, *Time Reversal Active Sensing for Health Monitoring of a Composite Plate*, Journal of Sound and Vibration, 2004.

[44] Wahyu, Lestari, 2001, *Damage of Composite Structures: Detection Technique, Dynamics Response and Residual Strength*, PhD Thesis, Georgia Institute of Technology

[45] Leissa, A., *Vibration of Plates*,Acoustical Society of America, Washington,DC, 1993.

[46] Kaczmarek, H., (2002), *Lamb Wave Interaction with Impact-induced Damage in Aircraft Composite: Use of the A0 Mode Excited by Air-coupled Transducer*, Journal of Composite Materials, Vol. 37, No. 3/2003.

[47] Kim, J.T., Stubbs, N., *Crack Detection in Beam Type Structures Using Frequency Data*, Journal of Sound and Vibration, 259 (1), pp. 146-160.

[48] Hu, N., et al., *Damage Assessment of Structures Using Modal Test Data*, International Journal of Solids and Structures, Vol. 38, pp. 3111-3126.

[49] Blotter, J. D., West, R. L., Sommerfeldt, S. D., *Spatially continuous power flow using a scanning laser Doppler vibrometer*, Journal of Vibration and Acoustics, Transactions of the ASME, v 124 n. 4, pp. 476-482.

[50] Farin, G., *Curves and Surfaces for CAGD: A Practical Guide*, Academic Press, 5th edition, 2002.

[51] Staszewski, W.J., Boller, C., Tomlinson, G., *Health Monitoring Of Aerospace Structures. Smart Sensors And Signal Processing*, Wiley & Sons Ltd., 2004.

[52] Michaels, T.E., Michaels, J.E., *Ultrasonic Signal Processing For Structural Health Monitoring*, Review of Progress in QNDE, 23, eds. D.O. Thompson, D.E. Chimenti, American Institute of Physics, 2004.

[53] Michaels, T.E., Michaels, J.E., *Sparse Ultrasonic Transducer Array For Structural Health Monitoring*, Review of Progress in QNDE, 23, eds. D.O. Thompson, D.E. Chimenti, American Institute of Physics, 2004.

[54] Ruzzene M., Jeong S.M., Michaels T.E., Michaels J.E., Mi B., *Simulation and Measurement of Ultrasonic Waves in Elastic Plates Using Laser Vibrometry*, Review of Progress in QNDE, 23, Eds. D.O. Thompson, D.E. Chimenti, Am. Inst. of Phys., 2004.

[55] Ing, K., Fink, M. *Time Reversed Lamb Waves*, IEEE Transactions on Ultrasonics, Ferroelectrics, and Frequency Control, Vol. 45, 4, pp. 1032-1043.

[56] Chakroun, N., Fink, M. Wu, F., *Time Reversal Processing In Ultrasonic Nondestructive Testing*, IEEE Transactions on Ultrasonics, Ferroelectrics, and Frequency Control, Vol. 42, 6, pp. 1087-1098.

[57] Staszewski, W.J. Lee B.C., Mallet L., and Scarpa, F., *Structural Health Monitoring Using Scanning Laser Vibrometry: I. Lamb Wave Sensing*, Smart Materials and Structures, 13 No 2 (April 2004) 251-260.

[58] Staszewski, W.J. Lee B.C., Mallet L., and Scarpa, F., *Structural Health Monitoring Using Scanning Laser Vibrometry: II. Lamb Wave For Damage Detection*, Smart Materials and Structures, 13 No 2 (April 2004) 261-269.

[59] Delsanto, P.P., Scalerandi, M. *A Spring Model For The Simulation Of The Propagation Of Ultrasonic Pulses Through Imperfect Contact Surfaces*, Journal of The Acoustical Society of America, 104(5), November 1998, pp. 2584-2591.

[60] Achenbach, J.D., *Wave Propagation In Elastic Solids*, North Holland, 1975.

[61] Graff, K.F., *Wave Motion In Elastic Solids*, Dover, NY, 1991.

[62] Michaels T.E., Michaels J.E., Mi B., Ruzzene, M., *Damage Detection in Plates Structures Using Sparse Ultrasonic Transducer Arrays and Acoustic Wavefield Imaging*, Review of Progress in QNDE, 23, Eds. D.O. Thompson, D.E. Chimenti, Am. Inst. of Phys., 2004.

[63] H. Lou and S. Hanagud, *Detection of Debondings in Thermal Protection System Tiles by using Non-Linear Structural Dynamic Response*, Georgia Institute of Technology, AIAA-98-1924. [47] H. Lou and S. Hanagud, "PVDF Sensor and Its Applications in Delamination Response Detection", Georgia Institute of Technology, AIAA-97-1218.

[64] Cawley, P. (1997), *Long Range Inspection of Structures Using Low Frequency Ultrasound*, in Structural Damage Assessment Using Advanced Signal Processing Procedures, Proceedings of DAMAS '97, University of Sheffield, UK, pp. 1-17.

[65] Prasad, Balasubramanium, Krishnamurthy, *Structural Health Monitoring of composite structures using Lamb wave tomography*, Smart Materials and Structures, 13 (2004) N73-N79 (copy in hand)

[66] Tua, Quek, Wang, *Detection of cracks in plates using piezo-actuated Lamb waves*, Smart Materials and Structures 13(2004) 643-660 (copy in hand)

[67] Ip, Mai, *Delamination detection in smart composite beams using Lamb waves*, Smart Materials and Structures 13(2004) 544-551 (copy in hand)

[68] Kessler, Spearing, Soutis, *Damage detection in composite materials using Lamb wave methods*, Smart Materials and Strcutures 11(2002) 269-278 (copy in hand)

[69] Monkhouse, Wilcox, Lowe, Dalton, *The rapid monitoring of structures using interdigital Lamb wave transducers*, Smart Materials and Strcutures 9(2000) 304-309

[70] Balis Crema, L., and Mastroddi, F. (1998), *A Direct Approach for Updating and Damage Detection by Using FRF Data*, Proceedings of ISMA23, Noise and Vibration Engineering, Leuven, Belgium.

[71] Carrasco, C., Osegueda, R., Ferregut, C., and Grygier, M. (1997), *Localization and Quantification of Damage in a Space Truss Model Using Modal Strain Energy*, Smart Systems for Bridges, Structures, and Highways, Proceedings of SPIE, Vol. 3,043,

[72] Staszewski, W.J., Boller, C., Tomlinson, G., *Health Monitoring Of Aerospace Structures. Smart Sensors And Signal Processing*, Wiley & Sons Ltd., 2004.

[73] Gudmundson P., "The Dynamic Behavior of Slender Structures With Cross-Sectional Cracks", *Journal of Mechanics, Physics and Solids*, Vol. 31, 1984, pp. 329-345.

[74] Ostachowicz W., Krawczuk M., "Analysis of The Effect of Cracks On The Natural Frequencies of A Cantilever Beam", *Journal of Sound and Vibration*, Vol. 138, 1990, pp. 115-134.

[75] Krawczuk M., "Application of spectral beam finite element with a crack and iterative search technique for damage detection". *Finite Elements in Analysis and Design*, 38(6), 2002, pp. 537-548.

[76] Krawczuk M., Ostachowicz, W., "Identification of delamination in composite beams by genetic algorithm" *Science and Engineering of Composite Materials*, 10(2),2002 147-155.

[77] Krawczuk M., Ostachowicz W., "Modelling and vibration analysis of a cantilever composite beam with a transverse open crack" *Journal of Sound and Vibration*, 183(1), 1995, pp. 69-89.

[78] Hellan K., *Introduction To Fracture Mechanics*, McGraw-Hill, New York, 1984.

[79] Atluri S.N., *Computational Methods In The Mechanics of Fracture* North Holland, Amsterdam, 1986.

[80] Haisty B.S., Springer W.T., "A General Beam Element For Use In Damage Assessment of Complex Structures", *ASME Journal of Vibration, Acoustics, Stress, and Reliabiliy in Design*, Vol. 110, 1988, pp. 356-359.

[81] Pozrikidis C., "Introduction to Finite and Spectral Element Methods using MATLAB", Section 1.7 Beam Bending, p. 101, 2005, Chapman Hall/CRC

[82] Cook R.D., Malkus D.S., Plesha M.E., Witt R.J., "Concepts and Applications of Finite Element Analysis", 4th Edition, 2004, John Wiley Sons, Inc.

[83] Christides S., Barr A.D.S., "One-dimensional Theory of Cracked Euler-Bernoulli Beams", *International Journal of Mechanical Sciences*, Vol. 26(11-12), 1984, pp. 639-648.

[84] Shen M.H., Pierre C., "Natural Modes of Euler-Bernoulli Beams With Symmetric Cracks", *Journal of Sound and Vibration*, Vol. 138, 1990, pp. 115-134.

[85] Qian G.L., Gu S.N., Jiang J.S., "The Dynamic Behavior AN Crack Detection of A Beam With A Crack", *Journal of Sound and Vibration*, Vol. 138, 1991, pp. 233-243.

[86] Azak A., Krawczuk M., Ostachowicz W. "Vibration of a laminated composite plate with closing delamination" *Journal of Intelligent Material Systems and Structures*, 12(8), 2001, pp. 545-551.

[87] Krawczuk M., "A rectangular plate finite element with an open crack", *Computers and Structures*, 2002.

[88] Krawczuk M., Palacz M., Ostachowicz W., "Wave propagation in plate structures for crack detection" *Finite Elements in Analysis and Design*, 40(9-10), 2004, pp. 991-1004.

[89] Jones D.S. *The Theory of Generalized Functions*, Cambridge University Press, 1982, Cambridge UK.

[90] Doebling S.W., Farrar C., Prime M.B. and Daniel W.S., *Damage Identification and Health Monitoring of Structural and Mechanical Systems from Changes in Their Vibration Characteristics: A Literature Review*, LA-13070-MS, May 1996.

[91] Staszewski, W.J., Boller, C., Tomlinson, G., *Health Monitoring Of Aerospace Structures. Smart Sensors And Signal Processing*, Wiley & Sons Ltd., 2004.

[92] Ho, Y.K., and Ewins, D.J., "On the Structural Damage Identification with Mode Shapes" *European COST F3 Conference on System Identification and Structural Health Monitoring*, Madrid, Spain, pp. 677-686.

[93] Kim, J.T., Stubbs, N., "Crack Detection in Beam Type Structures Using Frequency Data", *Journal of Sound and Vibration*, 259 (1), pp. 146-160.

[94] Cornwell P., Doebling S.W., Farrar C.R., "Application of the Strain Energy Damage Detection Method to Plate-like Structures, *Journal of Sound and Vibration*, 224(2), pp. 359-374.

[95] Rose, J.L. "A Baseline and Vision of Ultrasonic Guided Wave Inspection Potential" *Journal of Pressure Vessel Technology*, Vol. 124, pp. 273-282.

[96] Michaels, T.E., Michaels, J.E., "Ultrasonic Signal Processing For Structural Health Monitoring" *Review of Progress in QNDE*, 23, eds. D.O. Thompson, D.E. Chimenti, American Institute of Physics, 2004.

[97] Giurgiutiu, V., Bao, J., Zhao, W., "Piezoelectric Wafer Active Sensor Embedded Ultrasonics in Beams and Plates" *Experimental Mechanics*, Vol. 43, No. 4, December 2003, pp. 428-449.

[98] Sharma, V.K., Hanagud, S., Ruzzene, M., "Damage Index Estimation in Beams and Plates Using Laser Vibrometry", Proceeding of the *2005 International Workshop on Structural Health Monitoring (IWSHM)*, Stanford University, Stanford CA, 2005.

[99] Cook, R. D., Malkus, D. S., Plesha, M. E., Witt, R. J. 2001. *Concepts and Applications of Finite Element Analysis*, Fourth edition, Wiley, New York, NY.

[100] Farin, G., *Curves and Surfaces for CAGD: A Practical Guide*, Academic Press, 5th edition, 2002.

[101] Graff, K.F., *Wave Motion In Elastic Solids*, Dover, NY, 1991.

[102] Yim, H., Sohn, Y. "Numerical Simulation and Visualization of Elastic Waves Using Mass-Spring Lattice Model" *IEEE Transactions on Ultrasonics, Ferroelectrics, and Frequency Control*, Vol. 47, No. 3, May 2000, pp. 549-558.

[103] Sharma, V.K., Hanagud, S., Ruzzene, M., "Damage Index Estimation in Beams and Plates Using Laser Vibrometry", Proceeding of the *2005 International Workshop on Structural Health Monitoring (IWSHM)*, Stanford University, Stanford CA, 2005.

[104] Ruzzene, M., "Frequency-wavenumber Domain Filtering for Improved Damage Visualization", Smart Materials and Structures, Volume 16, Number 6, December 2007

[105] Apetre, N., Ruzzene, M., Hanagud, S., Sharma, V.,"Damage Measure Formulation Based on the Filtered Spectral Approximation of the Structural Response", AIAA 2007-2303, 48th AIAA/ASME/ASCE/AHS/ASC Structures, Structural Dynamics, and Materials Conference, 23-26 April 2007, Honolulu, Hawaii

[106] Drain, L.E., 1980. *The Laser Doppler Concepts*, John Wiley Sons, New York, NY.